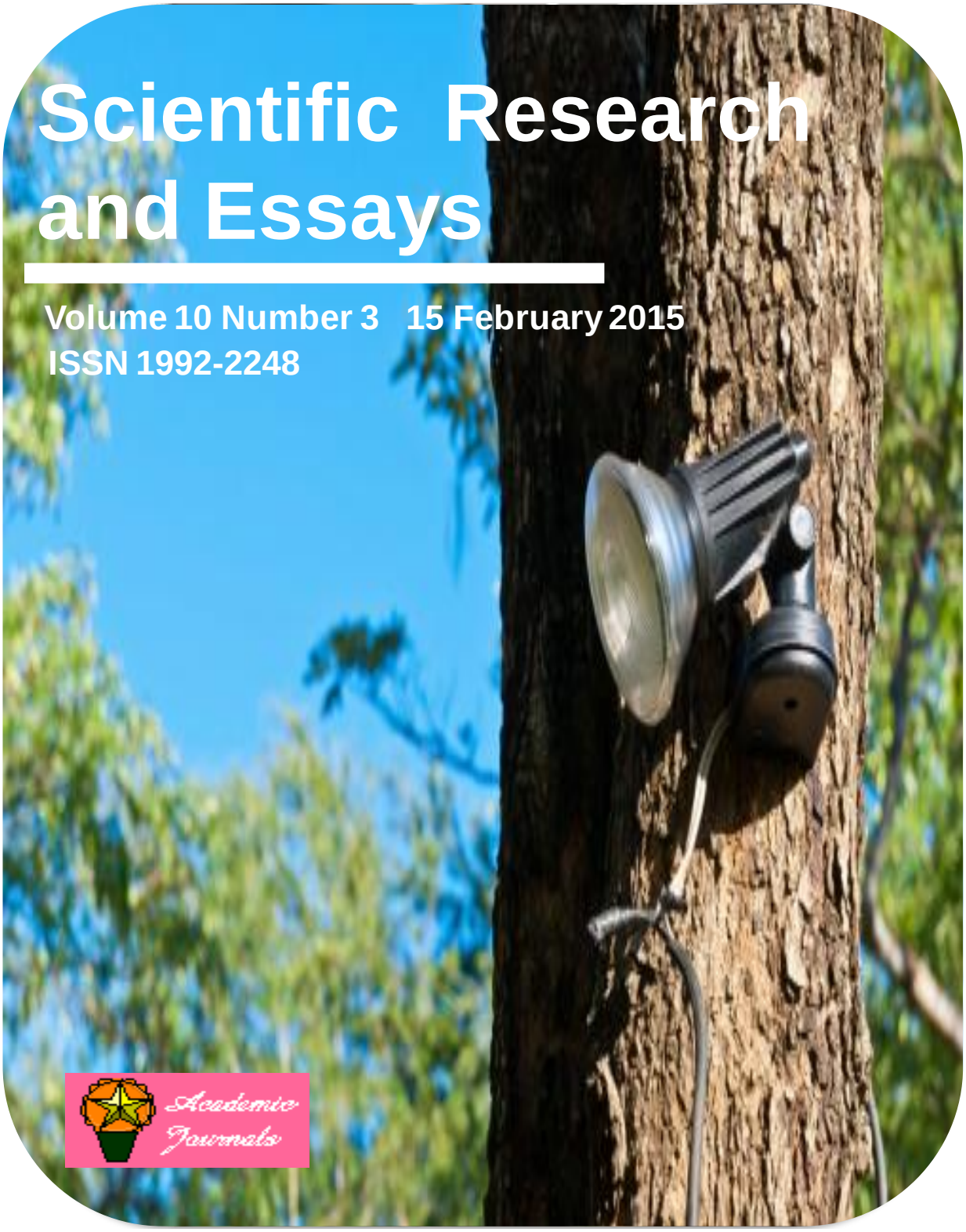

Scientific Research and Essays

Volume 10 Number 3 15 February 2015
ISSN 1992-2248

Academic Journals

ABOUT SRE

The **Scientific Research and Essays (SRE)** is published twice monthly (one volume per year) by Academic Journals.

Scientific Research and Essays (SRE) is an open access journal with the objective of publishing quality research articles in science, medicine, agriculture and engineering such as Nanotechnology, Climate Change and Global Warming, Air Pollution Management and Electronics etc. All papers published by SRE are blind peer reviewed.

SubmissionofManuscript

Submit manuscripts as email attachment to the Editorial Office at sre@academicjournals.org. A manuscript number will be mailed to the corresponding author shortly after submission.

The Scientific Research and Essays will only accept manuscripts submitted as e-mail attachments.

Please read the **Instructions for Authors** before submitting your manuscript. The manuscript files should be given the last name of the first author.

Editors

Dr.NJTonukari
Editor-in-Chief
ScientificResearchandEssays
AcademicJournals
E-mail:sre.research.journal@gmail.com

Dr.M.SivakumarPh.D. (Tech).
AssociateProfessor
SchoolofChemical&EnvironmentalEngineering
Faculty ofEngineering
UniversityofNottingham
JalanBroga,43500Semenyih
SelangorDarul Ehsan
Malaysia.

Prof.N.MohamedElSawiMahmoud*Departmentof*
Biochemistry,Facultyofscience,KingAbdulAzizuniv
ersity,
SaudiaArabia.

Prof. AliDelice
ScienceandMathematicsEducationDepartment,At
atürkFacultyofEducation,
MarmaraUniversity,
Turkey.

Prof.MiraGrdisa
RudjerBoskovicInstitute,Bijenickacesta54,
Croatia.

Prof.EmmanuelHalaKwon-
Ndung*NasarawaState*
UniversityKeffiNigeria PMB1022Keffi,
NasarawaState.
Nigeria.

Dr.CyrusAzimi
DepartmentofGenetics,CancerResearchCenter,
CancerInstitute,TehranUniversityofMedicalSciences,Kes
havarzBlvd.,
Tehran,Iran.

Dr.Gomez,NidiaNoemi
NationalUniversity ofSan Luis,
FacultyofChemistry,BiochemistryandPharmacy,
Laboratory ofMolecularBiochemistryEjercitodelos
Andes950-5700SanLuis
Argentina.

Prof.M.NageebRashed
ChemistryDepartment-FacultyofScience,Aswan
SouthValleyUniversity,
Egypt.

Dr.JohnW.Gichuki
KenyaMarine& FisheriesResearchInstitute,
Kenya.

Dr.WongLeongSing
DepartmentofCivilEngineering,C
ollegeofEngineering,UniversitiTe
nagaNasional,
Km7,JalanKajang-Puchong,
43009Kajang,SelangorDarulEhsan,M
alaysia.

Prof.XianyiLI
CollegeofMathematicsandComputationalScience
ShenzhenUniversity
Guangdong,518060
P.R.China.

Prof.MevlutDogan
KocatepeUniversity,ScienceFaculty,P
hysicsDept.Afyon/Turkey.
Turkey.

Prof.Kwai-LinThong
MicrobiologyDivision,Institut
eofBiologicalScience,
FacultyofScience,University
ofMalaya,50603,KualaLumpur,
Malaysia.

Prof.XiaocongHe
FacultyofMechanicalandElectricalEngineering,Ku
nming University
ofScienceandTechnology,253XueFuRoad,Kunmin
g,
P.R.China.

Prof.SanjayMisra
DepartmentofComputerEngineering
School ofInformationand CommunicationTechnology
FederalUniversityofTechnology,Minna,
Nigeria.

Prof.BurtramC.FieldingPr.Sci.Nat.*De*
partmentofMedicalBioSciencesUniver
sityoftheWesternCapePrivateBagX17
ModderdamRoad
Bellville,7535,
SouthAfrica.

Prof.NaqibUllahKhan
DepartmentofPlantBreedingandGenetics
NWFPAgriculturalUniversityPeshawar25130,P
akistan

EditorialBoard

Prof.AhmedM.Soliman
20MansourMohamedSt.,Apt51,Z amalek,Cairo, Egypt.

Prof.JuanJoséKasperZubillaga
Av.Universidad1953Ed.13depto304, MéxicoD.F.04340, México.

Prof.ChauKwok-wing
UniversityofQueensland

Prof.RajSenani
NetajiSubhasInstituteofTechnology, AzadHindFaujMarg,Sector3 , Dwarka,NewDelhi110075,In dia.

Prof.RobinJLaw
CefasBurnhamLaboratory, RemembranceAvenueBurnhamonCrouch,E ssexCM08HA, UK.

Prof.V.Sundarapandian
IndianInstitute ofInformation Technologyand Management-Kerala ParkCentre, TechnoparkCampus,KariavattomP.O., Thiruvananthapuram-695581,Kerala,India.

Prof.Tzung-PeiHong
DepartmentofElectricalEngineering, andattheDepartment ofComputerScienceand InformationEngineering NationalUniversity ofKaohsiung.

Prof.ZulfiqarAhmed
DepartmentofEarthSciences,box5070, Kfupm,dhahran-31261,SaudiArabia.

Prof.KhalifaSaif Al-Jabri
DepartmentofCivilandArchitecturalEngineering CollegeofEngineering,Sultan QaboosUniversity P.O.Box33,Al-Khod123,Muscat.

Prof.V.Sundarapandian
IndianInstitute ofInformationTechnology&Management-Kerala ParkCentre, Technopark,KariavattomP.O. Thiruvananthapuram-695581,KeralaIndia.

Prof.ThangaveluPerianan
DepartmentofMathematics,AditanarCollege,Ti ruchendur-628216India.

Prof.Yan-zePeng
DepartmentofMathematics, HuazhongUniversity ofScience and Technology,Wuhan430074,P.R. China.

Prof.KonstantinosD.Karamanos
UniversiteLibredeBruxelles, CP231Centre ofNonlinear Phenomena AndComplexsystems, CENOLIBoulevarddeTriomphe B-1050, Brussels,Belgium.

Prof.XianyiLI
SchoolofMathematicsandPhysics,Nanhu aUniversity,HengyangCity,HunanProvinc e, P.R.China.

Dr.K.W.Chau
HongKongPolytechnicUniversity DepartmentofCivil&StructuralEngineering,Ho ngKongPolytechnicUniversity,Hunghom,Kowl oon,HongKong, China.

Dr.AmadouGaye
LPAO-SF/ESPPoBox5085Dakar-FannSENEGAL UniversityCheikhAntaDiopDakarSE NEGAL.

Prof.MasnoGinting
P2F-LIPI,Puspiptek-Serpong, 15310IndonesianInstituteofSciences, Banten-Indonesia.

Dr.EzekielOlukayodeIdowu*Departme ntofAgriculturalEconomics,ObafemiAw olowoUniversity, Ife-Ife, Nigeria.*

Fees and Charges: Authors are required to pay a $550 handling fee. Publication of an article in the Scientific Research and Essays is not contingent upon the author's ability to pay the charges. Neither is acceptance to pay the handling fee a guarantee that the paper will be accepted for publication. Authors may still request (in advance) that the editorial office waive some of the handling fee under special circumstances.

Copyright:©2012,AcademicJournals.
All rights Reserved. In accessing this journal, you agree that you will access the contents for your own personal use But not for any commercial use. Any use and or copies of this Journal in whole or in part must include the customary bibliographic citation, including author attribution, date and article title.

Submissionofamanuscriptimplies:thattheworkdescribedhasnotbeenpublishedbefore(exceptintheformofan abstract oras part ofa publishedlecture,or thesis)that it is not underconsideration for publication elsewhere;that if andwhenthemanuscriptisacceptedforpublication,theauthorsagreetoautomatictransferofthecopyrighttothepublisher.

Disclaimer of Warranties

InnoeventshallAcademicJournalsbeliableforanyspecial,incidental,indirect,orconsequentialdamagesofanykindarising outofor in connection with the use ofthe articlesorothermaterial derivedfromtheSRE, whetherornotadvisedofthepossibilityofdamage,andonanytheoryofliability.
Thispublicationisprovided"asis"withoutwarrantyofanykind,eitherexpressedorimplied,including,butnot limitedto,theimpliedwarrantiesofmerchantability,fitnessforaparticularpurpose,ornon-infringement. Descriptionsof,or referencesto, productsorpublicationsdoes not implyendorsementofthatproductor publication. WhileeveryeffortismadebyAcademicJournalstoseethatnoinaccurateormisleadingdata,opinionorstatements appearinthispublication,theywishtomakeitclearthatthedataandopinionsappearinginthearticlesand advertisementshereinaretheresponsibilityofthecontributororadvertiserconcerned.AcademicJournalsmakesno warrantyofanykind,eitherexpressorimplied,regardingthequality,accuracy,availability,orvalidityofthedataorinformationi nthispublicationorofanyotherpublicationtowhich itmaybelinked.

ScientificResearchandEssays

Table of Contents: Volume 10 Number 3 15 February, 2015

ARTICLES

Research Articles

academicJournals

Vol. 10(3), pp. 86-96, 15 February, 2015
DOI: 10.5897/SRE2014.6159
Article Number:38A77C550344
ISSN 1992-2248
Copyright©2015
Author(s) retain the copyright of this article
http://www.academicjournals.org/SRE

Scientific Research and Essays

Full Length Research Paper

Exact solutions for the nonlinear KPP equation by using the Riccati equation method combined with the (G'/G)- expansion method

Elsayed M. E. Zayed* and Yasser A. Amer

Mathematics Department, Faculty of Sciences, Zagazig University, Zagazig, Egypt.

Received 15 January, 2015; Accepted 5 February, 2015.

The improved Riccati equation method combined with the improved (G'/G)- expansion method is an interesting approach to find more general exact solutions of the nonlinear evolution equations in mathematical physics. The objective of this article is to employ this method to construct exact solutions involving parameters of a nonlinear Kolmogorov-Petrovskii-Piskunov (KPP) equation. When these parameters are taken to be special values, the solitary wave solutions, the periodic wave solutions and the rational function solutions are derived from the exact solutions. The proposed method appears to be effective for solving other nonlinear evolution equations in the mathematical physics.

Key words: The Riccati equation method, the (G'/G)- expansion method, the nonlinear Kolmogorov-Petrovskii-Piskunov (KPP) equation, exact solutions, solitary wave solutions, periodic wave solutions, rational solutions.

PACS: 02.30.Jr, 05.45.Yv, 02.30.Ik.

INTRODUCTION

Many problems in the branches of modern physics are described in terms of suitable nonlinear models, and nonlinear physical phenomena are related to nonlinear differential equations, which are involved in many fields from physics to biology, chemistry, mechanics, and so on. Nonlinear wave phenomena are very important in nonlinear science, in recent years, much effort has been spent on the construction of exact solutions of nonlinear partial differential solutions. Many effective methods to construct the exact solutions of these equations have been established, such as, the inverse scattering transform method (Ablowitz and Clarkson, 1991), the Hirota method (Hirota, 1971), the truncated expansion method(Weiss et al., 1983), the Backlund transform method (Miura, 1979; Rogers and Shadwick, 1982), the exp-function method (He and Wu, 2006; Yusufoglu, 2008), the tanh- function method (Fan, 2000; Zhang and Xia, 2008), the Jacobi elliptic function method (Chen and Wang, 2005; Lu, 2005), the (G'/G)–expansion method (Wang and Zhang, 2008; Feng and Wan, 2011; Zayed

,*Corresponding author. E-mails: e.m.e.zayed@hotmail.com, yaser31270@yahoo.com
Author(s) agree that this article remain permanently open access under the terms of the Creative Commons Attribution License 4.0 International License

and Al-Joudi 2009; Zayed and Abdelaziz, 2010; Zayed and El-Malky, 2011), the modified simple equation (Jawad,et al .,2010; Zayed, 2011; Zayed and Hoda Ibrahim, 2012, Zayed and Hoda Ibrahim, 2014; Zayed and Arnous, 2012), the Riccati equation method (Zhu, 2008; Li and Zhang, 2010; Zayed and Arnous, 2013), the improved Riccati equation method (Li, 2012), the method of averaging (Leilei et al., 2014) and so on. The objective of this paper is to apply the improved Riccati equation method combined with the improved (G'/G) - expansion method to find the exact solutions of the following nonlinear Kolmogorov-Petrovskii-Piskunov (KPP) equation:

$$u_t - u_{xx} + \mu u + \gamma u^2 + \delta u^3 = 0, \quad (1)$$

Where μ, γ, δ are real constants. Equation (1) is important in the physical fields, and includes the Fisher equation, the Huxley equation, the Burgers- Huxley equation, the Chaffee-Infanfe equation and the Fitzhugh-Nagumo equation. Equation (1) has been investigated recently in (Feng and Wan, 2011) using the (G'/G)-expansion method and in (Zayed and Hoda Ibrahim, 2014) using the modified simple equation method. The rest of this paper is organized as follows: First is a description of the improved Riccati equation method combined with the improved (G'/G)- expansion method. Next is application of this method to solve the nonlinear KPP equation (1). Thereafter, the physical explanations of the obtained results are given, and conclusions are obtained.

Description of the Riccati equation method combined with the (G'/G)- expansion method

Suppose that we have the following nonlinear evolution equation:

$$F(u, u_t, u_x, u_{tt}, u_{xx}, ...) = 0, \quad (2)$$

Where *F* is a polynomial in *u*(*x*, *t*) and its partial derivatives, in which the highest order derivatives and the nonlinear terms, are involved. In the following, we give the main steps of the Riccati equation method combined with the (G'/G)- expansion method (Li, 2012):

Step 1. We use the traveling wave transformation

$$u(x,t) = u(\xi), \quad \xi = kx + \omega t, \quad (3)$$

Where k, ω are constants, to reduce Equation (1) to the following ordinary differential equation (ODE):

$$P(u, u', u'', ...) = 0, \quad (4)$$

Where P is a polynomial in $u(\xi)$ and its total derivatives, while the dashes denote the derivatives with respect to ξ.

Step 2. We assumes that Equation (4) has the formal solution:

$$u(\xi) = \sum_{i=-n}^{n} \alpha_i [f(\xi)]^i, \quad (5)$$

Where α_i $(i = -n, ..., n)$ are constants to be determined later $\alpha_n \neq 0$ *or* $\alpha_{-n} \neq 0$, while $f(\xi)$ satisfies the generalized Riccati equation:

$$f'(\xi) = p + rf(\xi) + qf^2(\xi), \quad (6)$$

Where *p, r* and *q* are real constants, such that $q \neq 0$ and $f(\xi)$ will be determined in the Step 4 below.

Step 3. The positive integer *n* in Equation (5) can be determined by balancing the highest-order derivatives with the nonlinear terms appearing in Equation (4).

Step 4. We determine the solutions $f(\xi)$ of Equation (6) using the improved (G'/G)-expansion method, by assuming that its formal solution has the form

$$f(\xi) = \sum_{i=-m}^{m} \beta_i \left(\frac{G'(\xi)}{G(\xi)} \right)^i, \quad (7)$$

Where β_i $(i = -m, ..., m)$ are constants to be determined later $\beta_m \neq 0$ *or* $\beta_{-m} \neq 0$, and $G(\xi)$ satisfies the following linear ODE:

$$G''(\xi) + \lambda G'(\xi) + \mu G(\xi) = 0, \quad (8)$$

Where λ and μ are constants.

Step 5. The positive integer *m* in Equation (7) can be determined by balancing $f'(\xi)$ and $f^2(\xi)$ in Equation (6) to get $m = 1$. Thus, the solution (7) reduces to.

$$f(\xi) = \beta_0 + \beta_1 \left[\frac{G'(\xi)}{G(\xi)} \right] + \beta_{-1} \left[\frac{G'(\xi)}{G(\xi)} \right]^{-1}, \quad (9)$$

Where $\beta_0, \beta_1, \beta_{-1}$ are constants to be determined,such that $\beta_1 \neq 0$ *or* $\beta_{-1} \neq 0$. Substituting Equation (9) along

with Equation (8) into Equation (6) and equating all the coefficients of powers of $\left(\frac{G'}{G}\right)$ to zero, yields a set of algebraic equations, which can be solved to get the following two cases:

Case 1

$$\beta_0 = \frac{-(\lambda + r)}{2q},\ \beta_1 = \frac{-1}{q},\ \beta_{-1} = 0,\ p = \frac{r^2 - \lambda^2 + 4\mu}{4q},\ q \neq 0.$$

In this case, the solution of Equation (6) has the form

$$f(\xi) = \frac{-(\lambda + r)}{2q} - \frac{1}{q}\left[\frac{G'(\xi)}{G(\xi)}\right]. \quad (10)$$

Case 2

$$\beta_0 = \frac{\lambda - r}{2q},\ \beta_1 = 0,\ \beta_{-1} = \frac{\mu}{q},\ p = \frac{r^2 - \lambda^2 + 4\mu}{4q},\ q \neq 0.$$

In this case, the solution of Equation (6) has the form

$$f(\xi) = \frac{\lambda - r}{2q} + \frac{\mu}{q}\left[\frac{G'(\xi)}{G(\xi)}\right]^{-1}. \quad (11)$$

From the Cases 1 and 2, we deduce that $\lambda^2 - 4\mu = r^2 - 4pq$. On solving Equation (8) we deduce that (G'/G) has the forms:

$$\frac{G'(\xi)}{G(\xi)} = \begin{cases} -\frac{\lambda}{2} + \frac{\sqrt{r^2 - 4pq}}{2}\left[\frac{c_1 \sinh\left(\frac{\xi}{2}\sqrt{r^2 - 4pq}\right) + c_2 \cosh\left(\frac{\xi}{2}\sqrt{r^2 - 4pq}\right)}{c_1 \cosh\left(\frac{\xi}{2}\sqrt{r^2 - 4pq}\right) + c_2 \sinh\left(\frac{\xi}{2}\sqrt{r^2 - 4pq}\right)}\right] & \text{if } r^2 - 4pq > 0 \quad (12) \\ -\frac{\lambda}{2} + \frac{\sqrt{4pq - r^2}}{2}\left[\frac{-c_1 \sin\left(\frac{\xi}{2}\sqrt{4pq - r^2}\right) + c_2 \cos\left(\frac{\xi}{2}\sqrt{4pq - r^2}\right)}{c_1 \cos\left(\frac{\xi}{2}\sqrt{4pq - r^2}\right) + c_2 \sin\left(\frac{\xi}{2}\sqrt{4pq - r^2}\right)}\right] & \text{if } r^2 - 4pq < 0 \quad (13) \\ -\frac{\lambda}{2} + \frac{c_2}{c_1 + c_2 \xi} & \text{if } r^2 - 4pq = 0 \quad (14) \end{cases}$$

Where c_1 and c_2 are arbitrary constants.

Step 6. Substituting Equation (5) along Equation (6) into Equation (4) and equating the coefficients of all powers of $f(\xi)$ to zero, we obtain a system of algebraic equations, which can be solved using the Maple or Mathematica to get the values of α_i, k and ω.\

Step 7. Substituting the values of α_i, k and ω as well as the solutions $f(\xi)$ given by Equation (10) or Equation (11) into Equation (5), we finally obtain the exact solutions of Equation (2) for the both Cases 1 and 2.

An application

Here we apply the proposed method just described to construct the exact solutions of the nonlinear KPP Equation (1). To the end, we use the wave transformation (3) to reduce Equation (1) to the following ODE:

$$\omega u'(\xi) - k^2 u''(\xi) + \mu u(\xi) + \gamma u^2(\xi) + \delta u^3(\xi) = 0. \quad (15)$$

By balancing u'' with u^3, we have $n = 1$. Consequently, we have the formal solution

$$u(\xi) = \alpha_0 + \alpha_1 f(\xi) + \alpha_{-1} f^{-1}(\xi), \quad (16)$$

Where $\alpha_0, \alpha_1, \alpha_{-1}$ are parameters to be determined later, such that $\alpha_{-1} \neq 0$ or $\alpha_1 \neq 0$.

Substituting Equation (16) along with Equation (6) into Equation (15) and equating the coefficients of all powers of $f(\xi)$ to zero, we get the following system of algebraic equations:

$$\begin{aligned}
f^3: &\quad -2k^2\alpha_1 q^2 + \delta\alpha_1^3 = 0, \\
f^2: &\quad \alpha_1 q\omega - 3\alpha_1 rqk^2 + \gamma\alpha_1^2 + 3\delta\alpha_0\alpha_1^2 = 0, \\
f: &\quad \omega\alpha_1 r - k^2(\alpha_1 r^2 + 2\alpha_1 pq) + \mu\alpha_1 + 2\gamma\alpha_0\alpha_1 + \delta(3\alpha_0^2\alpha_1 + 3\alpha_1^2\alpha_{-1}) = 0, \\
f^0: &\quad \omega(\alpha_1 p - \alpha_{-1} q) - k^2(\alpha_1 rp + r\alpha_{-1} q) + \mu\alpha_0 + \gamma(\alpha_0^2 + 2\alpha_1\alpha_{-1}) + \delta(\alpha_0^3 + 6\alpha_0\alpha_1\alpha_{-1}) = 0, \\
f^{-3}: &\quad -2k^2\alpha_{-1} p^2 + \delta\alpha_{-1}^3 = 0, \\
f^{-2}: &\quad -\alpha_{-1} p\omega - 3\alpha_{-1} rpk^2 + \gamma\alpha_{-1}^2 + 3\delta\alpha_0\alpha_{-1}^2 = 0, \\
f^{-1}: &\quad -\omega\alpha_{-1} r - k^2(\alpha_{-1} r^2 + 2\alpha_{-1} pq) + \mu\alpha_{-1} + 2\gamma\alpha_0\alpha_{-1} + \delta(3\alpha_0^2\alpha_{-1} + 3\alpha_{-1}^2\alpha_1) = 0.
\end{aligned}$$

By solving the above algebraic equations with the aid of Maple or Mathematical, we have the following results:

Result 1

$$\omega = \frac{\mu - k^2(r^2 - 4pq)}{\sqrt{r^2 - 4pq}},$$

$$\gamma = \frac{\left(2k^2(r^2 - 4pq) + \mu\right)\left((r^2 - 4pq) + r\sqrt{r^2 - 4pq}\right)\left((r^2 - 2pq) - r\sqrt{r^2 - 4pq}\right)}{4pq(r^2 - 4pq)\alpha_0},$$

$$\alpha_1 = 0,\ \delta = \frac{k^2\left((r^2 - 2pq) - r\sqrt{r^2 - 4pq}\right)}{\alpha_0^2}, \alpha_{-1} = \alpha_0\left(\frac{r + \sqrt{r^2 - 4pq}}{2q}\right).$$

provided that $r^2 - 4pq > 0$.

Now, the solution for the result 1 becomes

$$u(\xi)=\alpha_0+\alpha_0\left(\frac{r+\sqrt{r^2-4pq}}{2q}\right)f^{-1}(\xi), \tag{17}$$

Where

$$\xi=kx+\left(\frac{\mu-k^2(r^2-4pq)}{\sqrt{r^2-4pq}}\right)t. \tag{18}$$

Substituting Equation (10) into Equation (17) and using Equations (12) to (14) we have the hyperbolic wave solutions of Equation (1) as follows:

$$u(\xi)=\alpha_0-\alpha_0\left(r+\sqrt{r^2-4pq}\right)\left\{r+\sqrt{r^2-4pq}\left[\frac{c_1\sinh\left(\frac{\xi}{2}\sqrt{r^2-4pq}\right)+c_2\cosh\left(\frac{\xi}{2}\sqrt{r^2-4pq}\right)}{c_1\cosh\left(\frac{\xi}{2}\sqrt{r^2-4pq}\right)+c_2\sinh\left(\frac{\xi}{2}\sqrt{r^2-4pq}\right)}\right]\right\}^{-1}. \tag{19}$$

Substituting the formulas (8), (10), (12) and (14) obtained by Peng (2009) into Equation (19), we have respectively the following exact solutions for Equation (1):

(i) If $|c_1|>|c_2|$, then

$$u_1(\xi)=\alpha_0-\alpha_0\left(r+\sqrt{r^2-4pq}\right)\left\{r+\sqrt{r^2-4pq}\tanh\left(\frac{\xi}{2}\sqrt{r^2-4pq}+\operatorname{sgn}(c_1c_2)\psi_1\right)\right\}^{-1} \tag{20}$$

Where $\psi_1=\tanh^{-1}\left(\frac{|c_2|}{|c_1|}\right)$.

(ii) If $|c_2|>|c_1|\neq 0,$ then

$$u_2(\xi)=\alpha_0-\alpha_0\left(r+\sqrt{r^2-4pq}\right)\left\{r+\sqrt{r^2-4pq}\coth\left(\frac{\xi}{2}\sqrt{r^2-4pq}+\operatorname{sgn}(c_1c_2)\psi_2\right)\right\}^{-1} \tag{21}$$

Where $\psi_2=\coth^{-1}\left(\frac{|c_2|}{|c_1|}\right)$.

(iii) If $|c_2|>|c_1|=0,$ then

$$u_3(\xi)=\alpha_0-\alpha_0\left(r+\sqrt{r^2-4pq}\right)\left\{r+\sqrt{r^2-4pq}\coth\left(\frac{\xi}{2}\sqrt{r^2-4pq}\right)\right\}^{-1}, \tag{22}$$

(iv) If $|c_1|=|c_2|,$ then we have the trivial solution which is rejected.

Substituting Equation (11) into Equation (17) and using Equations (12) to (14) we have the hyperbolic wave solutions of Equation (1) as follows:

$$u(\xi)=\alpha_0+\alpha_0\left(r+\sqrt{r^2-4pq}\right)\left\{\lambda-r+4\mu\left[-\lambda+\sqrt{r^2-4pq}\left(\frac{c_1\sinh\left(\frac{\xi}{2}\sqrt{r^2-4pq}\right)+c_2\cosh\left(\frac{\xi}{2}\sqrt{r^2-4pq}\right)}{c_1\cosh\left(\frac{\xi}{2}\sqrt{r^2-4pq}\right)+c_2\sinh\left(\frac{\xi}{2}\sqrt{r^2-4pq}\right)}\right)\right]^{-1}\right\}^{-1}. \tag{23}$$

Substituting the formulas (8), (10), (12) and (14) obtained by Peng (2009) into Equation (23), we have respectively the following exact solutions for Equation (1):

(i) If $|c_1|>|c_2|$, then

$$u_4(\xi)=\alpha_0+\alpha_0\left(r+\sqrt{r^2-4pq}\right)\left\{\lambda-r+4\mu\left[-\lambda+\sqrt{r^2-4pq}\tanh\left(\frac{\xi}{2}\sqrt{r^2-4pq}+\operatorname{sgn}(c_1c_2)\psi_1\right)\right]^{-1}\right\}^{-1} \tag{24}$$

Where $\psi_1=\tanh^{-1}\left(\frac{|c_2|}{|c_1|}\right)$.

(ii) If $|c_2|>|c_1|\neq 0,$ then

$$u_5(\xi)=\alpha_0+\alpha_0\left(r+\sqrt{r^2-4pq}\right)\left\{\lambda-r+4\mu\left[-\lambda+\sqrt{r^2-4pq}\coth\left(\frac{\xi}{2}\sqrt{r^2-4pq}+\operatorname{sgn}(c_1c_2)\psi_2\right)\right]^{-1}\right\}^{-1} \tag{25}$$

Where $\psi_2=\coth^{-1}\left(\frac{|c_2|}{|c_1|}\right)$.

(iii) If $|c_2|>|c_1|=0,$, then

$$u_6(\xi)=\alpha_0+\alpha_0\left(r+\sqrt{r^2-4pq}\right)\left\{\lambda-r+4\mu\left[-\lambda+\sqrt{r^2-4pq}\coth\left(\frac{\xi}{2}\sqrt{r^2-4pq}\right)\right]^{-1}\right\}^{-1}, \tag{26}$$

(iv) If $|c_2|=|c_1|,$ then

$$u_7(\xi)=\alpha_0+\alpha_0\left(r+\sqrt{r^2-4pq}\right)\left\{\lambda-r+4\mu\left[-\lambda+\sqrt{r^2-4pq}\right]^{-1}\right\}^{-1}. \tag{27}$$

Result 2. Consider

$$\omega=\frac{k^2(r^2-4pq)-\mu}{\sqrt{r^2-4pq}},$$

$$\gamma=\frac{\left(2k^2(r^2-4pq)+\mu\right)\left((r^2-4pq)+r\sqrt{r^2-4pq}\right)\left((r^2-2pq)-r\sqrt{r^2-4pq}\right)}{4pq(r^2-4pq)\alpha_0},$$

$$\alpha_{-1}=0,\ \delta=\frac{k^2\left((r^2-2pq)-r\sqrt{r^2-4pq}\right)}{\alpha_0^2},\ \alpha_1=\alpha_0\left(\frac{r+\sqrt{r^2-4pq}}{2q}\right).$$

Now, the solution for the result 2, becomes

$$u(\xi)=\alpha_0+\alpha_0\left(\frac{r+\sqrt{r^2-4pq}}{2q}\right)f(\xi), \tag{28}$$

Where $\xi=kx+\left(\frac{k^2(r^2-4pq)-\mu}{\sqrt{r^2-4pq}}\right)t.$

Substituting Equation (10) into Equation (28) and using Equations (12) to (14) we have the hyperbolic wave solutions of Equation (1) as follows:

$$u(\xi)=\alpha_0-\frac{\alpha_0}{4q^2}\left(r+\sqrt{r^2-4pq}\right)\left\{r+\sqrt{r^2-4pq}\left[\frac{c_1\sinh\left(\frac{\xi}{2}\sqrt{r^2-4pq}\right)+c_2\cosh\left(\frac{\xi}{2}\sqrt{r^2-4pq}\right)}{c_1\cosh\left(\frac{\xi}{2}\sqrt{r^2-4pq}\right)+c_2\sinh\left(\frac{\xi}{2}\sqrt{r^2-4pq}\right)}\right]\right\} \quad (29)$$

Substituting the formulas (8), (10), (12) and (14) obtained by Peng (2009) into Equation (29), we have respectively the following exact solutions for Equation (1):

(i) If $|c_1|>|c_2|$, then

$$u_8(\xi)=\alpha_0-\frac{\alpha_0}{4q^2}\left(r+\sqrt{r^2-4pq}\right)\left\{r+\sqrt{r^2-4pq}\tanh\left(\frac{\xi}{2}\sqrt{r^2-4pq}+\operatorname{sgn}(c_1c_2)\psi_1\right)\right\}, \quad (30)$$

Where $\psi_1=\tanh^{-1}\left(\frac{|c_2|}{|c_1|}\right)$.

(ii) If $|c_2|>|c_1|\neq 0$, then

$$u_9(\xi)=\alpha_0-\frac{\alpha_0}{4q^2}\left(r+\sqrt{r^2-4pq}\right)\left\{r+\sqrt{r^2-4pq}\coth\left(\frac{\xi}{2}\sqrt{r^2-4pq}+\operatorname{sgn}(c_1c_2)\psi_2\right)\right\}, \quad (31)$$

Where $\psi_2=\coth^{-1}\left(\frac{|c_2|}{|c_1|}\right)$.

(iii) If $|c_2|>|c_1|=0$, then

$$u_{10}(\xi)=\alpha_0-\frac{\alpha_0}{4q^2}\left(r+\sqrt{r^2-4pq}\right)\left\{r+\sqrt{r^2-4pq}\coth\left(\frac{\xi}{2}\sqrt{r^2-4pq}\right)\right\}, \quad (32)$$

(iv) If $|c_2|=|c_1|$, then

$$u_{11}(\xi)=\alpha_0-\frac{\alpha_0}{4q^2}\left(r+\sqrt{r^2-4pq}\right)^2, \quad (33)$$

Substituting Equation (11) into Equation (28) and using Equation (12) to (14) we have the hyperbolic wave solutions of Equation (1) as follows:

$$u(\xi)=\alpha_0+\frac{\alpha_0}{4q^2}\left(r+\sqrt{r^2-4pq}\right)\left\{\lambda-r+4\mu\left[-\lambda+\sqrt{r^2-4pq}\left(\frac{c_1\sinh\left(\frac{\xi}{2}\sqrt{r^2-4pq}\right)+c_2\cosh\left(\frac{\xi}{2}\sqrt{r^2-4pq}\right)}{c_1\cosh\left(\frac{\xi}{2}\sqrt{r^2-4pq}\right)+c_2\sinh\left(\frac{\xi}{2}\sqrt{r^2-4pq}\right)}\right)\right]^{-1}\right\} \quad (34)$$

Substituting the formulas (8), (10), (12) and (14) obtained by Peng (2009) into Equation (34), we have respectively the following exact solutions for Equation (1):

(i) If $|c_1|>|c_2|$, then

$$u_{12}(\xi)=\alpha_0+\frac{\alpha_0}{4q^2}\left(r+\sqrt{r^2-4pq}\right)\left\{\lambda-r+4\mu\left[-\lambda+\sqrt{r^2-4pq}\tanh\left(\frac{\xi}{2}\sqrt{r^2-4pq}+\operatorname{sgn}(c_1c_2)\psi_1\right)\right]^{-1}\right\} \quad (35)$$

Where $\psi_1=\tanh^{-1}\left(\frac{|c_2|}{|c_1|}\right)$.

(ii) If $|c_2|>|c_1|\neq 0$, then

$$u_{13}(\xi)=\alpha_0+\frac{\alpha_0}{4q^2}\left(r+\sqrt{r^2-4pq}\right)\left\{\lambda-r+4\mu\left[-\lambda+\sqrt{r^2-4pq}\coth\left(\frac{\xi}{2}\sqrt{r^2-4pq}+\operatorname{sgn}(c_1c_2)\psi_2\right)\right]^{-1}\right\} \quad (36)$$

Where $\psi_2=\coth^{-1}\left(\frac{|c_2|}{|c_1|}\right)$.

(iii) If $|c_2|>|c_1|=0$, then

$$u_{14}(\xi)=\alpha_0+\frac{\alpha_0}{4q^2}\left(r+\sqrt{r^2-4pq}\right)\left\{\lambda-r+4\mu\left[-\lambda+\sqrt{r^2-4pq}\coth\left(\frac{\xi}{2}\sqrt{r^2-4pq}\right)\right]^{-1}\right\} \quad (37)$$

(iv) If $|c_2|=|c_1|$, then

$$u_{15}(\xi)=\alpha_0+\frac{\alpha_0}{4q^2}\left(r+\sqrt{r^2-4pq}\right)\left\{\lambda-r+4\mu\left[-\lambda+\sqrt{r^2-4pq}\right]^{-1}\right\} \quad (38)$$

Result 3. Consider

$$\omega=\pm k\sqrt{k^2(r^2-4pq)+2\mu},$$

$$\gamma=\frac{\left(k^2(r^2-2pq)+\mu+rk\sqrt{k^2(r^2-4pq)+2\mu}\right)\left(k^2(r^2-4pq)+2\mu-rk\sqrt{k^2(r^2-4pq)+2\mu}\right)}{p\alpha_0^2\left(2k^2pq-\mu\right)},$$

$$\alpha_{-1}=0,\ \delta=\frac{k^2(r^2-2pq)+\mu\pm rk\sqrt{k^2(r^2-4pq)+2\mu}}{\alpha_0^2},$$

$$\alpha_{-1}=\frac{kp\alpha_0\left(kr\mp\sqrt{k^2(r^2-4pq)+2\mu}\right)}{2k^2pq-\mu}.$$

Now, the solution for the result 3 becomes

$$u(\xi)=\alpha_0+\frac{kp\alpha_0\left(kr\mp\sqrt{k^2(r^2-4pq)+2\mu}\right)}{2k^2pq-\mu}f^{-1}(\xi) \quad (39)$$

Where

$$\xi=kx\pm k\sqrt{k^2(r^2-4pq)+2\mu}\,t, \quad \text{and}$$

$$k^2(r^2-4pq)+2\mu\geq 0. \quad (40)$$

Substituting Equation (10) into Equation (39) and using Equations (12) to (14) we have the exact solutions of Equation (1) as follows:

If $r^2-4pq>0$, we have the hyperbolic wave solutions

$$u(\xi)=\alpha_0-\frac{kp\alpha_0\left(kr\mp\sqrt{k^2(r^2-4pq)+2\mu}\right)}{2k^2pq-\mu}\left\{\frac{r}{2q}+\frac{\sqrt{r^2-4pq}}{2q}\left[\frac{c_1\sinh\left(\frac{\xi}{2}\sqrt{r^2-4pq}\right)+c_2\cosh\left(\frac{\xi}{2}\sqrt{r^2-4pq}\right)}{c_1\cosh\left(\frac{\xi}{2}\sqrt{r^2-4pq}\right)+c_2\sinh\left(\frac{\xi}{2}\sqrt{r^2-4pq}\right)}\right]\right\}^{-1} \quad (41)$$

Substituting the formulas (8), (10), (12) and (14) obtained by Peng (2009) into Equation (41), we have respectively the following exact solutions for Equation (1):

(i) If $|c_1| > |c_2|$, then

$$u_{16}(\xi) = \alpha_0 - \frac{kp\alpha_0\left(kr \mp \sqrt{k^2(r^2-4pq)+2\mu}\right)}{2k^2pq-\mu}\left\{\frac{r}{2q} + \frac{\sqrt{r^2-4pq}}{2q}\tanh\left(\frac{\xi}{2}\sqrt{r^2-4pq} + \mathrm{sgn}(c_1c_2)\psi_1\right)\right\}^{-1} \quad (42)$$

Where $\psi_1 = \tanh^{-1}\left(\frac{|c_2|}{|c_1|}\right)$.

(ii) If $|c_2| > |c_1| \neq 0$, then

$$u_{17}(\xi) = \alpha_0 - \frac{kp\alpha_0\left(kr \mp \sqrt{k^2(r^2-4pq)+2\mu}\right)}{2k^2pq-\mu}\left\{\frac{r}{2q} + \frac{\sqrt{r^2-4pq}}{2q}\coth\left(\frac{\xi}{2}\sqrt{r^2-4pq} + \mathrm{sgn}(c_1c_2)\psi_2\right)\right\}^{-1} \quad (43)$$

Where $\psi_2 = \coth^{-1}\left(\frac{|c_2|}{|c_1|}\right)$.

(iii) If $|c_2| > |c_1| = 0$, then

$$u_{18}(\xi) = \alpha_0 - \frac{kp\alpha_0\left(kr \mp \sqrt{k^2(r^2-4pq)+2\mu}\right)}{2k^2pq-\mu}\left\{\frac{r}{2q} + \frac{\sqrt{r^2-4pq}}{2q}\coth\left(\frac{\xi}{2}\sqrt{r^2-4pq}\right)\right\}^{-1}. \quad (44)$$

(iv) If $|c_2| = |c_1|$, then

$$u_{19}(\xi) = \alpha_0 - \frac{kp\alpha_0\left(kr \mp \sqrt{k^2(r^2-4pq)+2\mu}\right)}{2k^2pq-\mu}\left\{\frac{r}{2q} + \frac{\sqrt{r^2-4pq}}{2q}\right\}^{-1}. \quad (45)$$

If $r^2 - 4pq < 0$, we have the trigonometric wave solutions

$$u(\xi) = \alpha_0 - \frac{kp\alpha_0\left(kr \mp \sqrt{k^2(r^2-4pq)+2\mu}\right)}{2k^2pq-\mu}\left\{\frac{r}{2q} + \frac{\sqrt{4pq-r^2}}{2q}\left[\frac{-c_1\sin\left(\frac{\xi}{2}\sqrt{4pq-r^2}\right)+c_2\cos\left(\frac{\xi}{2}\sqrt{4pq-r^2}\right)}{c_1\cos\left(\frac{\xi}{2}\sqrt{4pq-r^2}\right)+c_2\sin\left(\frac{\xi}{2}\sqrt{4pq-r^2}\right)}\right]\right\}^{-1} \quad (46)$$

Now, we can simplify Equation (46) to get the following periodic wave solutions:

$$u_{20}(\xi) = \alpha_0 - \frac{kp\alpha_0\left(kr \mp \sqrt{k^2(r^2-4pq)+2\mu}\right)}{2k^2pq-\mu}\left\{\frac{r}{2q} + \frac{\sqrt{4pq-r^2}}{2q}\tan\left(\xi_1 - \frac{\xi}{2}\sqrt{4pq-r^2}\right)\right\}^{-1}, \quad (47)$$

Where $\xi_1 = \tan^{-1}\left(\frac{c_2}{c_1}\right)$,

and

$$u_{21}(\xi) = \alpha_0 - \frac{kp\alpha_0\left(kr \mp \sqrt{k^2(r^2-4pq)+2\mu}\right)}{2k^2pq-\mu}\left\{\frac{r}{2q} + \frac{\sqrt{4pq-r^2}}{2q}\cot\left(\xi_2 + \frac{\xi}{2}\sqrt{4pq-r^2}\right)\right\}^{-1} \quad (48)$$

Where $\xi_2 = \cot^{-1}\left(\frac{c_2}{c_1}\right)$.

If $r^2 - 4pq = 0$, we have the rational wave solutions

$$u_{22}(\xi) = \alpha_0 - \frac{kp\alpha_0\left(kr \mp \sqrt{2\mu}\right)}{2k^2pq-\mu}\left\{\frac{r}{2q} + \frac{1}{q}\left(\frac{c_2}{c_1 + c_2\xi}\right)\right\}^{-1}, \quad (49)$$

Where c_1, c_2 are arbitrary constants.

Substituting Equation (11) into Equation (39) and using Equations (12) to (14) we have the exact solutions of Equation (1) as follows:

If $r^2 - 4pq > 0$, we have the hyperbolic wave solutions

$$u(\xi) = \alpha_0 + \frac{kp\alpha_0\left(kr \mp \sqrt{k^2(r^2-4pq)+2\mu}\right)}{2k^2pq-\mu}\left\{\frac{\lambda-r}{2q} + \frac{\mu}{q}\left[-\frac{\lambda}{2} + \frac{\sqrt{r^2-4pq}}{2}\left(\frac{c_1\sinh\left(\frac{\xi}{2}\sqrt{r^2-4pq}\right)+c_2\cosh\left(\frac{\xi}{2}\sqrt{r^2-4pq}\right)}{c_1\cosh\left(\frac{\xi}{2}\sqrt{r^2-4pq}\right)+c_2\sinh\left(\frac{\xi}{2}\sqrt{r^2-4pq}\right)}\right)\right]^{-1}\right\}^{-1} \quad (50)$$

Substituting the formulas (8), (10), (12) and (14) obtained by Peng (2009) into Equation (50), we have respectively the following exact solutions for Equation (1):

(i) If $|c_1| > |c_2|$, then

$$u_{23}(\xi) = \alpha_0 + \frac{kp\alpha_0\left(kr \mp \sqrt{k^2(r^2-4pq)+2\mu}\right)}{2k^2pq-\mu}\left\{\frac{\lambda-r}{2q} + \frac{\mu}{q}\left[-\frac{\lambda}{2} + \frac{\sqrt{r^2-4pq}}{2}\tanh\left(\frac{\xi}{2}\sqrt{r^2-4pq} + \mathrm{sgn}(c_1c_2)\psi_1\right)\right]^{-1}\right\}^{-1} \quad (51)$$

Where $\psi_1 = \tanh^{-1}\left(\frac{|c_2|}{|c_1|}\right)$.

(ii) If $|c_2| > |c_1| \neq 0$, then

$$u_{24}(\xi) = \alpha_0 + \frac{kp\alpha_0\left(kr \mp \sqrt{k^2(r^2-4pq)+2\mu}\right)}{2k^2pq-\mu}\left\{\frac{\lambda-r}{2q} + \frac{\mu}{q}\left[-\frac{\lambda}{2} + \frac{\sqrt{r^2-4pq}}{2}\coth\left(\frac{\xi}{2}\sqrt{r^2-4pq} + \mathrm{sgn}(c_1c_2)\psi_2\right)\right]^{-1}\right\}^{-1}, \quad (52)$$

Where $\psi_2 = \coth^{-1}\left(\frac{|c_2|}{|c_1|}\right)$.

(iii) If $|c_2| > |c_1| = 0$, then

$$u_{25}(\xi) = \alpha_0 + \frac{kp\alpha_0\left(kr \mp \sqrt{k^2(r^2-4pq)+2\mu}\right)}{2k^2pq-\mu}\left\{\frac{\lambda-r}{2q} + \frac{\mu}{q}\left[-\frac{\lambda}{2} + \frac{\sqrt{r^2-4pq}}{2}\coth\left(\frac{\xi}{2}\sqrt{r^2-4pq}\right)\right]^{-1}\right\}^{-1} \quad (53)$$

(iv) If $|c_2| = |c_1|$, then

$$u_{26}(\xi) = \alpha_0 + \frac{kp\alpha_0\left(kr \mp \sqrt{k^2(r^2-4pq)+2\mu}\right)}{2k^2pq-\mu}\left\{\frac{\lambda-r}{2q} + \frac{\mu}{q}\left[-\frac{\lambda}{2} + \frac{\sqrt{r^2-4pq}}{2}\right]^{-1}\right\}^{-1} \quad (54)$$

If $r^2 - 4pq < 0$, we have the trigonometric wave solutions

$$u(\xi)=\alpha_0+\frac{kp\alpha_0\left(kr\mp\sqrt{k^2(r^2-4pq)+2\mu}\right)}{2k^2pq-\mu}\left\{\frac{\lambda-r}{2q}+\frac{\mu}{q}\left[-\frac{\lambda}{2}+\frac{\sqrt{4pq-r^2}}{2}\left(\frac{-c_1\sin\left(\frac{\xi}{2}\sqrt{4pq-r^2}\right)+c_2\cos\left(\frac{\xi}{2}\sqrt{4pq-r^2}\right)}{c_1\cos\left(\frac{\xi}{2}\sqrt{4pq-r^2}\right)+c_2\sin\left(\frac{\xi}{2}\sqrt{4pq-r^2}\right)}\right)\right]\right\}^{-1} \quad (55)$$

Now, we can simplify Equation (55) to get the following periodic wave solutions:

$$u_{27}(\xi)=\alpha_0+\frac{kp\alpha_0\left(kr\mp\sqrt{k^2(r^2-4pq)+2\mu}\right)}{2k^2pq-\mu}\left\{\frac{\lambda-r}{2q}+\frac{\mu}{q}\left[-\frac{\lambda}{2}+\frac{\sqrt{4pq-r^2}}{2}\tan\left(\xi_1-\frac{\xi}{2}\sqrt{4pq-r^2}\right)\right]^{-1}\right\}^{-1} \quad (56)$$

Where $\xi_1=\tan^{-1}\left(\frac{c_2}{c_1}\right)$,

and

$$u_{28}(\xi)=\alpha_0+\frac{kp\alpha_0\left(kr\mp\sqrt{k^2(r^2-4pq)+2\mu}\right)}{2k^2pq-\mu}\left\{\frac{\lambda-r}{2q}+\frac{\mu}{q}\left[-\frac{\lambda}{2}+\frac{\sqrt{4pq-r^2}}{2}\cot\left(\xi_2+\frac{\xi}{2}\sqrt{4pq-r^2}\right)\right]^{-1}\right\}^{-1}, \quad (57)$$

Where $\xi_2=\cot^{-1}\left(\frac{c_2}{c_1}\right)$.

If $r^2-4pq=0$, we have the rational wave solutions

$$u_{29}(\xi)=\alpha_0+\frac{kp\alpha_0\left(kr\mp\sqrt{2\mu}\right)}{2k^2pq-\mu}\left\{\frac{\lambda-r}{2q}+\frac{\mu}{q}\left(\frac{-\lambda}{2}+\frac{c_2}{c_1+c_2\xi}\right)^{-1}\right\}^{-1}, \quad (58)$$

Where c_1, c_2 are arbitrary constants.

Result 4. Consider

$$\omega=\pm k\sqrt{k^2(r^2-4pq)+2\mu},$$

$$\gamma=\frac{\left(k^2(r^2-2pq)+\mu+rk\sqrt{k^2(r^2-4pq)+2\mu}\right)\left(k^2(r^2-4pq)+2\mu-rk\sqrt{k^2(r^2-4pq)+2\mu}\right)}{q\alpha_0^2\left(2k^2pq-\mu\right)},$$

$$\alpha_{-1}=0,\delta=\frac{k^2(r^2-2pq)+\mu\pm rk\sqrt{k^2(r^2-4pq)+2\mu}}{\alpha_0^2},\alpha_1=\frac{kq\alpha_0\left(kr\pm\sqrt{k^2(r^2-4pq)+2\mu}\right)}{2k^2pq-\mu}.$$

Now, the solution for the result 4 becomes

$$u(\xi)=\alpha_0+\frac{kq\alpha_0\left(kr\pm\sqrt{k^2(r^2-4pq)+2\mu}\right)}{2k^2pq-\mu}f(\xi) \quad (59)$$

Where $\xi=kx\pm k\sqrt{k^2(r^2-4pq)+2\mu}\,t$, and

$$k^2(r^2-4pq)+2\mu\geq 0. \quad (60)$$

Substituting Equation (10) into Equation (59) and using Equations (12) to(14) we have the exact solutions of Equation (1) as follows:

If $r^2-4pq>0$, we have the hyperbolic wave solutions

$$u(\xi)=\alpha_0-\frac{kq\alpha_0\left(kr\pm\sqrt{k^2(r^2-4pq)+2\mu}\right)}{2k^2pq-\mu}\left\{\frac{r}{2q}+\frac{\sqrt{r^2-4pq}}{2q}\left[\frac{c_1\sinh\left(\frac{\xi}{2}\sqrt{r^2-4pq}\right)+c_2\cosh\left(\frac{\xi}{2}\sqrt{r^2-4pq}\right)}{c_1\cosh\left(\frac{\xi}{2}\sqrt{r^2-4pq}\right)+c_2\sinh\left(\frac{\xi}{2}\sqrt{r^2-4pq}\right)}\right]\right\}^{-1} \quad (61)$$

Substituting the formulas (8), (10), (12) and (14) obtained by Peng (2009) into Equation (61), we have respectively the following exact solutions for Equation (1):

(i) If $|c_1|>|c_2|$, then

$$u_{30}(\xi)=\alpha_0-\frac{kq\alpha_0\left(kr\pm\sqrt{k^2(r^2-4pq)+2\mu}\right)}{2k^2pq-\mu}\left\{\frac{r}{2q}+\frac{\sqrt{r^2-4pq}}{2q}\tanh\left(\frac{\xi}{2}\sqrt{r^2-4pq}+\operatorname{sgn}(c_1c_2)\psi_1\right)\right\}^{-1} \quad (62)$$

Where $\psi_1=\tanh^{-1}\left(\frac{|c_2|}{|c_1|}\right)$.

(ii) If $|c_2|>|c_1|\neq 0$, then

$$u_{31}(\xi)=\alpha_0-\frac{kq\alpha_0\left(kr\pm\sqrt{k^2(r^2-4pq)+2\mu}\right)}{2k^2pq-\mu}\left\{\frac{r}{2q}+\frac{\sqrt{r^2-4pq}}{2q}\coth\left(\frac{\xi}{2}\sqrt{r^2-4pq}+\operatorname{sgn}(c_1c_2)\psi_2\right)\right\}^{-1} \quad (63)$$

Where $\psi_2=\coth^{-1}\left(\frac{|c_2|}{|c_1|}\right)$.

(iii) If $|c_2|>|c_1|=0$, then

$$u_{32}(\xi)=\alpha_0-\frac{kq\alpha_0\left(kr\pm\sqrt{k^2(r^2-4pq)+2\mu}\right)}{2k^2pq-\mu}\left\{\frac{r}{2q}+\frac{\sqrt{r^2-4pq}}{2q}\coth\left(\frac{\xi}{2}\sqrt{r^2-4pq}\right)\right\}^{-1}. \quad (64)$$

(iv) If $|c_2|=|c_1|$, then

$$u_{33}(\xi)=\alpha_0-\frac{kq\alpha_0\left(kr\pm\sqrt{k^2(r^2-4pq)+2\mu}\right)}{2k^2pq-\mu}\left\{\frac{r}{2q}\pm\frac{\sqrt{r^2-4pq}}{2q}\right\}^{-1}. \quad (65)$$

If $r^2-4pq<0$, we have the trigonometric wave solutions

$$u(\xi)=\alpha_0-\frac{kq\alpha_0\left(kr\pm\sqrt{k^2(r^2-4pq)+2\mu}\right)}{2k^2pq-\mu}\left\{\frac{r}{2q}+\frac{\sqrt{4pq-r^2}}{2q}\left[\frac{-c_1\sin\left(\frac{\xi}{2}\sqrt{4pq-r^2}\right)+c_2\cos\left(\frac{\xi}{2}\sqrt{4pq-r^2}\right)}{c_1\cos\left(\frac{\xi}{2}\sqrt{4pq-r^2}\right)+c_2\sin\left(\frac{\xi}{2}\sqrt{4pq-r^2}\right)}\right]\right\}^{-1} \quad (66)$$

Now, we can simplify Equation (66) to get the following periodic wave solution:

$$u_{34}(\xi)=\alpha_0-\frac{kq\alpha_0\left(kr\pm\sqrt{k^2(r^2-4pq)+2\mu}\right)}{2k^2pq-\mu}\left\{\frac{r}{2q}+\frac{\sqrt{4pq-r^2}}{2q}\tan\left(\xi_1-\frac{\xi}{2}\sqrt{4pq-r^2}\right)\right\}^{-1}, \quad (67)$$

Where $\xi_1=\tan^{-1}\left(\frac{c_2}{c_1}\right)$,

$$u_{35}(\xi)=\alpha_0-\frac{kq\alpha_0\left(kr\pm\sqrt{k^2(r^2-4pq)+2\mu}\right)}{2k^2pq-\mu}\left\{\frac{r}{2q}+\frac{\sqrt{4pq-r^2}}{2q}\cot\left(\xi_2+\tfrac{\xi}{2}\sqrt{4pq-r^2}\right)\right\}^{-1}, \quad (68)$$

Where $\xi_2=\cot^{-1}\left(\frac{c_2}{c_1}\right)$.

If $r^2-4pq=0$, we have the rational wave solutions

$$u_{36}(\xi)=\alpha_0-\frac{kq\alpha_0\left(kr\pm\sqrt{2\mu}\right)}{2k^2pq-\mu}\left\{\frac{r}{2q}+\frac{1}{q}\left(\frac{c_2}{c_1+c_2\xi}\right)\right\}^{-1}, \quad (69)$$

Where c_1, c_2 are arbitrary constants.

Substituting Equation (11) into Equation (59) and using Equations (12) to (14) we have the exact solutions of Equation (1) as follows:

If $r^2-4pq>0$, we have the hyperbolic wave solutions

$$u(\xi)=\alpha_0+\frac{kq\alpha_0\left(kr\pm\sqrt{k^2(r^2-4pq)+2\mu}\right)}{2k^2pq-\mu}\left\{\frac{\lambda-r}{2q}+\frac{\mu}{q}\left[-\frac{\lambda}{2}+\frac{\sqrt{r^2-4pq}}{2}\frac{c_1\sinh\left(\frac{\xi}{2}\sqrt{r^2-4pq}\right)+c_2\cosh\left(\frac{\xi}{2}\sqrt{r^2-4pq}\right)}{c_1\cosh\left(\frac{\xi}{2}\sqrt{r^2-4pq}\right)+c_2\sinh\left(\frac{\xi}{2}\sqrt{r^2-4pq}\right)}\right]^{-1}\right\}^{-1} \quad (70)$$

Substituting the formulas (8), (10), (12) and (14) obtained by Peng (2009) into Equation (70), we have respectively the following exact solutions for Equation (1):

(i) If $|c_1|>|c_2|$, then

$$u_{37}(\xi)=\alpha_0+\frac{kq\alpha_0\left(kr\pm\sqrt{k^2(r^2-4pq)+2\mu}\right)}{2k^2pq-\mu}\left\{\frac{\lambda-r}{2q}+\frac{\mu}{q}\left[-\frac{\lambda}{2}+\frac{\sqrt{r^2-4pq}}{2}\tanh\left(\frac{\xi}{2}\sqrt{r^2-4pq}+\operatorname{sgn}(c_1c_2)\psi_1\right)\right]^{-1}\right\}^{-1}, \quad (71)$$

Where $\psi_1=\tanh^{-1}\left(\frac{|c_2|}{|c_1|}\right)$.

(ii) If $|c_2|>|c_1|\neq 0$, then

$$u_{38}(\xi)=\alpha_0+\left(\frac{k^2pr\alpha_0\pm\alpha_0k\,p\sqrt{k^2(r^2-4pq)+2\mu}}{2k^2pq-\mu}\right)\left\{\frac{\lambda-r}{2q}+\frac{\mu}{q}\left[-\frac{\lambda}{2}+\frac{\sqrt{r^2-4pq}}{2}\coth\left(\frac{\xi}{2}\sqrt{r^2-4pq}+\operatorname{sgn}(c_1c_2)\psi_2\right)\right]^{-1}\right\}^{-1}, \quad (72)$$

Where $\psi_2=\coth^{-1}\left(\frac{|c_2|}{|c_1|}\right)$.

(iii) $|c_2|>|c_1|=0$, then

$$u_{39}(\xi)=\alpha_0+\left(\frac{k^2pr\alpha_0\pm\alpha_0k\,p\sqrt{k^2(r^2-4pq)+2\mu}}{2k^2pq-\mu}\right)\left\{\frac{\lambda-r}{2q}+\frac{\mu}{q}\left[-\frac{\lambda}{2}+\frac{\sqrt{r^2-4pq}}{2}\coth\left(\frac{\xi}{2}\sqrt{r^2-4pq}\right)\right]^{-1}\right\}^{-1} \quad (73)$$

(iv) $|c_2|=|c_1|$, then

$$u_{40}(\xi)=\alpha_0+\left(\frac{k^2pr\alpha_0\pm\alpha_0k\,p\sqrt{k^2(r^2-4pq)+2\mu}}{2k^2pq-\mu}\right)\left\{\frac{\lambda-r}{2q}+\frac{\mu}{q}\left[-\frac{\lambda}{2}+\frac{\sqrt{r^2-4pq}}{2}\right]^{-1}\right\}^{-1}, \quad (74)$$

If $r^2-4pq<0$, we have the trigonometric wave solutions

$$u(\xi)=\alpha_0+\frac{kq\alpha_0\left(kr\pm\sqrt{k^2(r^2-4pq)+2\mu}\right)}{2k^2pq-\mu}\left\{\frac{\lambda-r}{2q}+\frac{\mu}{q}\left[-\frac{\lambda}{2}+\frac{\sqrt{4pq-r^2}}{2}\frac{-c_1\sin\left(\frac{\xi}{2}\sqrt{4pq-r^2}\right)+c_2\cos\left(\frac{\xi}{2}\sqrt{4pq-r^2}\right)}{c_1\cos\left(\frac{\xi}{2}\sqrt{4pq-r^2}\right)+c_2\sin\left(\frac{\xi}{2}\sqrt{4pq-r^2}\right)}\right]^{-1}\right\}^{-1} \quad (75)$$

Now, we can simplify Equation (75) to get the following periodic wave solution:

$$u_{41}(\xi)=\alpha_0+\frac{kq\alpha_0\left(kr\pm\sqrt{k^2(r^2-4pq)+2\mu}\right)}{2k^2pq-\mu}\left\{\frac{\lambda-r}{2q}+\frac{\mu}{q}\left[-\frac{\lambda}{2}+\frac{\sqrt{4pq-r^2}}{2}\tan\left(\xi_1-\tfrac{\xi}{2}\sqrt{4pq-r^2}\right)\right]^{-1}\right\}^{-1}, \quad (76)$$

Where $\xi_1=\tan^{-1}\left(\frac{c_2}{c_1}\right)$,

$$u_{42}(\xi)=\alpha_0+\frac{kq\alpha_0\left(kr\pm\sqrt{k^2(r^2-4pq)+2\mu}\right)}{2k^2pq-\mu}\left\{\frac{\lambda-r}{2q}+\frac{\mu}{q}\left[-\frac{\lambda}{2}+\frac{\sqrt{4pq-r^2}}{2}\cot\left(\frac{\xi}{2}\sqrt{4pq-r^2}+\xi_2\right)\right]^{-1}\right\}^{-1}, \quad (77)$$

Where $\xi_2=\cot^{-1}\left(\frac{c_2}{c_1}\right)$.

If $r^2-4pq=0$, we have the rational wave solutions

$$u_{43}(\xi)=\alpha_0+\frac{kq\alpha_0\left(kr\pm\sqrt{2\mu}\right)}{2k^2pq-\mu}\left\{\frac{\lambda-r}{2q}+\frac{\mu}{q}\left(\frac{-\lambda}{2}+\frac{c_2}{c_1+c_2\xi}\right)^{-1}\right\}^{-1} \quad (78)$$

Where c_1, c_2 are arbitrary constants.

Physical explanations of our obtained solutions

Solitary, periodic and rational waves can be obtained from the exact solutions by setting particular values in its unknown parameters. Here, we have presented some graphs of solitary and periodic waves constructed by taking suitable values of involved unknown parameters to visualize the underlying mechanism of the original Equation (1). By using the mathematical software Maple, the plots of some obtained solutions have been shown in Figures 1 to 4. The obtained solutions of Equation (1) incorporate three types of explicit solutions, namely the hyperbolic, trigonometric and rational solutions.

Some conclusions

We have used the Riccati equation method combined

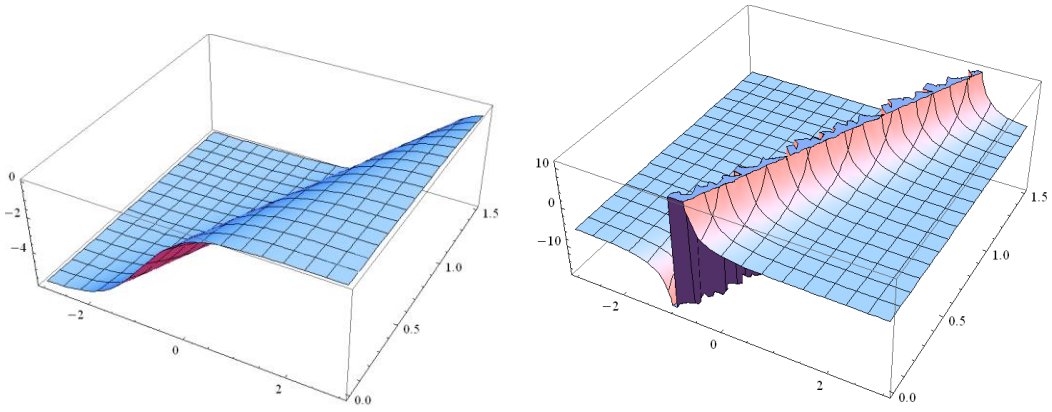

Figure 1. The plot of solutions u_1, u_2 with $\alpha_0 = p = q = k = \mu = 1, r = 3.$

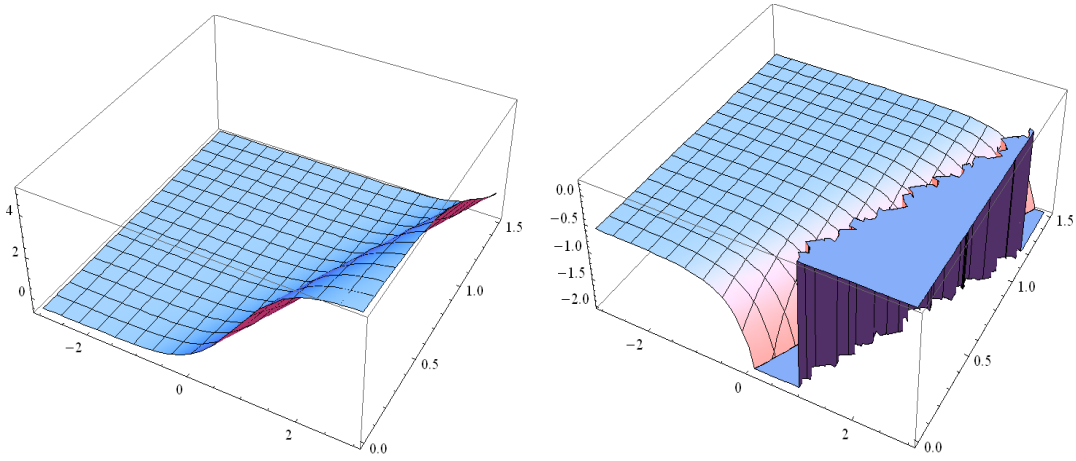

Figure 2. The plot of solutions u_4, u_5 with $\alpha_0 = p = q = k = \mu = \lambda = 1, r = 3.$

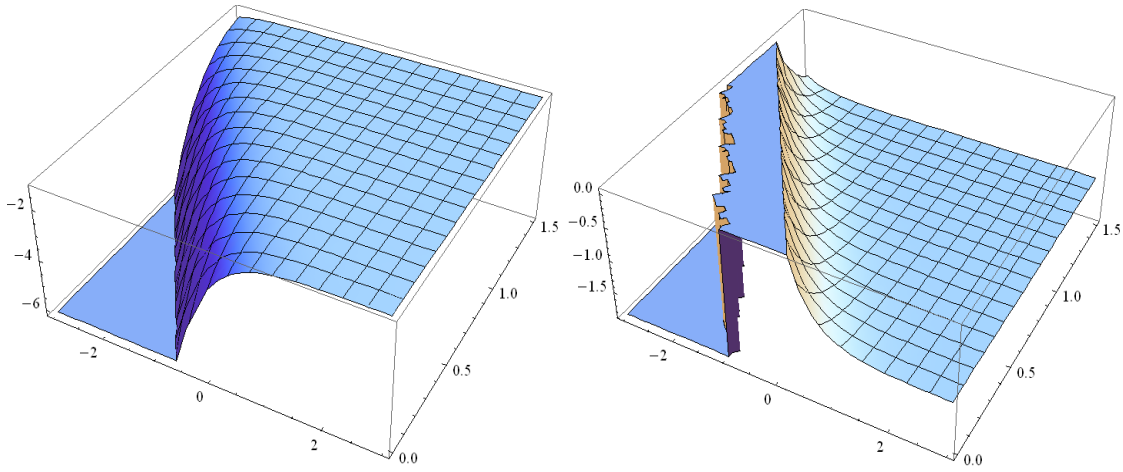

Figure 3. The plot of solutions u_{16}, u_{17} with $\alpha_0 = p = q = k = \mu = 1, r = 3.$

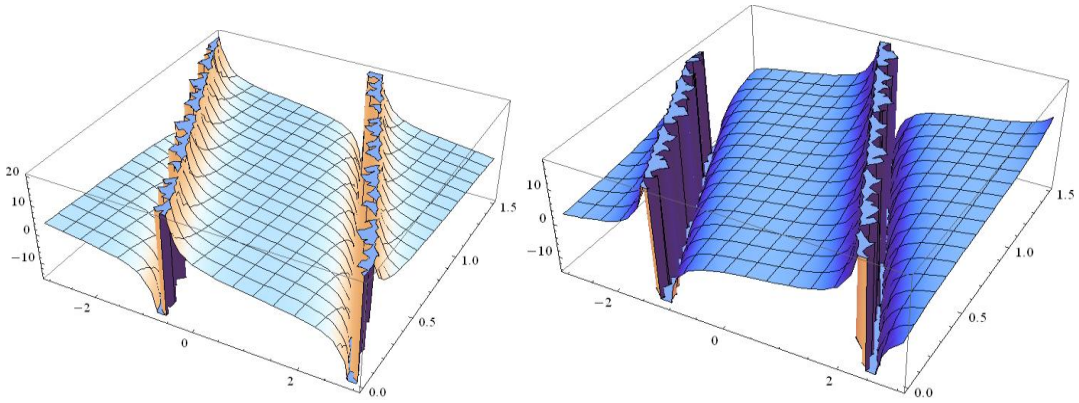

Figure 4. The plot of solutions u_{20}, u_{21} with $\alpha_0 = p = q = k = r = 1, \mu = 3.$

with the (G'/G)- expansion method to construct many new exact solutions of the nonlinear KPP Equation (1) involving parameters, which is expressed by the hyperbolic functions, the trigonometric functions and the rational functions. When the parameters are taken as special values the proposed method provides not only solitary wave solutions but also periodic wave solutions and rational wave solutions. These solutions will be of great importance for analyzing the nonlinear phenomena arising in applied physical sciences. This work shows that the proposed method is sufficient, effective and suitable for solving other nonlinear evolution equations in mathematical physics. Finally on comparing our results in this article with the results obtained in Feng et al. (2011) and Zayed and Hoda Ibrahim (2014), we conclude that our results are new and not reported elsewhere.

Conflict of Interest

The authors have not declared any conflict of interest.

ACKNOWLEDGMENT

The authors wish to thank the referees for their comments on this paper.

REFERENCES

Ablowitz MJ, Clarkson PA (1991). Solitons, nonlinear evolution equations and inverse scattering transform, Cambridge University Press New York, NY, USA.

Chen Y, Wang Q (2005). Extended Jacobi elliptic function rational expansion method and abundant families of Jacobi elliptic function solutions to(1+1)-dimensional dispersive long wave equation, Chaos, Solitons and Fractals, 24:745-757.

Fan E (2000). Extended tanh-function method and its applications to nonlinear equations Phys. Lett. A. 277:212-218.

Feng J, Li W, Wan Q (2011), Using $(G'/G$)-expansion method to seek the traveling wave solution of Kolmogorov-Petrovskii-Piskunov. Appl. Math. Comput. 217:5860-5865.

He JH, Wu XH (2006). Exp-function method for nonlinear wave equations. Chaos, Solitons Fractals 30:700-708.

Hirota R (1971). Exact solutions of the KdV equation for multiple collisions of solutions. Phys. Rev. Lett. 27:1192-1194.

Jawad AJM, Petkovic MD, Biswas A (2010). Modified simple equation method for nonlinear evolution equations. Appl. Math. Comput. 217:869-877.

Leilei J, Qihuai L, Ma Z (2014). A good approximation of modulated amplitude waves in Bose-Einstein condensates, Commun. Nonlinear Sci. Numer. Simula. 19:2715-2723.

Li X (2012). The improved Riccati equation method and exact solutions to mZK equation. Int. J. Differential equations, article ID 596762,11.

Li Z, Zhang X (2010). New exact kink solutions and periodic from solutions for a generalized Zakharov-Kuznetsov equation with varaible coefficients, Commun. Nonlinear Sci. Numer. Simul. 15:3418-3422.

Lu D (2005). Jacobi elliptic function solutions for two variant Boussinesq equations. Chaos, Solitons Fractals 24:1373–1385.

Miura MR (1979). Backlund transformation, Springer, Berlin, Germany.

Peng Z (2009). Comment on "Application of the (G'/G)-expansion method for nonlinear evolution equations [Phys. Lett. A, 372 (2008) 3400]," Commun. Theor. Phys. 52:206–208.

Rogers C, Shadwick WF (1982), Backlund Transformation and Their Applications, Vol. 161, Academec Press, New York, NY, USA.

Wang M, Li X, Zhang J (2008), The $(G'/G$)-expansion method and traveling wave solutions of nonlinear evolution equations in mathematical physics. Phys. Lett. A 372:417-423.

Weiss J, Tabor M, Carnevale G (1983). The Painlevé property for partial differential equations. J. Math. Phys. 24:552-526.

Yusufoglu E (2008). New solitary for the MBBM equations using Exp-function method. Phys. Lett. A 372:442-446.

Zayed EME (2011). A note on the modified simple equation method applied to Sharma-Tasso-Olver equation. Appl. Math. Comput., 218:3962-3964.

Zayed EME, Abdelaziz MAM (2010), Exact solutions for the generalized Zakharov-Kuznetsov equation with variable coefficients using the generalized $(G'/G$)-expansion method, AIP Conf. Proc. 1281:2216-2219.

Zayed EME, Al-Joudi S (2009). Applications of an improved $(G'/G$)-expansion method to nonlinear PDEs in mathematical physics, AIP Conf. Proc. 1168:371-376.

Zayed EME, Arnous AH (2012). Exact solutions of the nonlinear ZK-

MEW and the Potential YTSF equations using the modified simple equation method, AIP Conf. Proc. 1479: 2044-2048.
Zayed EME, Arnous AH (2013). Many Exact solutions for nonlinear dynamics of DNA model using the generalized Riccati equation mapping method, Sci. Res. Essays 8:340-346.
Zayed EME, EL-Malky MAS (2011). The (G'/G)-expansion method for solving nonlinear Klein-Gordon equations". AIP Conf. Proc. 1389:2020-2024.
Zayed EME, Hoda Ibrahim SA (2012). Exact solutions of nonlinear evolution equations in mathematical physcis using the modified simple equation method. Chin. Phys. Lett. 29:060201-060204.
Zayed EME, Hoda Ibrahim SA (2014). Exact Solutions of equation using the modified simple equation method, Kolmogorov-Petrovskii-Piskunov. Acta Math. Appl. Sinica, English Series 30:749-754.
Zhang S, Xia T (2008). A further improved tanh- function method exactly solving the (2+1) - dimensional dispersive long wave equations. Appl. Math. E-Notes 8:58-66.
Zhu SD (2008). The generalized Riccati equation mapping method in nonlinear evolution equation: application to (2+1)-dimensional Boiti-lion-Pempinelle equation. Chaos, Solitons Fractals 37:1335–1342.

academicJournals

Vol. 10(3), pp. 97-104, 15 February, 2015
DOI: 10.5897/SRE2014.6130
Article Number:6454B9650348
ISSN 1992-2248
Copyright©2015
Author(s) retain the copyright of this article
http://www.academicjournals.org/SRE

Scientific Research and Essays

Full Length Research Paper

Effects of a *Tabebuia avellanedae* extract and lapachol on the labeling of blood constituents with technetium-99m

Ana Cristina da Silva Braga[1], Maria Luisa Gomes[1], Joelma Fonseca de Oliveira Fernandes[1], Nasser Ribeiro Asad[1], Sebastião David Santos-Filho[1], Carlos Alberto Sampaio Guimarães[1], Eric Heleno Freire Ferreira Frederico[1,2]* and Mario Bernardo-Filho[1]

[1]Departamento de Biofísica e Biometria, Instituto de Biologia Roberto Alcantara Gomes, Universidade do Estado do Rio de Janeiro, Av. 28 de Setembro, 87, fundos, 4º andar, 20 551–030, Rio de Janeiro, RJ, Brazil.
[2]Programa de Pós-Graduação em Biociências, Instituto de Biologia Roberto Alcantara Gomes, Universidade do Estado do Rio de Janeiro, Av. 28 de Setembro, 87, fundos, 4º andar, 20 551–030 Rio de Janeiro, RJ, Brazil.

Received 4 November, 2014; Accepted 5 February, 2015.

Tabebuia avellanedae **extract has been used in folk medicine in the treatment of some clinical disorders. Lapachol is an active compound from this medicinal plant. The procedure of labeling of blood constituents with technetium-99m (^{99m}Tc) could be used as an *in vitro* assay to evaluate some properties of natural and synthetic drugs. The aim of this work was to evaluate the effect of a *T. avellanedae* extract and lapachol solutions on the labeling of blood constituents with ^{99m}Tc. Whole blood (*Wistar* rats) was incubated with an aqueous *T. avellanedae* extract or lapachol. After, stannous chloride (reducing agent) and ^{99m}Tc (sodium pertechnetate) were added. Blood cells (BC) and plasma (P) were isolated by centrifugation. Samples of BC and P were precipitated with trichloroacetic acid to separation of soluble (FS) and insoluble (IF) fractions. The radioactivity in each fraction was counted and the percentage of incorporated radioactivity (%ATI) was determined. The data obtained showed that *T. avellanedae* extract significantly ($p<0.05$) altered the %ATI on blood constituents while no effects were observed with lapachol. As the labeling of blood constituents with ^{99m}Tc depends on the presence of a reducing, the extract of *T. avellanedae* seems to have substances with redox properties. In addition, these findings would be not associated with the lapachol.**

Key words: *Tabebuia avellanedae*, lapachol, blood, stannous ion, technetium-99m.

INTRODUCTION

Medicinal plants widely used in traditional medicine constitute an important source of new, safer and maybe biologically active compounds against many disorders in the herbal medicine in various countries. Furthermore, the scientific interest in the determination of properties associated with medicinal herbs is increasing in the world

*Corresponding author. E-mail: ericfrederico@msn.com, Tel/Fax: +55(21)2868-8332.
Author(s) agree that this article remain permanently open access under the terms of the Creative Commons Attribution License 4.0 International License

(Adisakwattana et al., 2011; Ma et al., 2011). In addition,some authors have studied substances isolated from medicinal herbs, as the Bisabololoxide that is isolated from the *Matricaria recutita* L. (Ogata et al., 2010).

Tabebuia avellanedae is a tree from the Bignoniaceae family and native to Central and South America. It is known as “pau d’arco” , “taheebe”, “lapacho” or “ipe roxo” and its inner bark is used as antimicrobial (Machado et al., 2001), anti-inflammatory (Lira et al., 2008), analgesic, antinociceptive (de Miranda et al., 2001), and anti-tumor drugs (Ueda et al., 1994). Phytochemical analysis of *T. avellanedae* have demonstrated the presence of quinones (Sharma et al., 1998), furanonaphthoquinones (Díaz and Medina, 1994), naphthoquinones (Manners and Jurd, 1976), benzoic acid, benzaldehyde derivatives (Wagner et al., 1989), cyclopentene dialdehyde (Koyama et al., 2000), flavonoids and iridoids (Nakano et al., 1993) and phenolic glycosides (Warashina et al., 2004).

Lapachol (2-hydroxy-3-(-3-methyl-2-butanyl)-1,4-naphthoquinone) has been isolated from *T. avellanedae* extracts. There are interest in the studies of this substance due to its anti-tumor (Balassiano et al., 2005), anti-biotic (Santos et al., 2001), anti-leishmanial (Lima et al., 2004), anti-malarial (de Andrade Neto et al., 2004), anti-ulcer (Goel et al., 2004) and anti-inflammatory activities (Lira et al., 2008). Preparation of isolated of lapachol is commercially available and it was used in this study.

Radionuclides have been in various clinical evaluations (Saha, 2010) and in experimental models (Bustami et al., 2009; Santos et al., 2013; Frederico et al., 2014,). Technetium-99m (^{99m}Tc) has been widely used in these procedures due to its optimal physical characteristics (6 h physical half-life and gamma emission) that give a negligible environmental impact (Saha, 2010). Several authors have demonstrated the effects of synthetic and natural drugs on the labeling process of blood constituents with ^{99m}Tc (Fonseca et al., 2005; Bustami et al., 2009; Carmo et al., 2011).

Blood constituents labeled with ^{99m}Tc have been used as radiobiocomplexes for a number of applications in nuclear medicine. The labeling of blood cells and cell structures is based on the transmembrane transport of a reducing agent (Sn^{+2}) and pertecnetate ($^{99m}TcO_4^-$) ions into the red blood cells, reduction of $^{99m}TcO_4^-$ by Sn^{+2}, and subsequent binding of the reduced ^{99m}Tc to internal structures. The band-3 anion transport system and calcium channels may be involved in the transportion of $^{99m}TcO_4^-$ and Sn^{+2}, respectively. The fixation of ^{99m}Tc in plasma proteins also depends on the reducing agent action occurring at different proteins sites and albumin is the principal protein involved (Saha, 2010).

The effect of drugs altering the labeling of blood constituents could be due modification of the membrane structure (Braga et al., 2013), decreasing the efficiency of transmembrane transport system of $^{99m}TcO_4^-$ and Sn^{+2} ions into cells. Redox property and/or metal chelator could be another properties associated with the drugs.

In this investigation, the effect of a *T. avellanedae* extract and of a commercial preparation of lapachol on the labeling of the blood constituents with ^{99m}Tc was evaluated.

MATERIALS AND METHODS

Animals

Adult male *Wistar* rats (3-4 months of age, body weight 250-350 g) were maintained in a controlled environment. The animals had free access to water and food and the ambient temperature was kept at 25 ± 2ºC. Experiments were conducted in accordance with the Institutional Committee of Animal Care.

Preparation of *T. avellanedae* extract

T. avellanedae was purchased from *Estrella da Terra Produtos Naturais Ltda* (Brazil). To prepare the extracts, 2 g of bark were ground in 10 ml 0.9% NaCl at 100°C for 10 min. The crude extract was filtered, centrifuged (1500 rpm, 10 min) to obtain the final extract. The supernatant was considered to be 200 mg/ml. As the quantity of lapachol is about 7% of *T. avellanedae* (American Cancer Society, 2015), it is possible to consider a concentration of 14 mg/ml of lapachol. The concentrations of *T. avellanedae* used in the experiments were 12.5, 25, 50, 100 and 200 mg/ml, and respectively the concentrations of lapachol were 0.87, 1.75, 3.5, 7 and 14 mg/ml.

Preparation of lapachol solution

Lapachol is an important chemical compound of the *T. avellanedae* extract (Balassiano et al., 2005) and it is available in the market. It was purchased from *PVP Sociedade Anônima*. (Brazil) and the solutions were prepared in 0.02 N NaOH immediately before the use.

In vitro radiolabeling of blood constituents

Heparinized blood (500 µl), was withdrawn from *Wistar* rats and incubated with 100 µl of *T. avellanedae* extract (12.5, 25, 50, 100 and 200 mg/ml) or lapachol (0.05, 0.5, 5 and 50 mg/ml) for 1 hour (room temperature). Blood samples were also incubated with saline solution (0.9% NaCl) or 0.02N NaOH as control for *T. avellanedae* or lapachol, respectively. Afterwards, 500 µl of stannous chloride (1.20 µg/ml) was added and the incubation continued for further 1 h. After this period, 100 µl of ^{99m}Tc (3.7 MBq) as sodium pertechnetate ($Na^{99m}TcO_4$), recently milked from a $^{99}Mo/^{99m}$Tc generator (*Instituto de Pesquisas Energéticas e Nucleares, Comissão Nacional de Energia Nuclear,* São Paulo, Brazil) were added and the incubation was continued for 10 min. These samples were centrifuged in a clinical centrifuge (1500 rpm, 5 min) and aliquots of 20 µl of plasma (P) and blood cells (BC) were isolated. Another aliquots of 20 µl of P and BC were separated and precipitated in 1.0 ml of 5% trichloroacetic acid and centrifuged (1500 rpm, 5 min) to isolate soluble (SF) and insoluble fractions (IF). The radioactivity in P, BC, SF-P, IF-P, SF-BC and IF-BC were determined in a well counter (Packard, model C5002, Illinois, USA) and the percentage of incorporated radioactivity (%ATI) was

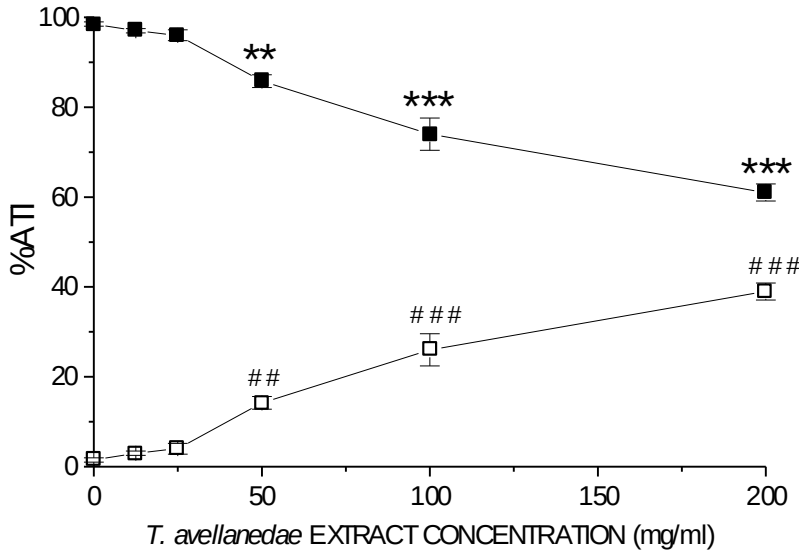

Figure 1. Effect of *T. avellanedae* extract on the distribution of the ^{99m}Tc in the plasma and blood cells (BC) compartments. Blood samples were incubated with *T. avellanedae* extract and after with $SnCl_2$ and with $Na^{99m}TcO_4$. After centrifugation, plasma (P) and blood cells (BC) were isolated. The radioactivity was counted in a gamma counter and the percentage of radioactivity incorporated (%ATI) was calculated for P and BC. ■, BC; □, P. **, $p \leq 0.01$, when compared to control group of plasma. ***, $p \leq 0.001$ when compared to control group of plasma. ##, $p \leq 0.01$, when compared to control group of blood cells. ###, $p \leq 0.001$, when compared to control group of blood cells

calculated as described elsewhere.

Histological analysis

Histological preparations were carried out with blood samples treated with various concentrations of *T. avellanedae* extract for 60 min at room temperature. Blood smears were prepared, dried, fixed and stained. After that, the morphology of the red blood cells was qualitatively evaluated under optical microscope.

Statistical analysis

Data are reported as (means ± SD) of %ATI and compared the treated (n=10 for each extract concentration) and control group (n=10) by One way analysis of variance - ANOVA, followed by Tukey post test, with a $p<0.05$ as significant level. InStat Graphpad software was used to perform statistical analysis (GraphPad InStat version 3.00 for Windows 95, GraphPad Software, San Diego California, USA).

RESULTS

Figure 1 shows the %ATI in blood cells and plasma compartments from whole blood treated with different concentrations of *T. avellanedae* extract. The analysis of these data indicates that *T. avellanedae* extract alters significantly ($p<0.05$) the distribution of radioactivity between the two blood compartments.

Figure 2 shows the %ATI in insoluble (IF-P) and soluble (SF-P) fractions isolated from plasma separated from whole blood treated with different concentrations of *T. avellanedae* extract. The analysis of these data indicates that *T. avellanedae* extract significantly ($p<0.05$) reduced the radioactivity fixation in IF-P.

Figure 3 shows the %ATI in insoluble (IF-BC) and soluble (SF-BC) fractions isolated from blood cells separated from blood treated with different concentrations of *T. avellanedae* extract. The analysis of these data indicates that the incubation with *T. avellanedae* extract significantly alters the radioactivity fixation on insoluble blood cells fraction at the higher concentrations used (200 mg/ml).

The qualitative comparison of the shape of the RBC (non-treated and treated with natural extracts) under optical microscopy has revealed strong morphological alterations due to the treatment of blood with *T. avellanedae* extract in the concentrations of 12.5 and 200 mg/ml. The histological preparation of a sample of blood (control-non-treated) with normal shape of RBC is shown in Figure 4. Figures 5 and 6 show histological preparations of blood treated with *T. avellanedae* in which are shown qualitative and strong alterations on the shape of the RBC.

Table 1 shows the distribution of the radioactivity in BC, IF-P and IF-BC treated with different concentrations of lapachol. The analysis of the results indicates that there

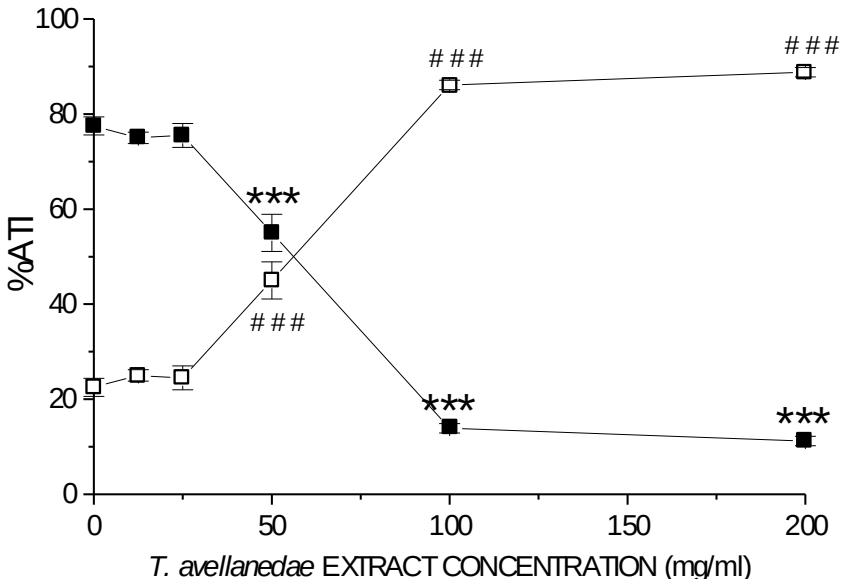

Figure 2. Effect of *T. avellanedae* extract on fixation of ^{99m}Tc by insoluble (IF-P) and soluble (SF-P) fractions of plasma (P). Blood samples were incubated with *T. avellanedae* extract (1 h) and after with $SnCl_2$ and with $Na^{99m}TcO_4$. Insoluble and soluble fractions of plasma (IF-P and SF-P) were obtained by precipitation and centrifuged. The radioactivity in these fractions were counted in a gamma counter and the percentage of radioactivity incorporated (%ATI) was calculated for each fraction. ■, IF-P; □, SF-P. ***, $p \leq 0.001$, when compared to control group of IF-P. ###, $p \leq 0.001$, when compared to control group of SF-P.

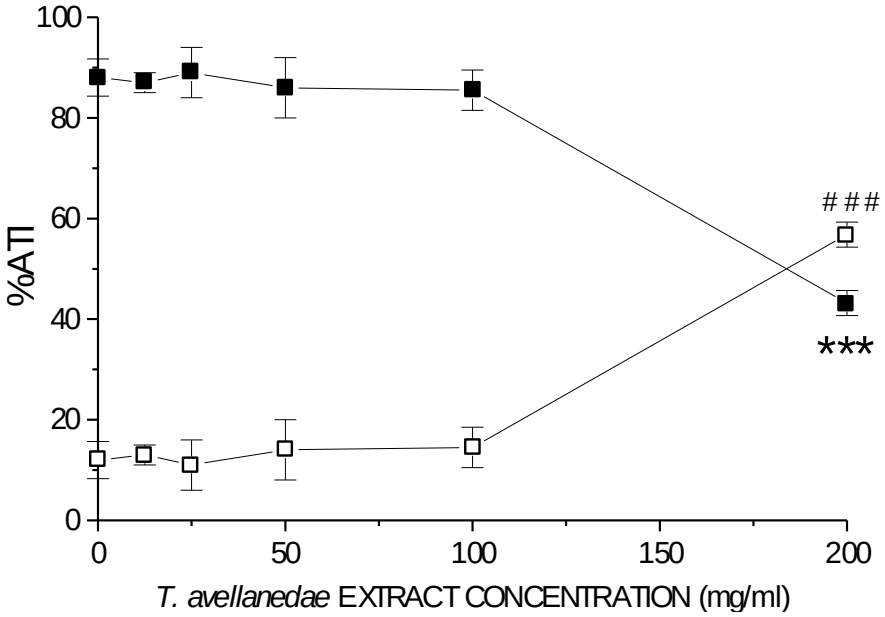

Figure 3. Effect of *T. avellanedae* extract on fixation of ^{99m}Tc by insoluble (IF-BC) and soluble (SF-BC) fractions of blood cells (BC). Blood samples were incubated with *T. avellanedae* extract, after with $SnCl_2$ and with $Na^{99m}TcO_4$. Insoluble and soluble fractions of blood cells (IF-BC and SF-BC) were obtained by precipitation and centrifuged. The radioactivity in these fractions was counted in a gamma counter and the percentage of radioactivity incorporated (%ATI) was calculated for each fraction. ■ IF-BC; □, SF-BC. ***, $p \leq 0.001$, when compared to control group of IF-BC. ###, $p \leq 0.001$, when compared to control group of SF-BC.

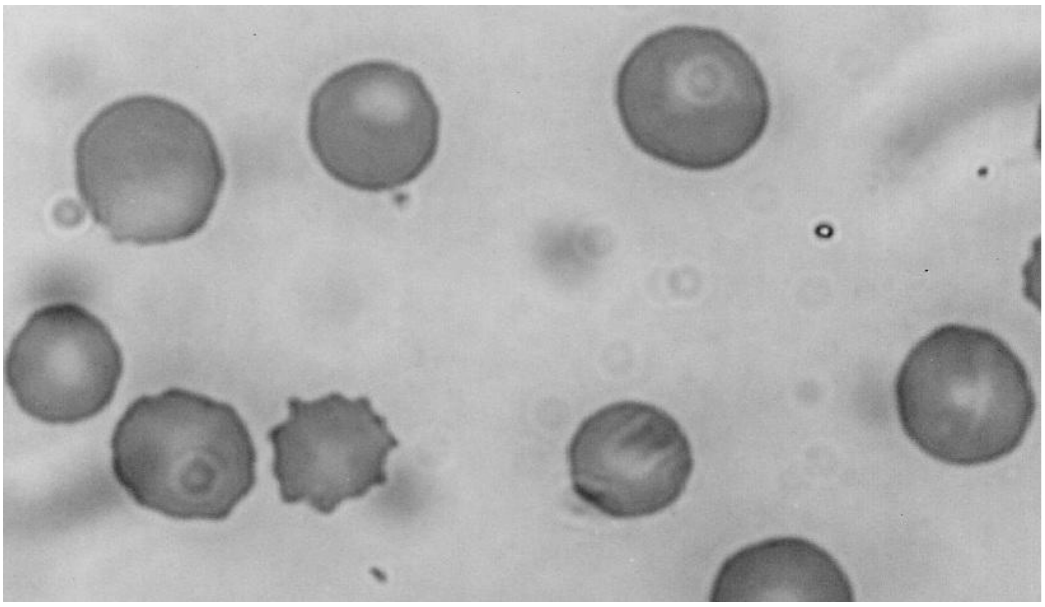

Figure 4. Samples of whole blood were incubated with 0.9% NaCl solution for 60 min. After that, stannous chloride solution was added and the incubation continued for 60 min. Then, ^{99m}Tc, as sodium pertechnetate was added. Blood smears were prepared, dried, fixed and staining. After that, the morphology of the red blood cells was evaluated under optical microscope (x1000).

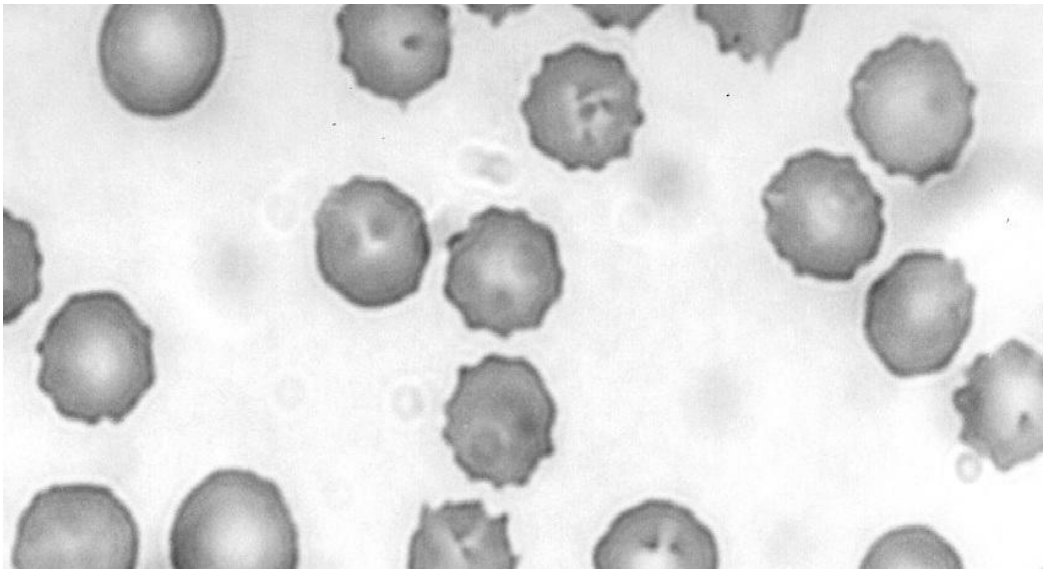

Figure 5. Samples of whole blood were incubated with 20.5 mg/ml of *T. avellanedae* extract for 60 min. After that, stannous chloride solution was added and the incubation continued for 60 min. Then, ^{99m}Tc, as sodium pertechnetate was added. Blood smears were prepared, dried, fixed and staining. After that, the morphology of the red blood cells was evaluated under optical microscope (x1000).

is no important alterations ($p>0.05$) of the %ATI on blood compartments, on IF-P and on IF-BC.

Heparinized blood samples of *Wistar* rats were incubated (1 h) with different concentrations of lapachol, saline solution or 0.02 N NaOH (control groups). After, stannous chloride and ^{99m}Tc were added, centrifuged and plasma (P) and blood cells (C) were separated. Another samples of P and BC were precipitated with trichloroacetic acid (5%) and insoluble fractions (IF) were separated. The radioactivity in C, IF-P and IF-BC

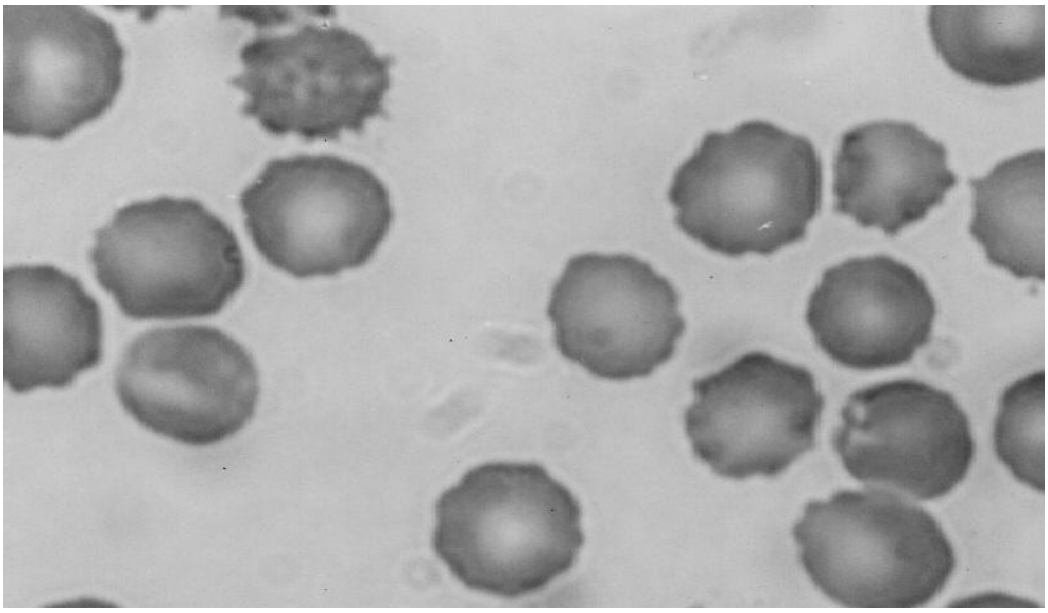

Figure 6. Samples of whole blood were incubated with 200 mg/ml of *T. avellanedae* extract for 60 min. After that, stannous chloride solution was added and the incubation continued for 60 min. Then, ^{99m}Tc, as sodium pertechnetate was added. Blood smears were prepared, dried, fixed and staining. After that, the morphology of the red blood cells was evaluated under optical microscope (x1000).

Table 1. Effect of different lapachol concentrations on labeling of blood constituents with ^{99m}Tc.

Lapachol (mg/ml)	Cells	IF-P	IF-BC
0.0	96.4±5.4	81.9±1.7	88.0±3.3
NaOH (0.02 N)	87.1±7.3	82.1±2.6	85.4±4.4
0.05	89.7±4.4	84.3±6.9	87.3±7.1
0.5	86.9±7.8	81.8±4.0	84.8±4.0
5.0	83.2±6.9	80.7±2.8	87.1±3.5
50	89.4±5.0	79.9±2.2	87.4±4.6

DISCUSSION

The evaluation of the influence of drugs on the labeling of blood constituents is highly relevant due to some products, as chocolate, can interfere in the quality of the examinations using red blood cells labeled with ^{99m}Tc (Bustami et al., 2009).

The analysis of data presented in Figure 1 show that the aqueous *T. avellanedae* extract can modify the distribution of ^{99m}Tc between the cellular and plasma compartments almost in all tested concentrations. However, the fixation of ^{99m}Tc in cellular proteins could be altered at high concentrations of this extract (Figure 3). The fixation of the ^{99m}Tc plasma proteins is also blocked by the presence of the *T. avellanedae* extract (Figure 2). This finding is interesting and it suggests that the entrance of the stannous and pertechnetate would be blocked on a depended matter (decreasing the radioactivity on the blood cells) (Figure 1). However, only in the highest concentration of the extract, the fixation of the ^{99m}Tc on the blood proteins would be blocked probably due to the anti-oxidant and/or scavenger activities of the substances in the *T. avellanedae* extract. These redox properties could be associated with the chemical analysis of *T. avellanedae* extracts revealed the presence of various compounds as naphthoquinones, flavonoids, quinoid compounds and phenolic glycosides (Warashina et al., 2004). The phenolic compounds presents in different herbal extracts have been described to possess antioxidant and chelating action and be able to inhibit peroxidation reaction in the living systems (Simoes-Pires et al., 2005; Soobrattee et al., 2005). On the other hand, It was described that antimicrobial effects of β-lapachol could be related to the formation of reactive oxygen species (Guiraud et al., 1994). Thus, some compounds present in *T. avellanedae* extracts could be

capable to impede or facilitate the oxidation of the stannous ions and alter the labeling of cellular proteins with ^{99m}Tc as well interfere with distribution of this radionuclide between plasma and cellular compartments.

Other hypothesis that could explain the effects of *T. avellanedae* extracts on labeling of blood cells with ^{99m}Tc is the interaction of constituents of this extract with ion channels. In fact, it was proposed that the antinociceptive effect of *T. avellanedae* may be related to an activation of the adenosine receptors (de Miranda et al., 2001). Other membrane proteins as band-3 and calcium channel may have their function altered by compounds present in *T. avellanedae* extract decreasing or impeding the transport of Sn^{+2} and $^{99m}TcO_4^-$ into blood cells and in consequence to modify de distribution of ^{99m}Tc between plasma and cellular compartments.

The data obtained in this work show that the labeling of plasma proteins with ^{99m}Tc could be decreased by the aqueous *T. avellanedae* extract used (Figure 2). Pharmacokinetics data have demonstrated that some compounds (as flavonoids) present in herbal extracts can be transported in blood attached to plasma proteins (Guiraud et al., 1994). Moreover, the already cited oxidant chelating properties of compounds present in *T. avellanedae* extract also could be related to effect obtained. Taken together, the binding in same proteins sites that the binding sites of ^{99m}Tc and oxidant/chelating properties of *T. avellanedae* extract compounds could explain the decreasing of labeling of plasma proteins with ^{99m}Tc.

In the procedure of labeling RBC with ^{99m}Tc, the stannous and pertechnetate ions pass through the plasma membrane (Gutfilen et al., 1992). Then, as reported to the tobacco extract (Oliveira et al., *2003*) and to *Maytenus ilicifolia* extract (Oliveira et al., 2000), histological alterations of the red blood cells could be responsible for modifications on the labeling of the RBC with ^{99m}Tc. Furthermore, the results obtained with the qualitative comparison of the shape of the RBC (treated and not treated with *T. avellanedae* extracts) under optical microscopy also justify the modifications in the fixation of ^{99m}Tc by the red blood cells. The achieved results have revealed strong morphological alterations due to the treatment of blood with *T. avellanedae* extract in two of the concentrations studied (Figures 5 and 6).

The analysis of Table 1 suggests that lapachol did not affect the distribution of ^{99m}Tc between cellular and plasma compartments or the binding of this radionuclide in cellular and plasma proteins. The pharmacological actions of lapachol include antitumor, antibiotic, antimalarial, antiinflammatory and antiulceric activities (Subramanian et al., 1998) besides molluscicidal, cercaricidal and trypanocidal activities (Santos et al., 2001; Lima et al., 2004). Oxidative stress and alkylation of cellular nucleophiles have been proposed to explain the lapachol effects on biological system (Bolton et al., 2000). In fact, it was described the generation of reactive oxygen species in the bioactivation of lapachol by P450 reductase (Kumagai et al., 1997) and an electrochemical study (Goulart *et al*., 2003). However, the absence of effects of lapachol labeling of blood constituents with ^{99m}Tc (Table 1) could be related to the concentrations used in this work, or this substance would be not responsible by our findings. Considering the quantity of lapachol in the *T. avellanedae*, probably the concentration of lapachol isolated used in the experiments (Table 1) would be small in comparison with the quantity of this molecule extract in the highest concentration. In consequence, the lapachol concentrations would be too low to induce any effect. In addition, the effect of a chemical compound in an extract is associated with an integrative and synergic action among several compounds (Galindo et al., 2010; Carmona and Pereira, 2013). This fact could occur with the lapachol when was used alone.

In conclusion as the labeling of blood constituents with ^{99m}Tc depends on the presence of a reducing, probably the extract of *T. avellanedae* has substances with redox properties. In addition, probably these properties are not associated with the lapachol or the concentration of lapchol used in this work was not sufficient to promote effect on the labeling process.

Conflict of Interest

The authors declare that they have no conflict of interest.

ACKNOWLEDGEMENTS

This study was supported by grants and financial support from CAPES, CNPq and FAPERJ.

REFERENCES

Adisakwattana S, Chanathong B (2011). Alpha-glucosidase inhibitory activity and lipid-lowering mechanisms of *Moringa oleifera* leaf extract. Eur. Rev. Med. Pharmacol. Sci: 15:803-08. 21780550.

American Cancer Society (2015). http://www.cancer.org/treatment/treatmentsandsideeffects/complementaryandalternativemedicine/herbsvitaminsandminerals/pau-d-arco, accessed on January 29th 2015.

Balassiano IT, De Paulo SA, Henriques Silva N, Cabral MC, da Gloria da Costa Carvalho M (2005). Demonstration of the lapachol as a potential drug for reducing cancer metastasis. Oncol. Rep. 13:329-33.

Bolton JL, Trush MA, Penning TM, Dryhurst G, Monks TJ (2000). Role of quinones in toxicology. Chem Res Toxicol. 13:135-160.

Braga ACS, Gomes ML, Santos JS, Oliveira JF, Amorim LF , Feliciano GD , Santos-Filho SD Bernardo-Filho M (2013). Evaluation of biologic effects of an *Ilex paraguariensis* aqueous extract on the labeling of blood constituents with technetium-99m and on the morphology of red blood cells. Afr. J. Pharm. 7(39):2685-2691.

Bustami H, Colavolpe C, Imbert-Joscht I, Havlik P, Pisano P, Guillet BA (2009). Chocolate intake associated with failed labeling of 99mTc red blood cells. J. Nucl. Med. Technol. 37:107-10.

Carmo FS, Diniz CL, Pereira MO, Santos-Filho SD, Bernardo-Filho M (2011). Characterization of physicochemical parameters and the effect on the labeling of blood constituents with technetium-99m of a *Solanum melongena* commercial extract. J. Med. Plants Res.5(23):5598-5604.

Carmona F, Pereira MAS (2013). Herbal medicines: old and new concepts, truths and misunderstandings. Braz. J. Pharmacog. 23(2):379-385.

de Andrade Neto VF, Brandão MGL, Oliveira FQ, Casali VW, Njaine B, Zalis MG, Oliveira LA, Krettli AU (2004). Antimalarial activity *of Bidens pilosa* L *(Asteraceae)* ethanol extracts from wild plants collected in various localities or plants cultivated in humus soil. Phytother Res.18:634-39.

de Miranda FG, Vilar JC, Alves IA, Cavalcanti SC, Antoniolli AR (2001). Antinociceptive and antiedematogenic properties and acute toxicity of *T. avellanedae* Lor. *ex Griseb*. inner bark aqueous extract. BMC Pharmacol. 1:6-10.

Díaz F, Medina JD (1996). Furanonaphthoquinones from *Tabebuia ochracea ssp*. Neochrysanta. J. Nat. Prod. 59:423-24.

Fonseca AS, Frydman JNG, Santos R, Bernardo-Filho M (2005). Influence of antipyretic drugs on the labeling of blood elements with technetium-99m. Acta Biol. Hung. 56:275-82.

Frederico EHFF, Carmo FS, Arnóbio A, Guedes SSV, Sá-Caputo DC, Bernardo LC, Guimarães CAS, Asad NR, Bernardo-Filho M (2014). Does the whole body vibration alter the effect of a *Coriandrum sativum* extract on the biodistribution of the radiopharmaceutical technetium-99m sodium pertechnetate and some biomarkers in *Wistar* rats? Int. J. Pharm. Sci. Res. 5(8):3529-3535.

Galindo LA, Pultrini AM, Costa M (2010). Biological effects of *Ocimum gratissimum* L. are due to synergic action among multiple compounds present in essential oil. J Nat Med. 64(4):436-41.

Goel RK, Pathak NK, Biswas M, Pandey VB, Sanyal AK (2004).Effect of lapachol, a naphthaquinone isolated from Tectona grandis, on experimental peptic ulcer and gastric secretion. J. Pharm. Pharmacol. 39:138-140.

Goulart MO, Falkowski P, Ossowski T, Liwo A (2003). Electrochemical study of oxygen interaction with lapachol and its radical anions. Bioelectrochem. 59:85-87.

Guiraud P, Steiman R, Campos-Takaki GM (1994). Comparison of antibacterial and antifungal activities of lapachol and beta-lapachone. Plant Med. 60:373-74.

Gutfilen B, Boasquevisque EM, Bernardo-Filho M (1992). Calcium channel blockers: interference on red blood cells and plasma proteins labeling with ^{99m}Tc. Rev. Espanõla Med. Nucl. 11:195-99.

Koyama J, Morita I, Tagahara K, Hirai K (2000). Cyclopentene dialdehydes from *Tabebuia impetiginosa*. Phytochem. 53:869-72.

Kumagai Y, Tsurutani Y, Shinyashiki M, Homma-Takeda S, Nakai Y, Yoshikawa T, Shimojo N (1997). Bioactivation of lapachol responsible for DNA scission by NADPH-cytochrome P450 reductase. Environ. Toxicol. Pharmacol. 3:245-250.

Lima NM, Correia CS, Leon LL, Machado GM, Madeira MF, Santana AE, Goulart MO (2004). Antileishmanial activity of lapachol analogues. Mem Inst Oswaldo Cruz. 99:757-61.

Lira AAM, Sester EA, Carvalho ALM, Strattmann Albuquerque MM, Wanderley AG, Santana DP (2008). Development of Lapachol Topical Formulation: Anti-inflammatory Study of a Selected Formulation. AAPS Pharm. Sci. Tech. pp. 163-168.

Ma JQ, Liu CM, Qin ZH, Jiang JH, Sun YZ (2011). Ganoderma applanatum terpenes protect mouse liver against benzo(α)pyren-induced oxidative stress and inflammation. Environ Toxicol Pharmacol; 31:460-68.

Machado TB, Pinto AV, Pinto MC, Leal IC, Silva MG, Amaral AC, Kuster RM, Netto-dos Santos KR (2001). *In vitro* activity of Brazilian medicinal plants, naturally occurring naphthoquinones and their analogues, against methicillin-resistant. *Staphylococcus aureus.* Int. J. Antimicrob. Agents 2:279-284.

Manners GD, Jurd L (1976). A new naphthaquinone from *Tabebuia guayacan*. Phytochem. 15:225-26.

Nakano K, Maruyama K, Murakami K, Takaishi Y, Tomimatsu T (1993). Iridoids from *Tabebuia avellanedae*. Phytochem. 32:371-73.

Ogata T, Kawanai E, Hashimoto, Nishimura Y, Oyama Y, Seo H (2010). Bisabololoxide A, One of the main Constituents in German chamomile extract, induces apoptosis in rat thymocytes. Archives toxicol. 84:45-52.

Oliveira JF, Braga AC, de Oliveira MB, Avila AS, Caldeira-de-Araújo A, Cardoso VN, Bezerra RJ, Bernardo-Filho M (2000). Assessment of the effect of *Maytenus ilicifolia* (espinheira santa) extract on the labeling of red blood cells and plasma proteins with technetium-99m. J. Ethnopharmacol. 72:179-84.

Oliveira JF, Santos-Filho SD, Catanho MTJA, Srivastava SC, Lima-Filho GL, Bernardo-Filho M (2003). Effect of extract of medicinal plants on the labeling of blood elements with technetium-99m and on the morphology of red blood cells (RBC): toxicological actions of roast coffee beans (Coffea arabica). Indian J. Nucl. Med. 18:52-56.

Saha GB (2010). Fundamentals of nuclear pharmacy, 6th ed. New York: Springer-Verlag.

Santos AF, Ferraz PA, de Abreu FC, Chiari E, Goulart MO, Sant'Ana AE (2001). Molluscicidal and trypanocidal activities of lapachol derivatives. Plant Med. 67:92-93.

Santos RRM, Carmo FS, Frederico EHFF, Dantas MP, Santos-Filho SD, Bernardo-Filho M (2013). Effects of licorice (*Glycyrrhiza uralensis* F.) commercial extract on the biodistribution of the radiopharmaceutical sodium pertechnetate, radiolabeling of blood constituents and on some biochemical parameters in *Wistar* rats. J. Med. Plants Res. 7:2590-2596.

Sharma PK, Khanna RN, Rohatgi BK, Thomson RH (1998). Tecomaquinone-III: A new quinone from Tabebuia pentaphylla. Phytochem. 27:632-633.

Simoes-Pires CA, Queiroz EF, Henriques AT, Hostettmann K (2005). Isolation and on-line identification of antioxidant compounds from three Baccharis species by HPLC-UV-MS/MS with post-column derivatisation. Phytochem. Analysis. 16:307-314.

Soobrattee MA, Neergheen VS, Luximon-Ramma A, Aruoma OI, Bahorun T (2005). Phenolics as potential antioxidant therapeutic agents: mechanism and actions. Mut Res. 579:200-13. Subramanian MMC, Ferreira M, Trsic A (1998). A structure-activity relationship study of lapachol and some derivatives of 1,4-naphthoquinones against carcinosarcoma Walker 256. Struct Chem. 9:47-57.

Ueda S, Umemura T, Dohguchi K, Matsuzaki T, Tokuda H, Nishino H, Iwashima A (1994). Production of anti-tumour-promoting furanonaphthoquinones in *Tabebuia avellanedae* cell cultures. Phytochem. 36:323-25.

Wagner H, Kreher B, Lotter H, Hamburger MO, Cordell GA (1989). Structure determination of new isomeric naphtha [2,3-b] furan-4,9-diones from *Tebebuia avellanedae* by the selective-INEPT technique. Helv Chim Acta. 72:659-67.

Warashina T, Nagatani Y, Noro T (2004). Constituents from the bark of *Tabebuia impetiginosa*. Phytochem. 65:2003-2011.

academicJournals

Vol. 10(3), pp. 105-113, 15 February, 2015
DOI: 10.5897/SRE2014.6146
Article Number:14908D250363
ISSN 1992-2248
Copyright©2015
Author(s) retain the copyright of this article
http://www.academicjournals.org/SRE

Scientific Research and Essays

Full Length Research Paper

A hybrid multilevel text extraction algorithm in scene images

Tahani Khatib*, Huda Karajeh, Hiba Mohammad and Lama Rajab

Department of Computer Information Systems, King Abdullah II School for Information Technology, University of Jordan, 11942 Amman, Jordan.

Received 15 December, 2014; Accepted 22 January, 2015

The textual pieces in scene images might often provide vital semantic data for visual content understanding, indexing and analysis; as a result, text extraction had become a significant research area in image processing and computer vision. In this paper, we propose a new hybrid multilevel algorithm to extract text in various scene images. The algorithm converts the Red – Green –Blue (RGB) image into grayscale for color reduction. Next, it applies edge detection and mathematical morphological operations to extract edges in the image preprocessing phase. The resultant binary image passes through three subsequent levels in a multi layer behavior. Connected components labeling and text candidates' selection take place in each level through different criteria analysis. We used the structural features of connected components as basis criteria for selecting candidate texts, those features include: area, width, length and condense intensity mean of connected components. Afterwards, Horizontal projection profile analysis is used to further refine the candidate text areas and to eliminate non-text regions. The proposed algorithm is evaluated on a set of fifty images chosen from a well known text locating test dataset: KAIST. Extensive experiments show high robustness under different environments such as indoor, outdoor, shadow, night and light, and for different text properties such as various font size, style and complexities of backgrounds and textures. The algorithm effectively extracts textual contents from scenes images with high average of Precision, Recall, and F-Score which are 90.1, 99, and 94.3%, respectively.

Key words: Multilevel text extraction, hybrid text extraction, edge detection, connected components, text candidates, morphological operations, horizontal projection profile.

INTRODUCTION

The development of digital technologies accelerated the rapid growth in digital content. However, as digitalization is expanding in all categories and materials, it becomes important to extract any textual content from digital media to acquire semantic clues to help in visual content illustration and analysis. Digital images, as an essential form of digital media, may include pieces of text that comprise useful information for automatic explanation and structuring of images (Mancas-Thillou et al., 2007). Furthermore, information in embedded text can be used to fully understand images and for specific applications such as page segmentation in (Jain and Zhong, 1996;

*Corresponding author. E-mail: tahani.khatib@ju.edu.jo
Author(s) agree that this article remain permanently open access under the terms of the Creative Commons Attribution License 4.0 International License

Tang et al., 1996), address block location (Yu et al., 1997), license plate location (Cui et al., 1997; Kim and Chien, 2001), and content-based image/video indexing and retrieval (Shim et al., 1998; Zhang et al., 1994). Text appears in images either in the form of documents such as scanned CD/book covers or as video images. The embedded text in video frames can broadly be classified into two categories: overlay text and scene text. Overlay text refers to those characters generated by graphic titling machines and superimposed on video frames/images (Zhang and Chang, 2003), while scene texts are those captured by a recording device such as text in signs, nameplates, food containers, etc. Scene text is more difficult to detect (Gatos et al., 2005; Choksi et al., 2013; Sumathi et al., 2012) and therefore researches and studies in this field are so limited. In contrast to caption texts, scene texts can have any orientation and may be distorted by the perspective projection and may often be affected by variations in scene and camera parameters (Jung et al., 2004 in Kim and Chien, 2004; Mancas-Thillou et al., 2007); they also have several varieties of fonts, sizes, styles, reflections and shadows. As a result, Text extraction in scene images has become a challenging issue due to previous problems in addition to the complicated background in the image itself.

Many algorithms have been developed and improved in scene image text extraction. The majority of text extraction algorithms could be classified either as connected component based technique or as texture based technique (Fu et al., 2006). Connected component-based methods use geometric constraints and information to choose text candidates by creating bounding boxes around connected regions in images (Pan et al., 2009). The algorithm proposed in (Leon et al., 2010) makes use of similarity measure to choose text regions; it combines texture information and geometric information in order to extract text in scene image. In Rajab et al. (2014), we presented a text extraction technique that employs image enhancement, morphological operations and different transformations in order to label text candidates.

Texture-based methods treat the text as a unique object that has some distinguishable features from the background. The researchers in Wen and Chou (2004) used Discrete cosine transform (DCT) based high pass filter to remove constant background. The problem of texture-based methods is the large computational complexity in texture classification; which leads to a confusion when text-like regions appear. The variations on text fonts, sizes, colors and complex backgrounds (Shivakumara et al. 2014; Mao et al., 2013) affect the performance of these algorithms and hence text cannot be extracted by using a single method only. Niti (2014) and Xiaoqing and Jagath (2006) improved a hybrid and multi-scale method that use Support Vector Machine (SVM) transformation along with some pre-processing and post-processing steps in order to extract text in complex images (Chandrasekaran and Chandrasekaran (2011).

In Jung and Han (2004), two methods for text localization in complex images were proposed. The first method was an automatic texture-base method that can increase the recall rates for complex images; while the second one was a connected component-based filtering that took advantage of geometry and shape information to enhance the precision rates.

This paper proposes a hybrid multilevel text extraction algorithm that can locate and extract texts in complex scene images and can resolve problems that some previous systems had. The algorithm uses both connected component-based and texture-based techniques in text candidates' selection. It begins with image preprocessing which includes both color reduction and edge extraction. In color reduction step, the RGB image is converted into a grayscale image. Afterwards, the binary image resulted from edge extraction in the preprocessing phase is sent to three subsequent levels. All levels contain both connected components labeling and text candidates' selection; however every level has its own criteria used in text candidates' selection. Criteria used in candidate selection include analyzing area, width, height and intensity mean of connected components. Adaptive background elimination through logical operations is performed in inner phases in addition to analyzing the horizontal projection profile of the image in order to eliminate tiny non textual areas.

MATERIALS AND METHODS

Proposed algorithm

In this study, we improved a hybrid multi level algorithm for text extraction in scene images. The proposed algorithm uses both connected component-based and texture-based techniques and it includes preprocessing phase in addition to three sequential levels; every level contains inner phases where candidate text regions are labeled gradually within inner phases of each level. The proposed algorithm is discussed methodically in the following:

Image preprocessing

Image preprocessing phase is extremely significant in achieving better performance in text detection and extraction techniques. The scene image may contain some noise or effects such as shadow or light spots; therefore we need to remove those effects before labeling and detecting the text candidates in the image in order to get a better input image for next phases. Preprocessing phase includes both color reduction and edge extraction inner phases:

i) ***Image preprocessing: Color Reduction***
In this phase, the acquired colored image is converted from Red – Green –Blue (RGB) color model into grayscale and passes as the input image to the next phase.
ii) ***Image preprocessing: Edge Extraction***
In this phase, the canny edge detection is applied on the saturation grayscale image. The edge detection is applied to get the edge map of the image. Afterwards, morphological image dilation is used on the resultant binary image with a suitable structuring element.

After image preprocessing, the resultant binary image passes through three subsequent levels as follows:

Level 1

Phase 1.1: Labeling text candidates' regions

In this phase, all elements in the connected components set *S* are labeled and then tested by using some selection criteria in order to find the text candidates set S_T. Those criteria contain mathematical analysis of width, height and area of each element. Connected components with area (A_i) greater than a certain portion of the overall area (A_I) of the image will be eliminated; the analysis of this criteria helps in excluding large connected components that are far away from being textual regions. Width and height of connected components are also tested so all components with width less than twice and half of height (the threshold used in the algorithm) are eliminated. Equations (1) and (2) in the following show the criteria used in eliminating non text regions in this phase.

$$S = S_E \cup S_T \quad (1)$$

$$S_T = \left\{ i \in S : A_i < \frac{A_I}{t_1} \text{ and } W_i < H_i * t_2 \right\} \quad (2)$$

In previous equations, *S* stands for the set of all connected components, S_E is the set of the eliminated components and S_T is the set of candidate text regions. The total area of image *I* is denoted by A_I, while *i* stands for an element in *S* with area, width and height denoted by A_i, W_i and H_i, respectively. Variables t_1 and t_2 are the thresholds used in our algorithm which were obtained from many experiments on large set of images and have values 18 and 2.5, respectively. Figure 1(a) shows a sample scene image used in algorithm testing, Figure 1(b) shows the result image after connected components labeling, while the result of text candidate selection is shown in Figure 1(c).

Phase 1.2: Text Extraction – level 1

In this phase, we apply multi-step operations on the text candidates in order to extract the text from the image. The inner steps of this phase are discussed in the following.

Step 1.2.1: Morphological operations: A set of morphological operations with filling procedures are applied on the image to facilitate edge enhancement; morphological operations include close and open operations followed by holes filling.

Step 1.2.2: Eliminate large non-text areas from the background using adaptive logical operator: In this step, we apply an adaptive (AND) operator between the binary image in Phase 1.1 and the enhanced edged image from Phase 1.2.1; this step gives excellent results in eliminating large non-text regions from the image background. Applying logical (AND) between both enhanced edge image and the adjusted monochrome version from the original helped in studying the foreground and the background of the image. However, if the intensity mean of the resultant image is greater than a certain threshold, an image negation operation is performed to keep the important foreground data; otherwise, the original image is converted to a monochrome version using different threshold. Figure 1(d) shows the result image after applying this phase, while the procedure is shown in the following pseudo code.

Pseudo code: (Adaptive AND Procedure)
Input (G, I, J)
Where: G is the grayscale image, I is the resultant image from Step 1.2.1 and J is the resultant image from Step 1.1

IF the intensity mean of J > 0.5 then

1. Find image negation of J, store the result in Jn
2. Calculate R = AND (I, Jn) ELSE
3. Find binary image of G with a larger threshold (0.75), store the result in Jnb
4. Calculate R = AND (J, Jnb)

End IF
Output (R)

Level 2

Phase 2.1: Labeling the text candidate regions

Text candidates are labeled by studying the condense intensity mean of white pixels (intensity = 1) for each connected component; if the mean is greater than a certain threshold, the region will be eliminated, otherwise it will be labeled as text region as shown in Equation (3).

$$S_T = \{ Mean(i) < t_3 \} \quad (3)$$

In the previous equation, S_T denotes the set of candidate texts, *i* is an element in S (the set of all connected components) and threshold *t3* = .80.

Phase 2.2: Text extraction – level 2

Step 2.2.1: Image post processing: After labeling the text candidates in Phase 2.1, border thinning operations are applied for text candidate regions to remove interior pixels. Filling operation is applied next to reduce gaps between pixels in connected components.

Step 2.2.3: Horizontal projection profile: A horizontal projection profile is defined as the sums of the candidate pixels over image rows (Ye et al., 2005). In this step, the small non textual regions are eliminated by using the horizontal projection profile of the result image after post processing. Pixel rows with intensity sum less than an acceptable threshold will be discarded. The threshold is relative to the total intensity mean of the horizontal projection profile of the image. Figure 2 illustrates eliminating small non-text regions by using the image horizontal projection profile. Figure 2(a) shows the image with small non-text regions, while Figure 2(b) shows the horizontal projection profile of the image with a red circle indicating the candidate image regions to be eliminated. The elimination is applied on all small curves indicating tiny intensity sum of row pixels. Figure 2(c) shows the resultant image after non-text elimination using projection profile analysis.

Level 3

Phase 3.1: Labeling the text candidate Regions

The principal objective of this final level is to ensure that all non-text components are eliminated in the image. In this phase, all criteria features studied earlier are examined for each text candidate again for the last time, those features are:

1. Area of the text candidate,
2. Height and width of the text candidate,
3. Intensity mean of the text candidates.

The text candidate area should be greater than 1/10 of the mean area of connected components with acceptable number of pixels, additionally it should not exceed 4 times of the mean area. The width and height of the text candidate should relatively conform to

Figure 1. The proposed algorithm results from Level 1 (a) Original image; (b) Result image after connected component labeling; (c) Result image after text candidates selection; (d) Result image after text extraction - level 1.

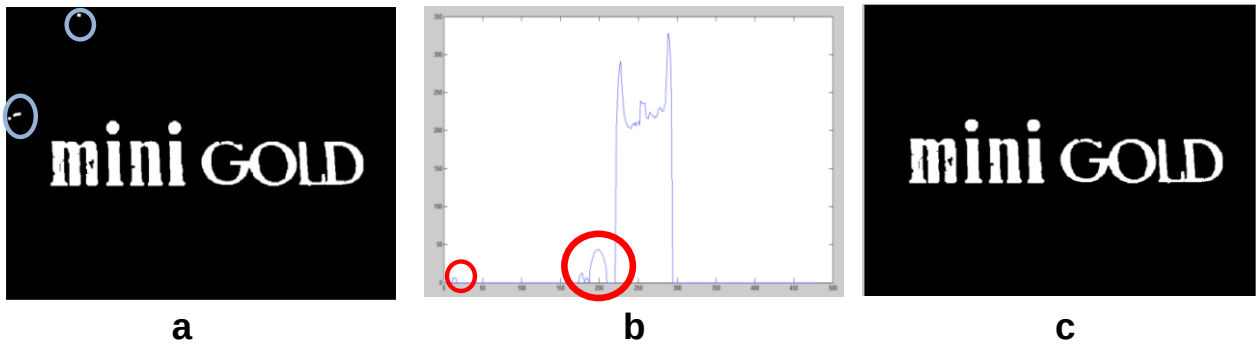

Figure 2. Eliminating small non-text regions by using the image horizontal projection profile (a) Small non-text regions are circled; (b) The horizontal projection profile; (c) Result after non-text elimination.

the English letters rules so that the width should not exceed the height*6 and vice versa. For the intensity mean of text candidate, we eliminated all components with intensity mean greater than 90%, so if the majority of the component texture is white, then the area cannot be a textual region; conversely, it may be a solid region or noise.

Phase 3.2: Final text extraction

After Level 3, the text candidate regions are extracted, and the final textual information in the image is detected. Figure 3 shows a sample final result of the extracted text at the end of this level. All levels, inner phases and steps of the proposed algorithm discussed previously are illustrated in the block diagram shown in Figure 4.

Testing dataset

The selected images from KAIST dataset are used to test the performance of the proposed algorithm (Jin and Seonghun, 2011). This dataset is developed by the Korean Advanced Institute of Science and Technology (KAIST) where the dataset name came from. KAIST dataset consists of scene text images with different properties such as (color, font size, orientation, and alignment) and were captured in five different environments: light, night, shadow, indoor, and outdoor. This dataset is grouped based into the languages: English, Korean, and mixed of English and Korean. Each of these groups is classified according the captured environment condition. All images in the dataset have been resized into 640 × 480. To test the performance of the proposed algorithm, a set of English language scene images have been selected from KAIST set. Testing was based on selecting some scene images with different properties such as (color, font size, orientation, and alignment) and that were captured in different environment.

RESULTS AND DISCUSSION

In this study, proposed text detection algorithm quantitatively and qualitatively were evaluated. The analysis of results is based on various experiments and measurements and is discussed in the subsequent subsection.

Procedure

The performance of the proposed algorithm is evaluated under 50 scene images selected from KAIST dataset with different properties and captured in different environments. The availability of ground truth images in the KAIST dataset provides a better opportunity to compare the proposed algorithm resultant image with the ground truth image quantitatively and qualitatively. An example on a scene image and its ground truth from KAIST dataset is shown in Figure 5.

Selecting optimum values for thresholds used in our algorithm was not an easy task; extensive testing on

Figure 3. The final extracted text.

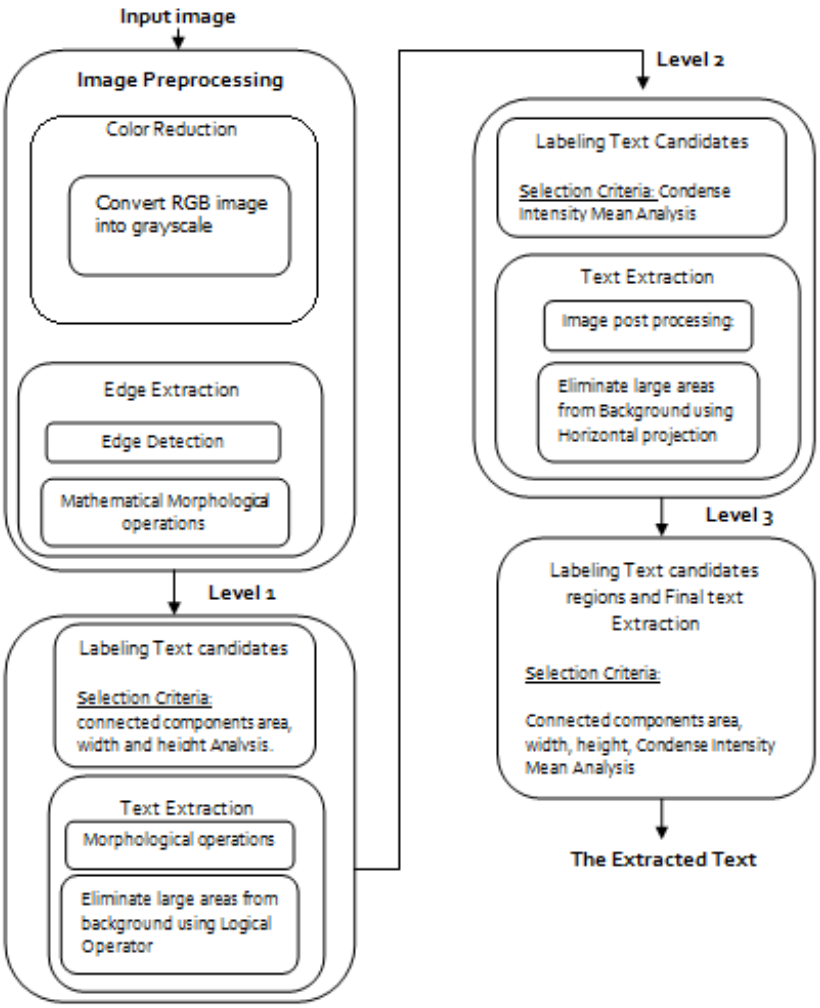

Figure 4. The block diagram for the multilevel text detection algorithm.

Figure 5. A KAIST image and its corresponding ground truth a. The original image; b. Ground truth image.

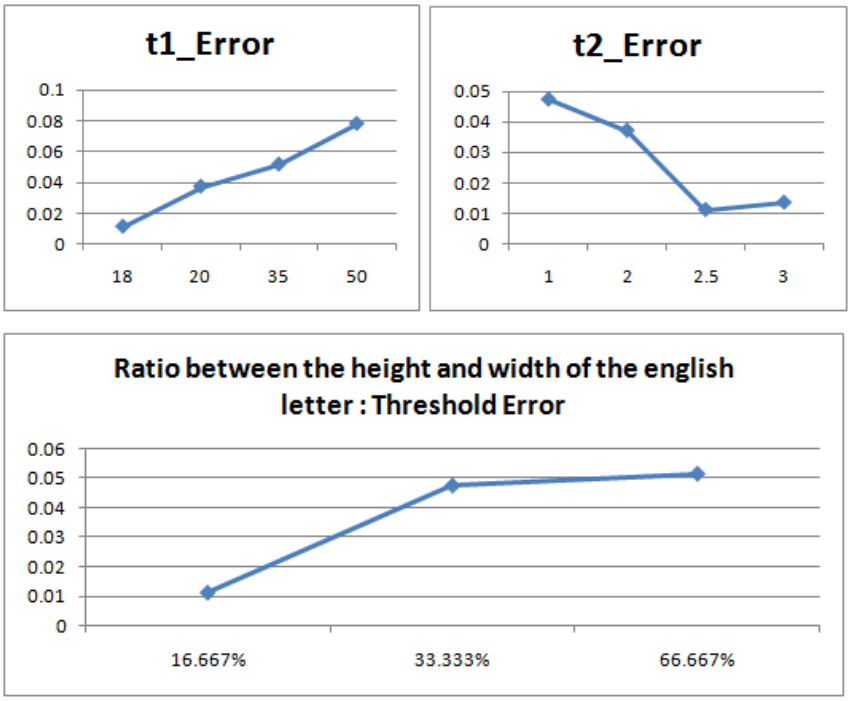

Figure 6. Choosing some thresholds optimum values. The upper charts compare between t1, t2 thresholds probabilities; while the bottom chart compares between threshold probabilities for the ratio between height and width in English letters.

many images had been performed to choose the best value for each one. Figure 6 shows comparisons between the algorithm testing results when applied on one KAIST image with different threshold probabilities. Figure charts compare between error percentages for threshold probabilities. The minimum error values: 18, 2.5 were selected for thresholds, demonstrated previously in this study: t1, t2 respectively. Also, the third chart shows the best threshold for the ratio between height and width for English letters which is 16.667 or 1:6%.

Quantitative metric

The performance of the proposed text extraction algorithm is evaluated quantitatively by calculating three measurement metrics: Precision, Recall, and F-Score. The calculation of these metrics is based on computing the number of corresponding match text between the algorithm's detected text area and the ground truth image. This yields calculating three measurements: true positive *tp*, false positive *fp*, and false negative *fn*. True positive (*tp*) represents the number of pixels that are truly classified as text in the algorithm's detection result, and false positive (*fp*) represents the number of pixels that are falsely classified as text in the algorithm's detection result while it is a background in the ground truth. False negative (*fn*) represents the number of pixels that are falsely classified as background in the algorithm's detection result while it is a text in the ground truth. Based on these measurements, Precision, Recall, and F-Score are calculated as in the following equations:

$$Precision = \frac{tp}{tp + fp} \quad (4)$$

$$Recall = \frac{tp}{tp + fn} \quad (5)$$

$$F - Score = \frac{2 \times Precision \times Recall}{Precision + Recall} \quad (6)$$

Precision value measures the percentage of the correctly detected text from the whole detected text area while the Recall value measures the probability of the text detection algorithm of correctly detecting the text area. F-Score value represents a harmonic mean of the precision and recall to give a single value to measure the effectiveness of the detection results.

Analysis

The proposed text extraction algorithm was improved to resolve the problems encountered in our system proposed

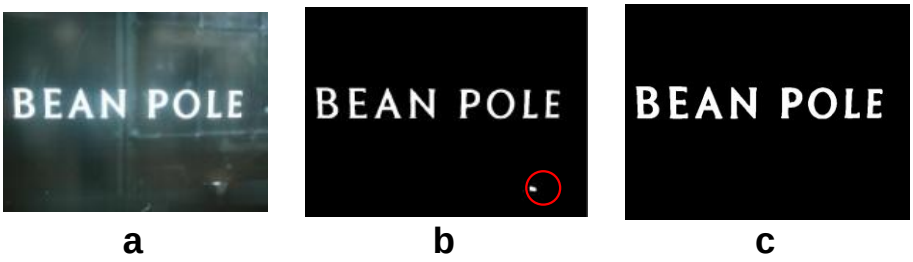

Figure 7. False text detection in the old algorithm and the improvement in the new one a. Original image; b. Lama Rajab et.al (2014) Algorithm; c. Proposed algorithm.

in (Rajab et al., 2014). The previous system presented a connected component-based text extraction technique that employs image enhancement, morphological operations and different transformations such as Hough transform in order to label and extract text candidates. However in this paper, a hybrid multi-level text extraction that uses both connected component-based and texture-based techniques in text candidates' selection was present. The algorithm applies color reduction and edge enhancement on input image followed by three subsequent levels. Each level applies multiple inner phases like connected components labeling and text candidates' selection based on criteria analysis of connected components' area, width, height and intensity mean in addition to image horizontal projection profile analysis.

The old system proved its robustness in text extraction on many images but unfortunately it failed in extracting the text from shadow images and it was detecting the light spot falsely as a text. Figure 7 shows a sample image with a light spot detected as text in the old technique. However, the current Algorithm utilized completely different techniques and presented a novel methodology to improve the performance of text extraction in such images.

The improvement of the current algorithm performance was experimented by testing both algorithms on a set of common images from about 15% of the overall test set. The precision, Recall and F_score values of the proposed algorithm for this set of images are 0.868, 0.991, 0.924, respectively, while they are 0.853, 0.955 and 0.889, respectively for algorithm (Rajab et al., 2014). Comparisons between these metrics for both algorithms are shown in the chart (Figure 8).

Relatively to the comparative analysis above, the effectiveness of the proposed text extraction algorithm is tested also individually on fifty selected scene images from KAIST dataset that have different properties and were captured in different environments. The results under five different environments: indoor, outdoor, light, night, and shadow are shown in Figure 9; two images were selected from each environment.

Obviously, the detection results from the proposed technique are very accurate and robust in detecting text from scene images that have different properties such as font size and type, color, orientation, and alignment. Moreover, the proposed algorithm detects the text accurately from images that have been affected to strong light or those which have dark or bright illumination spots (Figure 9c and d). It also detects the large characters accurately as well as the small ones in both indoor and outdoor environments (Figure 9a and i), as well as in images which have shadow areas as in Figure 9g and h. Moreover, it proved to be robust and effective in detecting images with curved texts (Figure 9b).

As stated previously, the performance of the proposed technique is evaluated quantitatively using three metrics: Precision, Recall, and F-Score that obtained from comparing the output image from the proposed algorithm with the ground truth. These three measurements are calculated for 50 images that were selected from KAIST dataset. The average of Precision, Recall, and F-Score on this set consisting of fifty KAIST images is 90.1, 99, and 94.3%, respectively.

Noticeably, the average of the Recall metric is very high (99%) due to the high probability of our text detection algorithm of correctly detecting the text area in the scene image and this is obvious in the Figure. As a result, our proposed algorithm is robust and consistent under the different environments and under variant properties.

Unfortunately in some cases, the algorithm detects some small areas falsely if they have similar properties to texts. Therefore, the algorithm will label these background areas as candidate text regions which will be detected as textual contents in the further steps. Thus, the existence of some small areas which are similar to text properties will decrease the precision since these areas were extracted falsely to be texts while they are in fact background areas as we can see in Figure 9b, e, and h, and that affects the value of Precision metric.

Conclusion

Text extraction in scene images is a significant and promising research area in computer vision. In this paper, we propose a new and improved multilevel and hybrid algorithm that can detect and extract the textual content

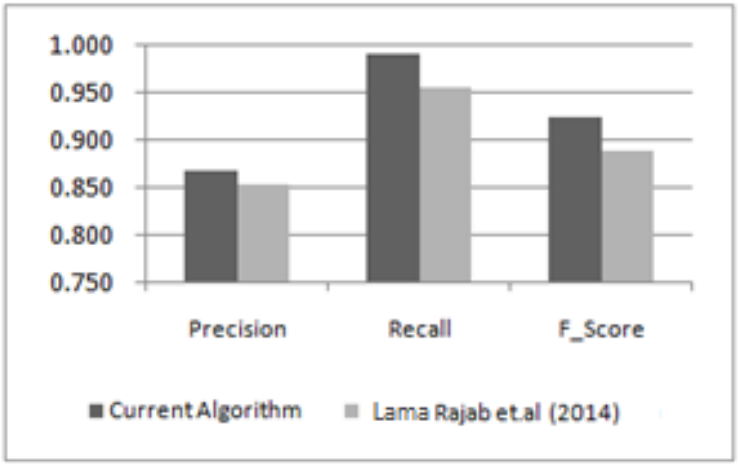

Figure 8. Comparisons of Precision, Recall and F_Score between both: our new and old techniques.

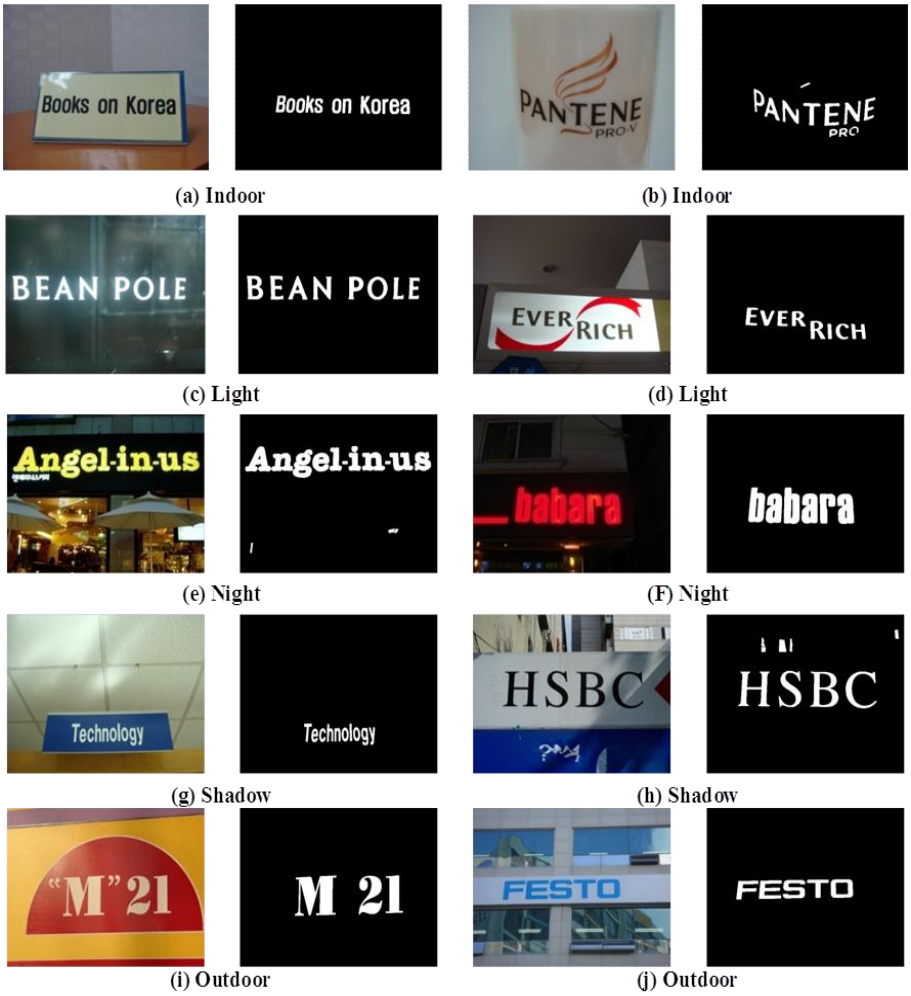

Figure 9. Set of images from KAIST dataset with detected text area using the proposed technique. (a) and (b) were captured on a indoor environment. (c) and (d) were captured on light. (e) and (f) were captured on night environment. (g) and (h) are two images that were captured at shadow. (i) and (j) are two images that were captured at outdoor.

in various scene images. The algorithm uses both connected component-based and texture-based techniques in text candidates' selection. The improvement is represented by using a hybrid multilevel detection method with subsequent multi phases in order to extract the text progressively. We have anticipated through the proposed algorithm to resolve problems that our some previous systems had in text extraction field.

In the preprocessing step, the algorithm used the grayscale version from the RGB image and then applied edge extraction on the resultant image. Various techniques in three subsequent levels are applied after preprocessing such as connected component labeling, text candidate selection with different criteria testing, morphological operations, and projection profile based technique for non-text regions elimination. As a result, candidate text areas will be labeled, detected and extracted in a multi layer behavior in inner phases.

The effectiveness of the proposed technique is tested on 50 images from KAIST dataset that were captured in different environments (shadow, light, outdoor, indoor, and night). Precision, Recall, and F-Score metrics are used to test the accuracy of the text detection rate for the proposed technique quantitatively. The results show that the proposed algorithm detects the text with high average of Precision, Recall, and F-Score to be 90.1, 99, and 94.3%, respectively. The algorithm also proved to be robust and consistent in terms of detecting the textual content from scene images that have various properties and which were captured in different environments.

Conflict of Interest

The authors have not declared any conflict of interest.

REFERENCES

Jain AK, Zhong Y (1996). Page segmentation using texture analysis. Pattern Recognition 29(5):743-770. DOI: 10.1016/0031-3203(95)00131-X

Chandrasekaran R, Chandrasekaran RM (2011). Morphology based Text Extraction in Images. Int. J. Comput. Sci. Technol. 2:4.

Choksi A, Desai N, Chauhan A, Revdiwala V, Patel K (2013). Text Extraction from Natural Scene Images using Prewitt Edge Detection Method. Int. J. Adv. Res. Comput. Sci. Software Eng. 3:12 DOI 10.1007/11595755_59.

Cui Y, Huang Q (1997). Character extraction of license plates from video. In Computer Vision and Pattern Recognition, Proceedings IEEE Computer Society Conference. pp. 502-507. DOI :10.1109/CVPR.1997.609372

Kim DS, Chien SI (2001). Automatic car license plate extraction using modified generalized symmetry transform and image warping. In Industrial Electronics, 2001. Proceedings. ISIE 2001. IEEE International Symposium 3:2022-2027. DOI:10.1109/ISIE.2001.932025

Fu H, Liu X, Jia Y (2006). Maximum-Minimum similarity training for text extraction, King et al. (Eds.): ICONIP 2006, Part III, LNCS 4234:268-277. DOI: 10.1007/11893295_31.

Gatos B, Pratikakis I, Perantonis S (2005). Towards text recognition in natural scene images. Proc. Int. Conf. Automation Technol. pp. 354-359, doi:10.1.1.76.9618

Jin HK, Seonghun L (2011) http://www.iapr-tc11.org/mediawiki/index.php/KAIST_Scene_Text_Database accessed on (2014-07)

Jung K, Han J (2004). Hybrid approach to efficient text extraction in complex color images. Pattern Recognit. Lett. 25(6):679-699. DOI:10.1016/j.patrec.2004.01.017.

Jung, K, Kim K, Jain KA (2004). Text information extraction in images and video: A survey. Pattern recognit. 37(5):977-997. http://dx.doi.org/10.1016/j.patcog.2003.10.012.

Lama R, Mohammad H, Karajeh H, Al Khatib T (2014). An improved text extraction technique based on linear transformation. Life Sci. J. 11(7):83-88.

Leon M, Vilaplana V, Gasull A, Marques F (2010). Region-based caption text extraction. In Image Analysis for Multimedia Interactive Services (WIAMIS), 2010 11th International Workshop on IEEE. ISBN: 978-1-4244-7848-4. pp. 1-4.

Mancas-Thillou C, Gosselin B (2006). Natural scene text understanding. na. Vision Systems: Segmentation and Pattern Recognition, Goro Obinata and Ashish Dutta (Ed.), ISBN: 978-3-902613-05-9, In Tech, DOI: 10.5772/4966. Available from: http://www.intechopen.com/books/vision_systems_segmentation_and_pattern_recognition/natural_scene_text_understanding

Mao J, Li H, Zhou W, Yan S, Tian Q (2013). Scale based region growing for scene text detection. Proceedings of the 21st ACM international conference on Multimedia ACM Multimedia, pp.1007-1016 , DOI:10.1145/2502081.2502108.

Niti S, Naresh K, (2014).Text extraction in images using dwt, gradient method and svm classifier. Int. J. Emerging Technol. Adv. Eng. 4:6 ISSN 2250-2459, ISO 9001:2008 Certified Journal.

Pan Y, Hou X, Liu C (2009). Text Localization in Natural Scene Images based on conditional Random Field .10th International Conference on Document Analysis and Recognition. DOI 10.1109/ICDAR.2009.97

Shim J, Dorai C, Bolle R (1998). Automatic text extraction from video for content-based annotation and retrieval. Proc. Int. Conf. Pattern Recognit. (1):618-620. DOI: 10.1109/ICPR.1998.711219

Shivakumara P, Kumar NV, Guru DS, Tan CL (2014). Separation of Graphics (Superimposed) and Scene Text in Video Frames. In Document Analysis Systems (DAS), 2014 11th IAPR International Workshop on IEEE. pp. 344-348. DOI :10.1109/DAS.2014.20.

Sumathi C, Santhanam T, Gayathri G (2012). A survey on various approaches of text extraction in images. Int. J. Comput. Sci. Eng. Survey. 3:4. DOI: 10.5121/ijcses.2012.3403.

Tang Y, Lee S, Suen C (1996). Automatic document processing: A Survey. Pattern Recognit. 29(12):1931-1952. DOI: 10.1016/S0031-3203(96)00044-1.

Xiaoqing L, Jagath S (2006). Multiscale edge-based text extraction from complex images. Conference: Proceedings of the 2006 IEEE International Conference on Multimedia and Expo, Toronto, Ontario, Canada. DOI: 10.1109/ICME.2006.262882

Ye Q, Huang Q, Gao W, Zhao D (2005). Fast and robust text detection in images and video frames. Image Vision Comput. 23(6):565-576. DOI: 10.1145/1101149.1101250

Yu B, Jain AK, Mohiuddin M (1997). Address block location on complex mail pieces. In Document Analysis and Recognition, Proceedings of the Fourth International Conference on IEEE. 2:897-901. DOI: 10.1109/ICDAR.1997.620641.

Zhang D, Chang S (2003). Accurate overlay text extraction for digital video analysis, in international conference on information technology: Research and Education (ITRE) DOI:10.1.1.134.7724

Zhang H, Gong Y, Smoliar SW, Tan SY (1994). Automatic parsing of news video. In Multimedia Computing and Systems. Proc. Int. Conf. IEEE. pp. 5-54. DOI :10.1109/MMCS.1994.292432.

academicJournals

Vol. 10(3), pp. 114-119, 15 February, 2015
DOI: 10.5897/SRE2014.6135
Article Number:8BFC61550373
ISSN 1992-2248
Copyright©2015
Author(s) retain the copyright of this article
http://www.academicjournals.org/SRE

Scientific Research and Essays

Full Length Research Paper

Ultrastructural changes in the neuronal superior colliculus in the early stage of streptozotocin-induced diabetes mellitus in rats

Tosawan Upachit, Passara Lanlua and Sirinush Sricharoenvej*

Prannok Road, Department of Anatomy, Faculty of Medicine Siriraj Hospital, Mahidol University, Bangkoknoi, Bangkok 10700, Thailand.

Received 20 November, 2014; Accepted 5 February, 2015

The superior colliculus (SC) is a visuomotor center involved in the autonomic reflex adjustments of eye movements in response to visual stimuli. Diabetes mellitus (DM) is known to affect some visual pathway structures, but few studies have assessed the effects of diabetes on the SC. The aim of this study was to investigate the ultrastructural changes of SC neurons in the early period of streptozotocin (STZ)-induced diabetes. The ultrastructure was assessed by transmission electron microscopy (TEM). Twenty male Sprague–Dawley rats were divided into two groups (n=10 per group) and were intraperitoneally injected with either STZ (60 mg/kg) in citrate buffer (pH 4.5) to induce DM or with buffer alone as a positive control. The rats were sacrificed 4 weeks after injection and the SC was processed for TEM. Most of the SC neurons in the DM group exhibited either chromatolysis or pyknosis. Chromatolytic neurons had an enlarged nucleus with some chromatin clumping and disruption of the cell membrane. These neurons also exhibited mitochondrial enlargement with rupture of the cristae, distended Golgi complexes and rough endoplasmic reticulum, and numerous secondary lysosomes. By contrast, the pyknotic neurons in the DM group exhibited severe chromatic condensation and dark electron-dense structures in the cytoplasm. The organelles were smaller and had an irregular outline. The neuropil of DM rats had coarse, irregular, swollen dendrites and axons, together with demyelination. In conclusion, this study has provided clear evidence of ultrastructural degeneration in the SC of STZ-induced DM rats. These ultrastructural changes might contribute to the impairments of autonomic eye movement, optokinetic and vestibulo-ocular reflexes, and vision-related learning and memory in patients with DM.

Key words: Superior colliculus, diabetes mellitus, streptozotocin.

INTRODUCTION

The superior colliculus (SC) is an important visuomotor center that controls and adjusts eye movement in response to environmental stimuli, and is influential in automatic perceptual visual function. The SC is the laminar structure located in the midbrain. It consists of alternating neurons and nerve fiber layers, which are

*Corresponding author. E-mail: sirinush.sri@mahidol.ac.th, Tel: +66-2-419-8592. Fax: +66-2-419-8523.
Author(s) agree that this article remain permanently open access under the terms of the Creative Commons Attribution License 4.0 International License

divided into two functional parts: the superficial layer and intermediate and deep layers (May, 2006). The superficial layer receives incoming optic signals from the retinas and the visual cortex. The many variously sized and shaped neurons in this layer receive visual inputs and transmit signals to neurons in the deeper sublayers to integrate the autonomic eye movement reflexes. The intermediate and deep layers of the SC are involved in eye movement, by receiving visual input signals from the superficial layers and afferent projections of several systems related to autonomic eye movement reflexes, including the optokinetic and vestibulo-ocular reflexes (May, 2006).

Diabetes mellitus (DM) is one of the most common chronic metabolic disorders, and affects more than 285 million people worldwide. Prolonged hyperglycemia caused by insulin insufficiency (type 1 DM or insulin-dependent DM) or insulin resistance (type 2 DM or non-insulin-dependent DM) also affect the metabolism of carbohydrate, protein, and lipid (Zhang, 2008). DM is associated with a number of complications, some of which affect components of the nervous system, including visual function. Visual loss, blurred vision, visual defects, and impaired visual acuity are commonly found in patients with DM (Negi and Vernon, 2003). There are also numerous reports of early visual neuronal abnormalities in DM, including histological, physiological, and clinical abnormalities (Antonetti, 2006; Ozawa, 2011). To date, however, few studies have focused on the efferent visual pathways involved in ocular motility and visual reflexes. Prior studies have revealed prolonged reaction times and slower eye movement reflexes, including the loss of eye fixation and gaze shift problem, which are controlled by the SC, in patients with DM (Virtaniemi, 1993; Alessandrini, 1999). Consequently, patients with these visual impairments have difficulties performing daily-life activities, complex task activities, learning, and cognition (Sanders and Gillig, 2009). Therefore, the aim of this study was to assess the ultrastructural changes in the SC in streptozotocin (STZ)-induced diabetic rats using transmission electron microscopy (TEM). So that, the hypothesis of this study was to demonstrate degeneration of neurons and nerve fibers in the SC. These damages will cause the impairment of the eye movement and reflexes in the diabetic patients.

MATERIALS AND METHODS

Twenty male adult Sprague–Dawley rats aged 5 to 8 weeks, weighing 200 to 270 g, were obtained from the National Laboratory Animal Center, Mahidol University, Salaya, Nakhonpathom. The Mahidol University Council's Criteria for Care and Use of Laboratory Animal was adhered to in this study. After acclimatization, the animals were divided into two groups, a DM (n = 10) and a positive control (n = 10) groups.

Rats in the DM group were intraperitoneally injected with a single dose of STZ (60 mg/kg body weight; Across Organics, Janssen Pharmaceuticals, Geel, Belgium) in citrate buffer at pH 4.5. Rats in the positive control group were injected with an equal volume of buffer per kilogram body weight. After a 10 h fast, the urine glucose levels and body weights were monitored daily. Whole-blood glucose levels were measured at 48 and 72 h after injection, and before sacrifice. The animals were sacrificed 4 weeks after injection, corresponding to the early period of DM by halothane inhalation.

The ultrastructural technique was described as in the previous studies (Lanlua, 2012; Sricharoenvej, 2012). After cutting the rib cage to expose the thoracic cavity, 0.1 M phosphate-buffered saline (PBS) was injected into the ascending aorta, and 500 ml of 2.5% glutaraldehyde in 0.1 M PBS was injected to preserve the tissues. Then, the SC was removed and cut into small cubes of about 1 mm^3. These specimens were postfixed in 1% osmium tetroxide in 0.1 M PBS, dehydrated in a graded series of ethanol, cleared in propylene oxide, and soaked in propylene oxide: araldite plastic. The specimens were then embedded in the araldite plastic. The tissue blocks were then sectioned on an ultramicrotome (Leica EM UC6; Leica Microsystems, Vienna, Austria). Semi-thin sections (1–1.5 µm) were stained with toluidine blue and representative areas were observed under a light microscope (Olympus BX41; Olympus, Tokyo, Japan). Next, the embedded specimens containing neurons were serially sectioned (80 to 85 nm thick) using the ultramicrotome and the thin serial sections were stained with 1% uranyl acetate and lead citrate. The neuronal ultrastructure on each SC tissue section was observed and photographed by TEM (JEOL JEM100S; JEOL Ltd., Tokyo, Japan).

Statistic analysis

Quantitative analysis of body weights in each group was expressed as a mean ± a standard deviation (SD). The comparison on the body weights of the positive control and the diabetic groups was performed by using Mann-Whitney U test (SPSS 16.0 software). The value of $p<0.05$ was considered to indicate statistical significance.

RESULTS

At 48 h after injection of STZ in the DM, the mean urine glucose concentration was > 500 mg/dL and the mean whole-blood glucose concentration was > 300 mg/dL, while those in the control were 0 and <300 mg/dL. The body weight was significantly lower in the DM group (256.43 ± 14.07 g) than in the control group (372.33 ± 11.64, $p< 0.05$).

TEM revealed that the ultrastructures of all layers of the SC in the control group were similar in appearance. The normal neurons had large, round, electron lucent nuclei with evenly dispersed fine chromatins and a large dense nucleolus. The nuclear membrane was generally smooth, although some membranes were wrinkled or invaginated. Numerous organelles were concentrically arranged around the nucleus (Figure 1A). By contrast, there were several changes in the neurons in all of the layers of the SC in the DM group. In this group, the neurons in each of the layers exhibited two major degenerative features: chromatolysis or pyknosis. The chromatolytic neurons were enlarged compared with the control neurons. Although most of the nuclear membranes of DM neurons were intact, the chromatin particles were distributed and

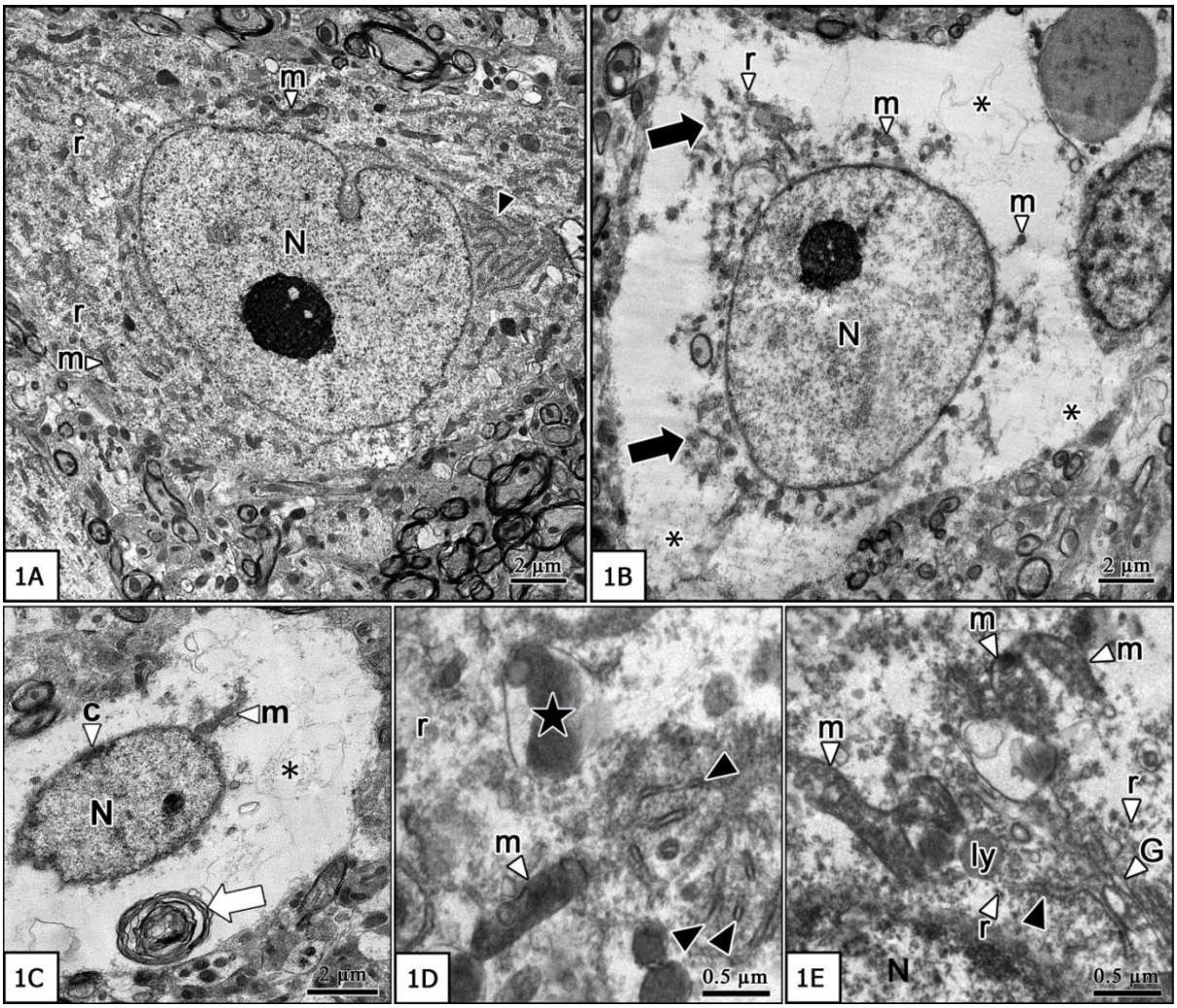

Figure 1. Transmission electron micrographs of SC cross-sections in the control (A) and DM (B–E) groups. Nucleus (N), mitochondria (m), rER (black arrowhead), ribosomes (r), unidentified particles aggregated around the nucleus (black arrows), empty peripheral areas (asterisks), chromatin clumping (C),a large membrane-bound vacuole (a white arrow), Golgi complex (G), primary lysosome (Ly), and a secondary lysosome (a black star).

often formed clumps beneath the nuclear membrane (Figures 1B, C and 2A). Regarding cytoplasmic changes, the SC neurons displayed a loss of organelles, including ribosomes, rough endoplasmic reticulum (rER), and mitochondria in the peripheral area of the perikaryon. The cell organelles also formed clusters around the nucleus (Figures 1B, C and 2A). At higher magnifications, rupture of the rER with short cisternae or small fragments, as well as ribosomal disintegration were also seen. Moreover, enlarged mitochondria with disrupted cristae or ruptured outer membranes were illustrated (Figures 1D and E). Distension of the Golgi complex was also clearly noticed (Figure 1E). Numerous, small secondary lysosomes with dark contents were visible in the cytoplasm (Figure 1D). Large membrane-bound vacuoles, containing a membranous structure, were also observed in the degenerated neurons (Figure 1C).

The second type of neurons in the DM group was pyknotic neurons. These neurons were dark, electron-dense cells with significant abnormalities of the nucleus and cytoplasm. The nuclei and organelles of these neurons were poorly defined, small, and had irregular outlines (Figure 2B). Moreover, the normal neuropils contained several neuronal and glial processes, including dendrites, myelinated axons, and unmyelinated axons (Figure 3A). Both types of axons contained abundant neurofilaments and microtubules, with long and extremely slender mitochondria, but rER and free ribosomes were not observed (Figure 3C). The neurons had enlarged dendrites containing vacuoles with electron-lucent regions (Figures 3B, D and E). The neurofilaments and microtubules were irregularly arranged and the cytoplasmic mitochondria were enlarged (Figures 3D and E). Demyelination was also apparent in the enlarged

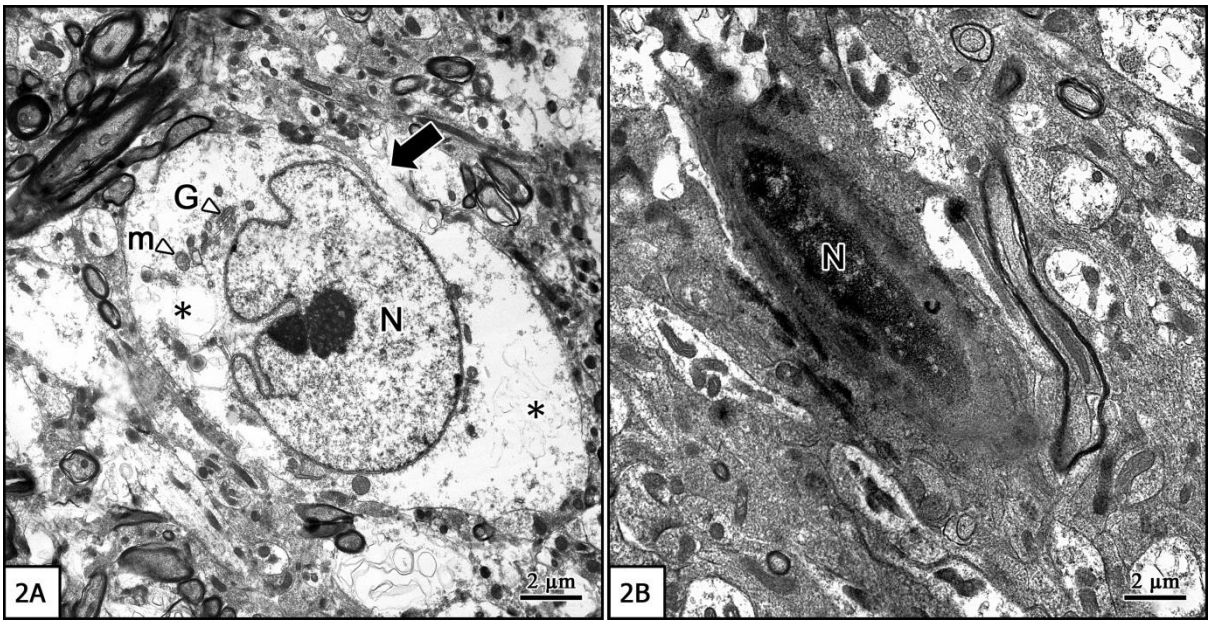

Figure 2. Transmission electron micrographs of chromatolytic neurons (A) and pyknotic neurons (B) in SC cross-sections in the DM group. Nucleus (N), mitochondria (m), Golgi complex (G), clear empty peripheral area (asterisks), and ruptured cell membrane (a black arrow).

neuropils (Figures 3B, D and E). The myelinated axons exhibited localized disarrangement of the myelin sheath, and of neurofilaments and microtubules in the axon cytoplasm (Figures 3D and E).

DISCUSSION

The STZ was used to induce the DM because of the selective destruction of pancreatic beta cells and inhibition of insulin synthesis. Therefore, hyperglycemia occurs due to insulin deficiency (Anderson, 1974; Junod, 1967; Yamamoto, 1981). The most common diabetic complication, which is caused by prolonged hyperglycemia, is microangiopathy. Then, the destruction of vascular wall and reduction of blood supply occur, that affects on the nervous system (Huber, 2006; Li, 1998). The degenerative SC neurons in DM rats in the present study could be classified into two types; chromatolytic and pyknotic neurons. Features of the chromatolytic neurons included enlargement, slight condensation of chromatin in the nucleus, clear cytoplasm with distended cell organelles, and destruction of the neurofilaments. Similar features were observed in the hypothalamic and dorsal motor nuclei of the vagus nerve neurons in previous studies of neurodegeneration (Bestetti and Rossi, 1980; Tay and Wong, 1994). Hyperglycemia in the diabetic state increases the accumulation of glutamate in the extracellular matrix, leading to glutamate excitotoxicity. Glutamate is taken up by neurons via *N*-methyl-D-aspartate (NMDA) and non-*N*-methyl-D-aspartate (non-NMDA) receptors (Portera-cailliau, 1997; Schurr and Payne, 2003). Binding of glutamate to NMDA induces chromatolysis by stimulating cellular intake of calcium ions (Ca^{2+}) that is released from the ER. The accumulation of Ca^{2+} near the cell membrane increases water influx into the neurons (Berridge, 1998) causing cell enlargement with a clear peripheral cytoplasm. Intracellular Ca^{2+}also acts as a second messenger to stimulate protease, lipase, and endonuclease activities (Sundaram, 2012). Intracellular Ca^{2+} also increases the nitric oxide (NO) concentration (Berridge, 1998). Elevated NO and Ca^{2+}concentrations in the mitochondria activate G-proteins, which stimulates the Ras and mitogen-activated protein kinases (MAPK) pathway. MAPK enters the nucleus, where it activates extracellular signal-regulated kinases, FOS, and Ced-3. This signaling pathway promotes the synthesis of proteases, endonucleases and phospholipases, such as calpain and caspase-3, which ultimately degrade the neurofilaments in axons and dendrites (Sundaram, 2012).

Hyperglycemia also increases the generation of reactive oxygen species (ROS), which activate and release cytochrome C from mitochondria to the cytoplasm. Cytochrome C stimulates the expression of caspase-3 (Davi, 2005), which increases the synthesis of endonucleases to cleave DNA, causing chromatin condensation (Huppertz, 1999). High levels of ROS also cause lipid peroxidation of unsaturated fatty acids in the lipid bilayers of cell and organelle membranes. This increases the permeability of the cell's outer membrane, as well as the membranes of the rER, Golgi complex, and

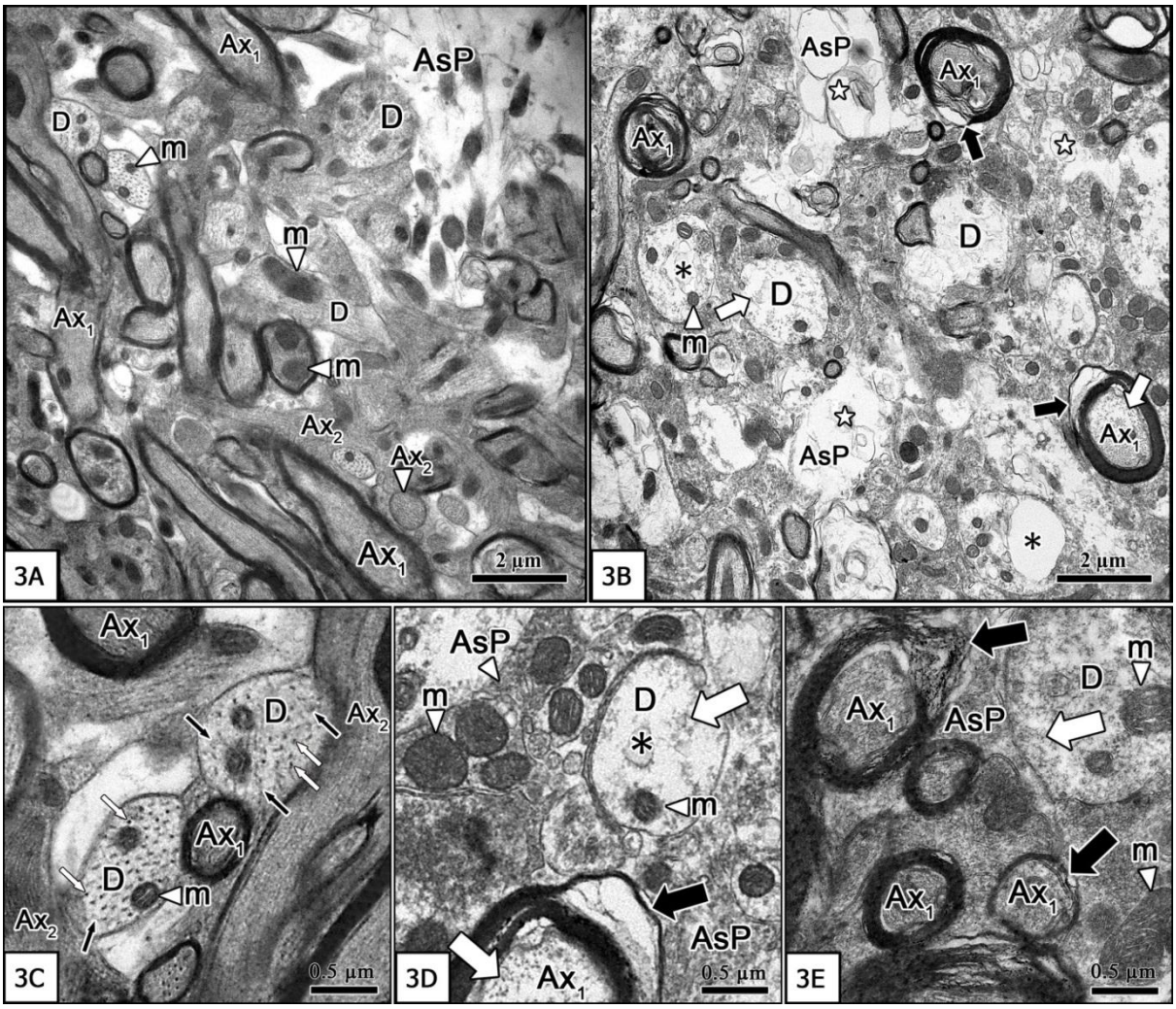

Figure 3. Transmission electron micrographs of SC cross-sections in the control (A,C) and DM (B,D, E) groups. Dendrites (D), myelinated axons (Ax1), unmyelinated axons (Ax2), mitochondria (m), astrocytic process (AsP), vacuolated appearances (asterisks), local disarrangement of myelin sheath (black arrows), degenerations of neurofilaments and microtubules (white arrows), large electron-lucent vacuoles (stars), microtubules (small white arrows), and neurofilaments (small black arrows).

mitochondria. The resulting influx of water causes enlargement of the neurons and cell organelles (Davi, 2005).

Numerous degenerated fragments of organelles in small lysosomes (autophagic membrane-bound vacuoles) in the neurons were observed because of the activity of hydrolytic enzymes. Some secondary lysosomes also contain degenerated membranous organelles, such as mitochondria, which form a concentric pattern known as the myelin figure. These myelin figures have been observed in anoxic-ischemic condition, in cells exposed to potent pro-apoptotic chemicals, and in the diabetic state (Park, 2003; Lanlua, 2012).

Other degenerative features of SC neurons in DM rats were chromatin condensation, cytoplasmic condensation with unidentified cell organelles, and cell shrinkage. These features were consistent with pyknosis or apoptosis, which were observed in previous studies of Park (2003) and Logvinov (2010). As mentioned above, glutamate accumulates in the extracellular matrix. Through an as-yet unknown mechanism, binding of glutamate to non-NMDA receptors increases the mitochondrial Ca^{2+}concentration (Saliñska, 2005). Intracellular Ca^{2+} also upregulates the expression of endonucleases, proteinases, and phospholipases, which leads to degradation of chromatin, rER, Golgi complex, cell membrane, and cytoskeleton in the neurons, as occurs in chromatolysis. These processes result in chromatin condensation and the destruction of cell organelles causes cytoplasmic condensation.

It is also notable that the levels of neurotrophic factors,

such as insulin, insulin-like growth factor-1, neurotrophin-3, and their corresponding receptors are lower in the diabetic state (Lee, 2001; Li, 2005). The changes in these signaling pathways leads to mitochondrial dysfunction, and promote the release of cytochrome C. Cytochrome C stimulates the production of endonucleases, which are responsible for DNA cleavage (Huppertz, 1999). Therefore, cell shrinkage occurs through a variety of processes involving the destruction of the cell membrane, cytoskeleton, and cell organelles.

In conclusion, the results of this study provide clear evidence for significant ultrastructural changes in SC neurons at the early stage of DM in rats. These changes are expected to contribute to the early neurodegenerative changes in the central nervous system in DM. These changes may also contribute to the visual impairments in DM, including autonomic eye movement, optokinetic reflexes, vestibulo-ocular reflexes, and vision-related learning and memory. The present results should provide a foundation for further research to develop therapeutic approaches to prevent or reduce the severity of nervous system disorders affecting vision and related processes that might improve the quality of life of patients with DM.

Conflict of Interest

The authors have not declared any conflict of interest.

ACKNOWLEDGMENTS

This study was supported by a Siriraj Graduate Thesis Scholarship, 2011, and the Chalermprakiet Fund from the Faculty of Medicine, Siriraj Hospital, Mahidol University.

REFERENCES

Alessandrini M, Parisi V, Bruno E, Giacomini PG (1999). Impaired saccadic eye movement in diabetic patients: the relationship with visual pathways function. Doc. Opthalmol. 99(1):11-20.

Anderson T, Schein PS, McMenamin MG, Cooney DA (1974). Streptozotocin diabetes correlation with extent of depression of pancreatic islet nicotinamide adenine dinucleotide. J. Clin. Invest. 54(3):672-677.

Antonetti D, Barber A, Bronson S, Freeman W, Gardner T, Jefferson L, Kester M, Kimball S, Krady J, LaNoue K, Norbury C, Quinn G, Sandirasegarane L, Simpson I (2006). Perspectives in diabetes: diabetic retinopathy seeing beyond glucose-induced microvascular disease. Diabetes 55:2401-2411.

Berridge M (1998). Neuronal calcium signaling. Neuron 21: 13-26.

Bestetti G, Rossi G (1980). Hypothalamic lesion in rats with long-term streptozotocin-induced diabetes mellitus. Acta Neuropathol. 52:119-127.

Davi G, Falco A, Patrono C (2005). Lipid peroxidation in diabetes mellitus. Antioxid. Redox Signal. 7(1-2):256-268.

Huber JD, VanGilder RL, Houser KA (2006). Streptozotocin-induced diabetes progressively increases blood-brain barrier permeability in specific brain regions in rats. Am. J. Physiol. Heart Circ. Physiol. 291:H2660-H2668.

Huppertz B, Frank HG, Kaufmann P (1999). The apoptosis cascade-morphological and immunohistochemical methods for its visualization. Anat. Embryol. 200(1):1-18.

Junod A, Lambert AE, Orci L, Pictet R, Gonet AE, Renold AE (1967). Studies of the diabetogenic action of streptozotocin. Proc. Soc. Exp. Biol. Med. 126(1):201-205.

Lanlua P, Chotimol P, Sricharoenvej S, Baimai S, Piyawinijwong S (2012). Cardiac ultrastructure in streptozotocin-induced diabetic rats. Siriraj Med. J. 64(Suppl1):49-53.

Lee PG, Hohman TC, Cai F, Regalia J, Helke CJ (2001). Streptozotocin-induced diabetes causes metabolic changes and alterations in neurotrophin content and retrograde transport in the cervical vagus nerve. Exp. Neurol. 170:149-161.

Li C, Li PA, He QP, Ouyang YB, Siesjo BK (1998). Effects of streptozotocin-induced hyperglycemia on brain damage following transient ischemia. Neurobiol. Dis. 5:117-128.

Li ZG, Zhang W, Sima A (2005). The role of impaired insulin/IGF action in primary diabetic encephalopathy. Brain Res. 1037:12-24.

Logvinov V, Plotnikov B, Zhdankina A, Smolyakova L, Ivanov S, Kuchin V, Chukicheva V, Varakuta Y (2010). Morphological changes in retinal neurons in STZ-induced DM and their correlation with an isobornylphenol derivative. Neurosci. Behav. Physiol.40(7):779-782.

May P (2006). The mammalian superior colliculus: laminar structure and connections. Prog. Brain Res. 151:321-378.

Negi A, Vernon S (2003). An overview of the eye in diabetes. J. R. Soc. Med. 96:266-272.

Ozawa Y, Kurihara T, Sasaki M, Ban N, Yuki K, Kubota S, Tsubota K (2011).Neural degeneration in the retina of the streptozotocin-induced type 1 diabetes model. Exp. Diabetes Res. pp. 1-7.

Park SH, Park JW, Park SJ, Kim KY, Chung JW, Chun MH, Oh SJ (2003). Apoptotic death of photoreceptors in the streptozotocin-induced diabetic rat retina. Diabetologia 46:1260-1268.

Portera-cailliau P, Price D, Martin L (1997). Non-NMDA and NMDA receptor- mediated excitotoxic neuronal deaths in adult brain are morphologically distinct: further evidence for apoptosis-necrosis continuum. J. Comp. Neurol. 378:70-87

Saliñska E, Danysz W, £azarewicz JW (2005). The role of excitotoxicity in neurodegeneration. Folia Neuropathol. 43(4):322-339.

Sanders RD, Gillig PM (2009). Cranial nerves III, IV, and VI: oculomotor function. Psychiatry 6(11):34-39.

Schurr A, Payne RS (2003). Hyperglycemia and neuronal damage in cerebral ischemia and beyond. Crit. Care Shock 6(4):184-190.

Sricharoenvej S, Siratechawiwat A, Lanlua P, Niyomchan A, Baimai S (2012). Ultrastructural changes of hepatic stellate cells in streptozotocin-induced diabetic rats. Siriraj Med. J. 64(Suppl1): S45-S48.

Sundaram RS, Gowtham L, Manikandan P, Venugopal V, Kamalakannan D (2012). Neuronal apoptosis and necrosis: role of excitotoxins, calcium, oxidative stress. Int. J. Res. Pharm. Biomed. Sci. 3(2):567-575.

Tay S, Wong W (1994). Short-and long-term effects of streptozotocin-induced diabetes on the dorsal motor nucleus of the vagus nerve in the rat. Acta Anat.150:274-281.

Virtaniemi J, Laakso M, Nuutinen J, Karjalinen S, Vartiainen E (1993). Voluntary eye movement test in patients with insulin-dependent diabetes mellitus. Acta Otolarigol. 113:123-127.

Yamamoto H, Uchigata Y, Okamoto H (1981). Streptozotocin and alloxan induce DNA strand breaks and poly (ADP-ribose) synthetase in pancreatic islets. Nature. 294:284-286.

Zhang X, Gregg EW, Cheng YJ, Thompson TJ, Geiss LS, Duenas MR, Saaddine JB (2008). Diabetes mellitus and visual impairment: national health and nutrition examination survey, 1999-2004. Arch. Ophthalmol. 126(10):1421-1427.

academicJournals

Vol. 10(3), pp. 120-126, 15 February, 2015
DOI: 10.5897/SRE2013.5753
Article Number:378E0F050379
ISSN 1992-2248
Copyright©2015
Author(s) retain the copyright of this article
http://www.academicjournals.org/SRE

Scientific Research and Essays

Full Length Research Paper

Determination of the priority areas for the rehabilitation of degraded forest lands

Ali İhsan KADIOĞULLARI[1]* and İbrahim TURNA[2]

[1]Discipline of Forest Management, Faculty of Forestry, Karadeniz Technical University, 61080, Trabzon-Turkey.
[2]Discipline of Silviculture, Faculty of Forestry, Karadeniz Technical University, 61080, Trabzon-Turkey.

Received 24 November 2013; Accepted 6 December, 2013

Turkey has more than 21.67 million ha forest areas and 10.11 million ha of these forest areas are still degraded or highly degraded in 2012 year. These areas can only be transformed into a productive state with implementation of rehabilitation treatments. Determination of the priority of degraded forest areas for the rehabilitation is important issue and affected by many parameters in Turkey. Some important indicators such as slope, aspect, elevation, social pressure, roads near forest and tree species, were used to determine priority of forest rehabilitation areas by using Geographic Information Systems (GIS). In this study, we developed a spatial database including topographic parameters, forest stand type maps and stand type parameters, forest stratification, roads and settlement areas and its proximity tables with forest stands. Slope, aspect and elevation maps of the study area were created by employing a digital elevation model (DEM) produced from contour curves (10 m height accuracy). The study area is naturally covered by *Pinus brutia, Pinus nigra, Abies cilicica, Cedrus libani, Juniperus* spp., and *Quercus* spp., the most widely distributed species in the Mediterranean region. Total degraded forest areas consist of 2.880 sub compartments with 11.363 ha. Finally, we designed a priority map of the forest rehabilitation based on these sub compartments and other indicators by using GIS techniques. It is shown that 6364 ha of degraded forest areas has high priority index value (>=16 and =<19) and 1254 ha of degraded forest areas has very high priority values with higher than 19 priority index value.

Key words: Forest rehabilitation, Geographic Information Systems (GIS), forest management plans, Digital Elevation Model (DEM), priority areas, slope, aspect, proximity, degraded forest.

INTRODUCTION

Forest rehabilitation has always been a sophisticated issue based on not only wood production but also ecological and social services of forest areas in Turkey. Instead of forestry depending on only wood production, what is expected as a forestry concept to answer ecologic, economic and social functions in spoiled forest regions is to have maximum benefit from progress and growth energy of current stands, and to make forest areas efficient with rehabilitation requiring less work and costs by preserving current species in the region without

*Corresponding author. E-mail: alikadi@ktu.edu.tr, Tel: +90 462 377 3243. Fax: +90 462 325 7499.
Author(s) agree that this article remain permanently open access under the terms of the Creative Commons Attribution License 4.0 International License

spoiling the forest ecosystem.

In Turkey, conifers, broadleaved and mixed area in spoiled forest regions, whichhas no chance of being recovered by natural rejuvenation and silvicultural treatment, and the bare spaces in these forest regions are considered for rehabilitation.

In this perspective, forest rehabilitation practices have been applied to large areas and three different pytho-geographical regions (Euro-Siberian, Mediterranean and Irano-Turanian) for a long time (Ürgenç and Boydak, 1985; Saatçioğlu, 1961) in Turkey.

Rehabilitation treatments have been applied in 1453392 ha areas between 1998 and 2010 throughout Turkey (Çolak et al., 2010). By adding the treated area, 346902 ha, in 2010 and 345000 ha area objective for 2011, the total treated area is obtained as 2145394 ha (Anonymous, 2002). These treatment operations, purposely, make important contributions to decrease erosion rate, preserve the soil and manage it in a sustainable way, preserve water bodies, prevent sedimentation in dams, lakes and ponds and guarantee water and electricity generation, minimize floods and overflows, especially, minimize the negative effects of climate change and desertification.

The first forest management plans of Karaisali Forest Enterprise which includes the biggest dam basins and the major portion of Cukurova containing the most important agricultural areas of Turkey, has been designed in 1969. The spoiled forest areas have been decreased from 46851.9 ha area in 1969's forest management plans to 15848 ha in the plans of 2012. Successful forestry applications and rehabilitations work in the last 10 years have been effective in this process. Thanks to these treatments, the spoiled forest areas have been decreased to 8642 ha in the last 10 years (Kadioğullari et al., 2013). Instead of these successful and convenient treatments, the parameters required setting priority order in the rehabilitation sites and which areas have the priority for the intervention are not clear and not considered, which is an important downside. In the abstract, area difference, rehabilitation and forestation effects on the products and services of forest ecosystem have been investigated in this study (Farley et al., 2005; Ilstedt et al., 2007; Chen et al., 2000; Andres and Ojeda, 2002; Şahin and Hall, 1996; Zinn et al., 2002; Louis Awanyo et al., 2011; Zhuang, 1997; Kadioğullari, 2013; Başkent and Kadioğullari, 2007; Kadioğullari et al., 2008; Sağlam et al., 2008).

This study aims to determine the priority of degraded forest areas for the rehabilitation in the Karaisali Forest Enterprise year of 2012 based on forest-stand-type maps by using a Geographic Information System (GIS). In this context, the objective of this study is to contribute to the understanding of the priority index of rehabilitation areas using topographic parameters with different class for the tree species, distance from settlement areas for social pressure and nearness of the roads in the Mediterranean forests of southeastern Turkey.

METHODS

Study area

The study area of Karaisali State Forest Enterprise included Çatalan, Kizildağ, Çukurova, Karaisali, Akarca and Hacili Forest Planning Units located in Adana Province in the Eastern Mediterranean Region of Turkey, UTM European 50 datum 36 zones 668970 to 716792 E, 4103218 to 4151137 N (GDF, 2012). The area consists of mountain forests, flat agricultural land and scattered settlements and highlands. The altitude varies between 20 and 2420 m (Figure 1) (Kadioğullari et al., 2013).

The region is naturally covered degraded forest by *Pinus brutia, Pinus nigra, Abies cilicica, Cedrus libani, Juniperus* spp*., and Quercus* spp*.* the most widely distributed species in the Mediterranean region. In this study, there are 11,363 ha degraded forest that consist of above species with 2,880 sub compartments (Number of patch; NP). According to stand-type maps, the forests in 2012 were mostly classified into BÇz (degraded *P. brutia*; calabrian pine), BÇz-E (degraded *P. brutia*-erosion), BÇz-T (degraded *P. brutia*-stony), BAr (degraded *Juniperus* spp.; juniper), BÇk (degraded *P. nigra*), BÇk-T (degraded *P. nigra*-stony), BG (degraded *Abies cilicica*; fir), BS (degraded *Cedrus libani*; cedar), BM (degraded *Quercus* spp*;* oak) degraded forest stand types with areas of 5848 ha (number of patch (NP) value is 1984), 311 ha (NP value is 167), 938 ha, 3398 ha (NP is 372), 108 ha, 69 ha, 32 ha, 145 ha and 511 ha (NP is 74) respectively.

Database development

In this study, stand parameter data of forest stand type were obtained from the Karaisali forest management plans carried out in 2012 (GDF, 2012). The forest-stand-type maps for 2012 were produced with digital collared infrared aerial photos and controlled field survey data. These plan maps merged and saved as a single database by using ArcInfo 10.0^{TM}. Settlement areas and degraded forest stand type were gathered using this database. Road maps of study area was gathered from management plans and controlled by ortho-photos created by using digital aerial photograph in the year of 2011 (Figure 2).

Topographic parameters such as slope, aspect and elevation were created by using a digital elevation model (DEM) produced from contour curves (10 m height accuracy). Slope maps produced from this data and average slope value was measured using area weighted methods based on per sub compartment. At the same time, elevation value was measured using area weighted methods based on per sub compartment. However, there are other aspect value of per sub compartment that are used to select dominant aspect value with covered area based on per sub compartment (Figure 2).

Determining of priority index

Priority index was determined by using same topographic parameters based on tree species except for elevation. The reason for this is that all the tree species were distributed in different stages of elevation and tree species grow best when elevation varies. Therefore, regardless of the tree species, for all stands slope, aspect, distance to the road, the distance from residential (settlement) area and stony-erosion according to the characteristics of the sub compartment basically used the same parameters.

Index of stony-erosion was classified into three, while other

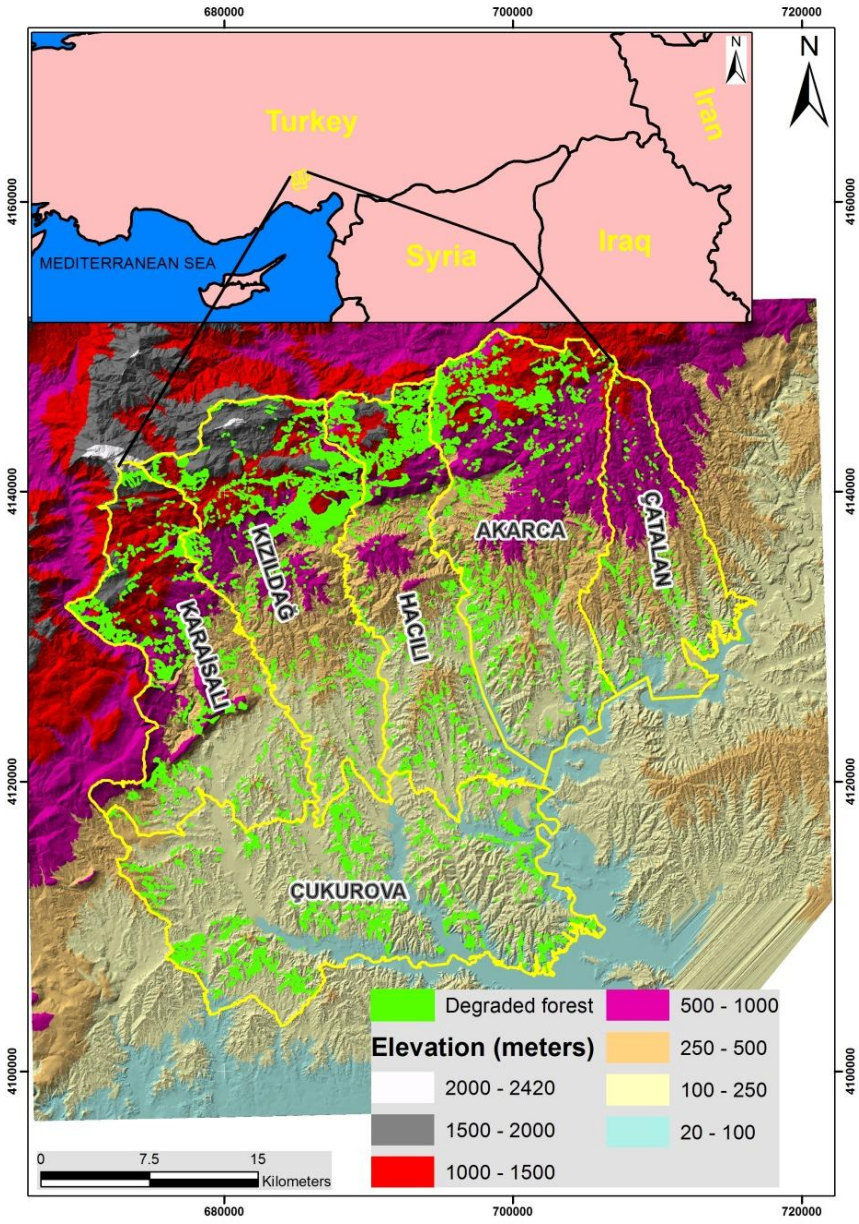

Figure 1. Study area.

indexes were classified into four. All sub compartments were classified into three for erosion-stony index; stony, erosion and normal stand with index of 1, 2 and 3. According to slope index, all sub compartments were classified into four for slope (%; percent) using area weighted method; <20%, 20-40%, 40-60% and >60% with index of 4, 3, 2 and 1. Furthermore, for other parameters such as distance to road index, all sub compartments were classified into four; 0 m, 0.1-250 m, 251-500 m and >500 meter with index of 4, 3, 2 and 1. For parameters as distance from settlement areas, all sub compartments were classified into four; <500 m, 501-1000 m, 1001-1500 m and >1500 m with index of 1, 2, 3 and 4. For other main aspect parameters, all sub compartments were classified into four; north, east, west and south aspects with index of 4, 3, 2 and 1. Lastly, all the tree species were distributed in different stages of elevation and classified into four based on elevation. For the *Pinus brutia* (calabrian pine; Çz) and *Quercus* (Oak; M) species for all sub compartments were classified into four; <500 m, 501-1000 m, 1001-1500 m and >1500 m with index of 4, 3, 2 and 1, respectively. For the *Pinus nigra* (Çk), *Abies cilicica* (G) and *Cedrus libani* (S) species for all sub compartments were classified into four; 900-1250 m, 1250-1500 m, 1500-1750 m and >1750 m with index of 4, 3, 2 and 1, respectively. For the last species as *Juniperus sps*, (Ar) for all sub compartments were classified into four; 250-750 m, 750-1250 m, 1250-1750 m and >1750 m with index of 4, 3, 2 and 1, respectively. To end this calculated priority index for each sub compartment, total priority index is determined by summing these six indexes. This index value for each sub compartment is changed from 6 to 23. To better understand the spatial distribution of priority index, it is classified into four classes as, <=10, 11-15, 16-19 and>=20 (Figure 3).

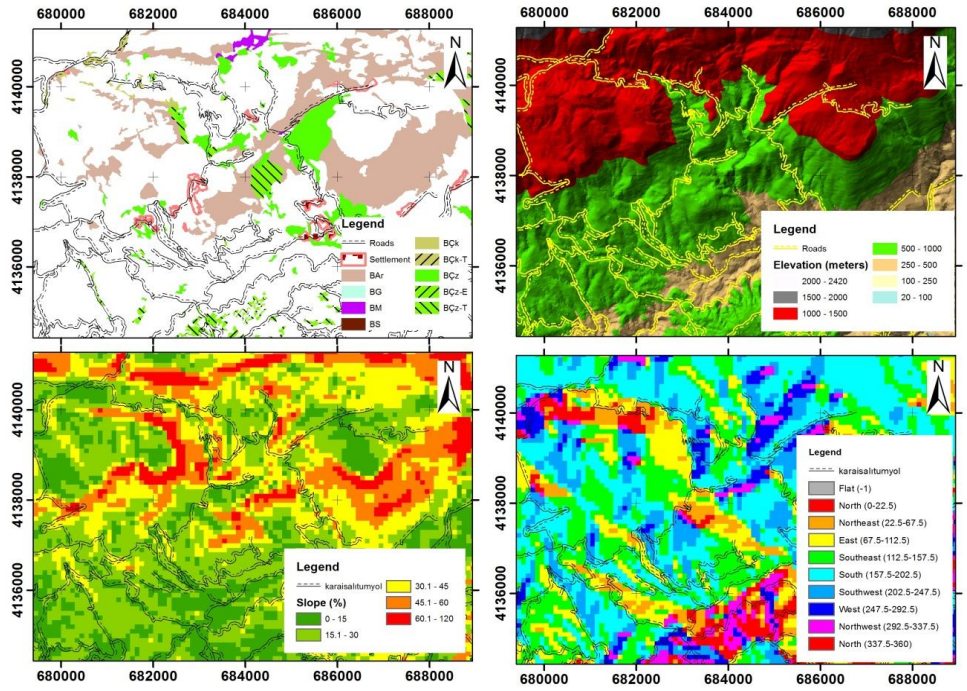

Figure 2. Database development of study area.

Table 1. Priority index of rehabilitations areas based on degraded stand types.

Stand type		BÇk	BÇk-T	BAr	BÇz	BÇz-E	BÇz-T	BG	BM	BS	Total
Priority index	**Priority group**	**Area (ha)**									
10	Low			5.1							5.1
11				24.2	16.0		93.9			3.8	137.9
12			42.7	97.1	26.5		176.8			8.0	351.1
13	Medium		11.4	496.7	93.3		215.3	2.5		5.0	824.2
14		2.3	2.5	603.7	377.4	11.1	81.5	11.1	14.6	25.9	1130.1
15		23.2	3.8	653.2	330.4	9.8	153.0		88.8	31.4	1293.5
16		30.5	6.5	602.2	818.6	58.7	98.7		49.4	23.5	1688.1
17	High	18.2		429.4	977.4	92.4	54.4	16.6	158.2	34.0	1780.5
18		24.8	2.4	282.8	1168.1	80.9	49.0	2.1	29.3	3.5	1643.1
19		8.8		101.1	1060.6	37.7	15.6		31.7		1255.5
20		0.8		84.0	558.6	18.5			108.7	10.2	780.9
21	Very high			19.1	326.7	2.1			29.4		377.3
22					93.4	0.5			1.3		95.2
23					1.3						1.3
Total		**108.7**	**69.4**	**3398.4**	**5848.5**	**311.6**	**938.2**	**32.2**	**511.5**	**145.4**	**11363.9**

RESULTS

According to the priority index of rehabilitation are asbased on degraded forest stand type map in the 2012, there are four classes: low (index value =<10), medium (10< index value <16), high (16<= index value =<19), and very high (index value>=20) priority classes (Table 1, Figure 3). Priority index class was generally concentrated into high class (6367.2 ha, NP value is 1911 (sub compartment), very high value class (1254.7 ha, NP is 481) and medium class (3736.8 ha, NP value is 487) (Table 1, Figures 3 and 4). The low class has very low

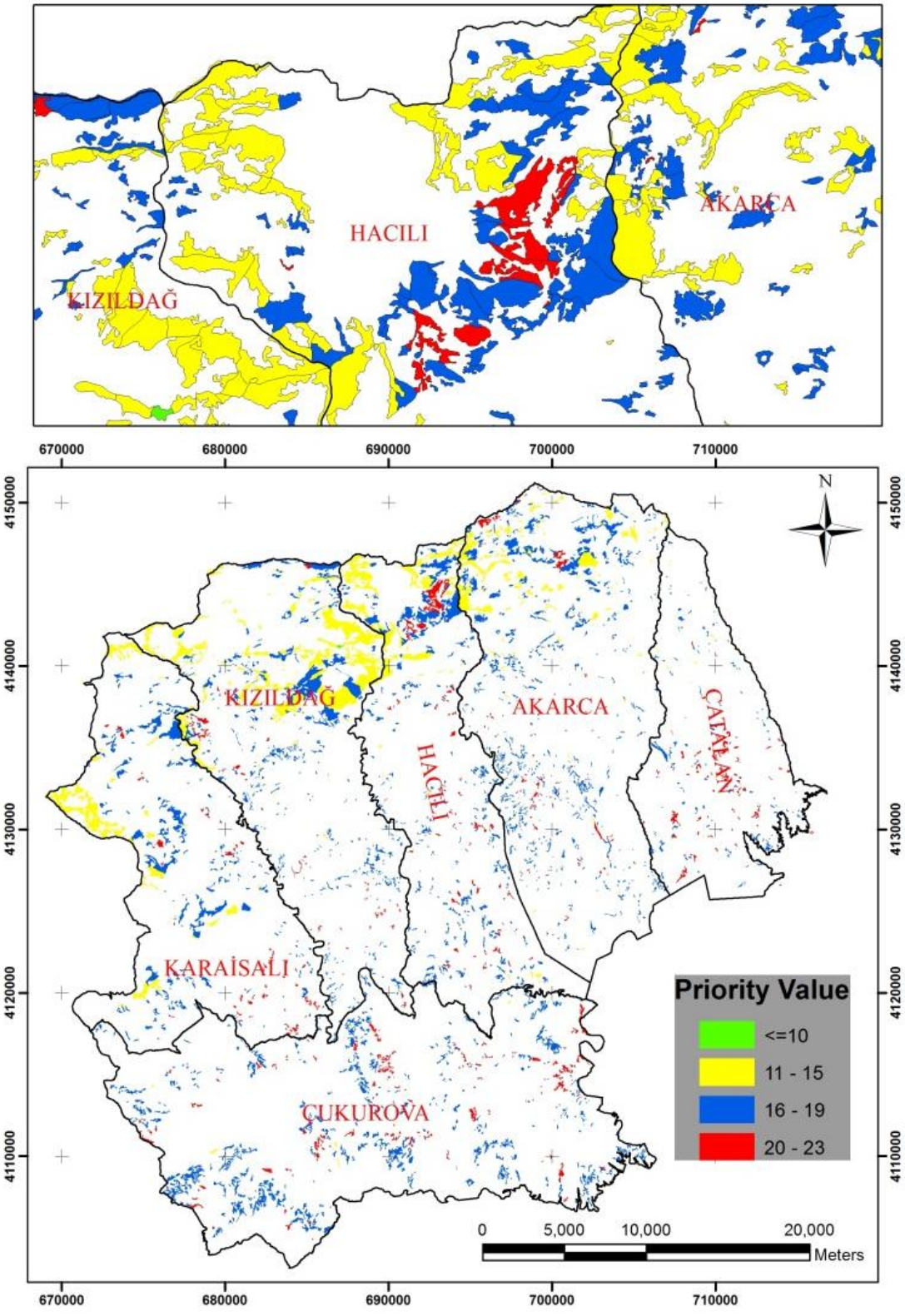

Figure 3. Priority maps of rehabilitations area.

priority areas of 5.1 ha. These results showed that, degraded forest areas have different priority index values and these values may help the plan makers decide which areas have the priority for rehabilitation in the first

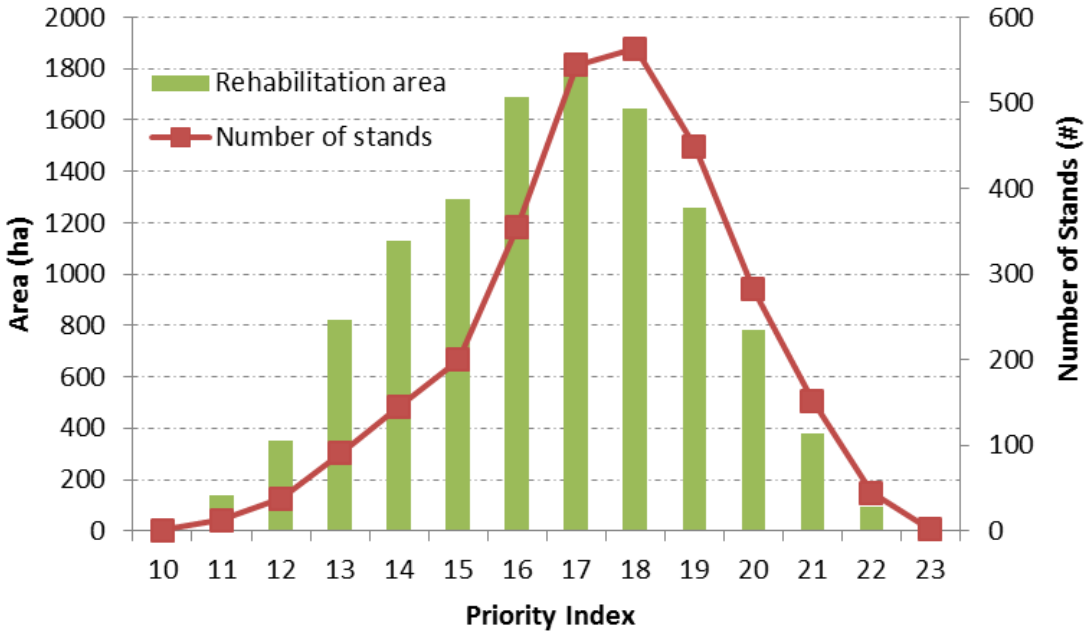

Figure 4. The distribution of the number of sub compartment of rehabilitations area.

forest management planning period.

DISCUSSION

This study was a determination of the priority of degraded forest areas for rehabilitation in the Karaisali Forest Enterprise by using a Geographic Information System (GIS). This study analyzed priority index of rehabilitation by using topographic parameters with different class for the tree species, distance from settlement areas for social pressure and closeness of the roads based on degraded forest stand type maps of the year 2012 in the Mediterranean forests of southeastern Turkey. The results of priority class in the study area show that the high priority areas have bigger areas than other classes and the same stand type has different priority index based on other parameters. At the same time, user change the parameters used for determined priority index of each degraded forest stand type which may be useful for planning other study areas.

Conclusions

Determined priority index for rehabilitation areas and mapping by using GIS for the planning of sustainable forest resources have become increasingly important during the preparation of Ecosystem Based Multi Objective (ETÇAP) forest management plans. This study examined the priority index by using only a number of topographic parameters in Karaisali Forest Enterprise, but for the following studies, adjacency/proximity parameters and opening size parameters should be used for determining the priority index for each degraded forest stands in order to prevent area of forest ecosystems from turning into monotonous block and fragmented areas.

Conflict of Interest

The authors have not declared any conflict of interest.

REFERENCES

Andres C, Ojeda F (2002). Effects of afforestation with pines on woody plant diversity of Mediterranean heathlands in southern Spain. Biodivers. Conserv. 11:1511–1520

Anonymous (2002) Forestry Statistics, 2012. Republic of Turkey, Ministry of Environment and Forestry, Ankara (in Turkish).

Başkent EZ, Kadioğullari Aİ (2007). Spatial and temporal Dynamics of land use pattern in Turkey: A case study in İnegöl. Landsc. Urban Plan. 81(4):316-327 (in Turkish).

Chen CR, Condron LM, Davis MR, Sherlock RR (2000). Effects of afforestation on phosphorus dynamics and biological properties in a New Zealand grassland soil. Plant Soil 220:151–163.

Çolak AH, Kirca S, Rotherham JD, İnce A (2010). Restoration and Rehabiltation of Deforested and degraded forest Landscapes in Turkey. Ministry of Environment and Forestry General Directorate of Afforestation and Erosion Control, Ankara.

Farley KA, Jobbagy EG, Jackson RB (2005). Effects of afforestation on water yield: A global synthesis with implications for policy. Glob Chang. Biol. 11:1565–1576.

GDF (2012). General Directorate of Forestry of Turkey. Forest Management Plans of Karaisali, Akarca, Kizildağ, Çatalan, Hacili and Çukurova Forest Planning Units, Ankara (in Turkish).

Ilstedt U, Malmer A, Verbeeten E (2007). The effect of afforestation on water infiltration in the tropics: A systematic review and meta-analysis. For. Ecol. Manage. 251(1–2):45–51.

Kadioğullari Aİ, Keleş S, Başkent EZ, Günlü A (2008). Spatiotemporal Changes in Landscape Pattern in Response to Afforestation in Northeastern Turkey: A Case Study of Torul. Scott. Geogr. J. 4:259-273.

Kadioğullari Aİ, Sayin MA, Çelik DA, Borucu S, Bulut S, Çil B (2013). Understanding land-cover change and forest dynamics using temporal forest management plans. Environ. Monit. Assess. (DOI 10.1007/s10661-013-3520-9).

Kadioğullari Aİ (2013). Assessing implications of land use and land cover changes in forest ecosystems of NE Turkey. Environ. Monit. Assess.185:2095–2106 (DOI 10.1007/s10661-012-2691-0).

Louis Awanyo L, Attuah EM, McCarron M (2011). Rehabilitation of forest-savannas in Ghana: The impacts of land use, shade, and invasive species on tree recruitment. Orig. Res. Art. Appl. Geogr. 31(1):181-190.

Saatçioğlu F (1961). Türkiyede orman davasi ve bazi memleketlerin ağaçlandirma çalişmalari. I.U. Rev. Fac. For., Istanbul Univ. Ser. A. 11(2):1-11 (in Turkish).

Sağlam B, Dinc Durmaz B, Bilgili E, Kadioğullari Aİ, Küçük Ö (2008). Spatio-Temporal Analysis of Forest Fire Risk and Danger Using LANDSAT Imagery. Sens. 8:3970–3987.

Şahin V, Hall MJ (1996). The effects of afforestation and deforestation on water yields. J. Hydrol. 178(1–4): 293–309. (15 April).

Ürgenç S, Boydak M (1985) Current Situation of reforestation and afforestation activities in Turkey and their objectives. I.U. Rev. Fac. For. Istanbul Univ. Ser. A. 35(2):8-18.

Zhuang X (1997). Rehabilitation and development of forest on degraded hills of Hong Kong. Orig. Res. Art. For. Ecol. Manage. 99(1–2):197-201.

Zinn YL, Resck DVS, da Silva JE (2002). Soil organic carbon as affected by afforestation with *Eucalyptus* and *Pinus* in the Cerrado region of Brazil. For. Ecol. Manag. 166:285–294.

academicJournals

Related Journals Published by Academic Journals

- International NGO Journal
- International Journal of Peace and Development Studies